Dynamical Mass Generation and Confinement at Finite Temperature

by

Michael Strickland

Department of Physics
Duke University

Date: ______________________________

Approved:

____
Dr. Berndt Müller, Supervisor

____
Dr. Calvin Howell

____
Dr. Joshua Socolar

____
Dr. Roxanne Springer

____
Dr. Stephen Teitsworth

Dissertation submitted in partial fulfillment of the
requirements for the degree of Doctor of Philosophy
in the Department of Physics
in the Graduate School of
Duke University

1997

ABSTRACT

(Physics)

Dynamical Mass Generation and Confinement at Finite Temperature

by

Michael Strickland

Department of Physics
Duke University

Date: ______________________

Approved:

____
Dr. Berndt Müller, Supervisor

____
Dr. Calvin Howell

____
Dr. Joshua Socolar

____
Dr. Roxanne Springer

____
Dr. Stephen Teitsworth

An abstract of a dissertation submitted in partial fulfillment of the requirements for the degree of Doctor of Philosophy in the Department of Physics in the Graduate School of Duke University

1997

Abstract

We study the quark propagator at finite temperature through non-perturbative solution of a truncated Scwhinger-Dyson (SD) equation for the quark self-energy. The truncation used ignores the coupling to the gluon and ghost self-energy equations by modeling the gluon propagator. We study several different Ansätze for the gluon propagator which allow us to study both strongly coupled QED and QCD. To model confinement within QCD the gluon propagator is chosen to be a sum of a delta function, which models the strong infrared enchancement expected in the gluon propagator, and a perturbative piece, which models the short range aspects. It is shown that this model can describe both the deconfinement and chiral symmetry phase transitions and provides insight into the relation between them. In solving the SD equation we have gone beyond the bare vertex approximation by applying the finite temperature Ward-Takahashi identity allowing us to write the finite temperature quark-gluon vertex function in terms of the finite temperature quark propagator. It is shown that vertex improvement restores gauge invariance of the results. Numerical solution of the SD equation shows that at low temperature the quark propagator does not contain any poles on the real $\underline{\mathrm{p}}^2$ axis, instead having a pair of timelike complex conjugate poles. The imaginary part of the position of these poles is suggested to be related to the rapid decay of the quark propagator due to dynamical pair generation. We find that at a critical temperature, T_c^{dc}, these complex conjugate poles combine into a single pole on the real timelike $\underline{\mathrm{p}}^2$ axis signaling quark deconfinement. In addition, we demonstrate that the chiral and deconfinement phase transitions are coincident in the limit of vanishing bare quark mass. For finite bare quark mass we find that the chiral transition occurs prior to the deconfinement transition, with the separation between the two being on the order of the bare quark mass.

Acknowledgements

I would like to thank my wife Melissa Trachtenberg for her help and support. I would also like to thank my parents, Donald and Mary Ann Strickland, for always being there for me, my advisor, Berndt Müller, for countless meetings and good advice, and all of my friends (you know who you are!) for providing healthy distractions.

Thanks also to the North Carolina Supercomputing Center for use of their Cray T90.

"When the going gets weird, the weird turn pro."

Hunter S. Thompson

Contents

List of Tables

List of Figures

Chapter 1

Introduction

Although there have been significant advances made in the study of high energy particle physics in the last few decades, the current theory of the sub-nuclear degrees of freedom, the quarks and gluons, is far from well understood. High energy experimental data from proton-proton and electron-proton collisions have provided incontrovertible evidence for the existence of quarks, and the symmetry properties of the quark model alone are sufficient to explain the qualitative structure of the nuclear particle spectrum. However, to this day the low-energy properties of QCD are still a mystery. One of the most extraordinary aspects of the physics of quarks and gluons is that they are never observed in isolation. The particles which are observed are always colorless composite states of two or three quarks called hadrons. This property is called "quark confinement". Through numerical lattice simulations it has been shown that the theory which is believed to govern quark and gluon interactions, quantum chromodynamics (QCD), is confining; however, the exact mechanism that produces confinement has yet to be determined.

The QCD coupling constant has been shown to be a decreasing function of temperature, and it is therefore believed that QCD will undergo a phase transition at very high temperatures, $T \approx 200\,\mathrm{MeV} \approx 2 \times 10^{12}\,\mathrm{K}$, to a state in which colored states can propagate more or less freely. This new state of matter is called a quark gluon plasma (QGP), in analogy to the familiar electromagnetic plasma. An understanding of this phase transition is crucial for two reasons. The first is that it provides a testing ground for QCD itself. QCD has had much success in describing high energy scattering data; however, at low-energies theories which only take into account the

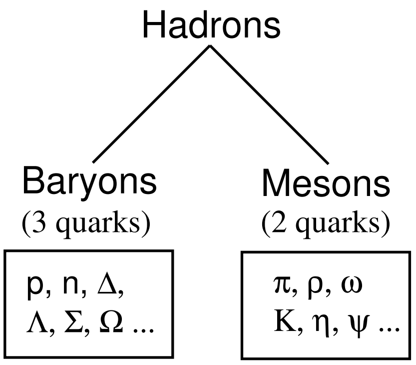

Figure 1.1: The classification of strongly interacting particles.

hadronic degrees of freedom are more reliable. A QGP is expected to be a weakly coupled system, so the problems that are encountered at low energies can be avoided. The second, more compelling, reason to study this phase transition is that if we trace the history of our universe backwards in time, this is the most recent phase transition involving fundamental quantum fields thought to be encountered, occurring about 10 μs after the "Big Bang". The electroweak phase transition is believed to have taken place at $t \approx 10^{-11}\,\mathrm{s}$ ($T \approx 100\,\mathrm{GeV}$) and the splitting of the electroweak and strong interactions is hypothesized to have taken place at $t \approx 10^{-35}\,\mathrm{s}$; however, the QGP phase transition is the only one which we can currently access in a laboratory setting.

In addition to deconfinement, QCD is expected to undergo another phase transition, the chiral phase transition. The chiral phase transition describes how, when the temperature is increased, the dynamically generated mass of the quark vanishes. Dynamical mass generation is the process by which mass can be generated purely from the interactions of particles with the vacuum. Dynamical mass generation can be illustrated by considering the condensed matter example of an electron moving through a crystal lattice. As the electron moves past the nuclei of the atoms at each lattice site, it gently pulls the nuclei in its direction, and as it moves away the nuclei recoil and oscillate slightly. The immediate effect of this movement is that nearby lattice sites oscillate in response to this perturbation. The oscillations of these nuclei will then, in turn, affect the movement of the electron through the lattice and can make the electron's mass appear to be larger than its physical mass. In order to translate this analogy to QCD we replace the lattice with the vacuum itself, and the electron with a quark moving through the vacuum. However, in this case, the mass that results from the quark's interaction with the vacuum is not an artifact of the "crystal", but is instead manifest as the physical mass of the particle which is observed.

1.0.1 QGP experiments

In order to study the formation of a QGP in a laboratory setting, it is expected that one must collide heavy-ions at ultra-relativistic energies. There are two facilities being planned for ultra-relativistic heavy-ion experiments. The Relativistic Heavy-Ion Collider (RHIC) [1] at Brookhaven National Labs in New York and the Large Hadron Collider (LHC) [2] at European Centre for Particle Physics (CERN), in Geneva, Switzerland. RHIC will accelerate and collide ions from protons to heavy nuclei, such as Au, at center of mass energies up to 500 GeV for protons and 200 GeV per nucleon pair for Au nuclei. LHC will concentrate on Pb + Pb collisions at center of mass energies around 5.4 TeV per nucleon pair.

When nuclei are collided at these energies it is expected that in the central collision region a very hot dense pocket of nuclear matter will be formed. In the evolution of this collision event, we identify three regimes. In the first stage, the rescattering of quarks and gluons is expected to lead to a quasithermal phase space distribution (prequilibrium). Further rescattering of these quarks and gluons is expected to lead to a thermalized QGP about 1 fm/c ($\approx 10^{-23}$ s) after the initial collision (thermal QGP). The thermalized QGP then expands and cools until it reaches the critical temperature, $T_c \approx 200$ MeV, at which time the quarks begin to coalesce back into hadrons (hadronization).

With lifetimes expected to be on the order of 10^{-22} seconds the experiments that will study QGP formation will not be able to directly probe this new state of matter. Instead, experimentalists will rely on measurements of the particles which are produced from within the QGP itself and produced as the QGP cools. Although there are a great number of detector systems which will be utilized, the three most important are hadron spectrometers, lepton pair spectrometers, and photon spectrometers. Photons and lepton pairs (e^+e^-, $\mu^+\mu^-$, etc.) are expected to be the cleanest signatures of the existence of a QGP because they probe the earliest stages of QGP evolution and are not affected by final-state interactions [3]. Using hadron spectrometers experimentalists will also be able to measure the momentum and rapidity distributions of a variety of hadronic particles produced in the latter stages of QGP evolution, including decays and resonances.

To determine whether not a QGP plasma is formed or not, one must compare the predictions of models which include only hadronic degrees of freedom with those which assume that a thermally equilibrated QGP has been formed. If it is in fact the case that a thermalized QGP has been formed, then the middle stage of the QGP evolution should be parameterized by one parameter, the temperature as a function of proper time. In order to calculate the temperature as a function of time, one needs to understand the microscopic dynamics of the scattering of quarks, gluons, and meson resonances within the plasma. The scattering processes are important because these enter directly into the equation of state for the QGP. When the thermal state cools down and reaches the critical temperature the hadronization cross sections are necessary in order to predict the types, numbers, and momentum distributions of hadrons produced in a QGP event. Both of these calculations require as input the finite temperature quark propagator. For the thermal scattering processes it may be sufficient to perform perturbative finite temperature calculations, as long as one is not close to the critical temperature; however, when calculating hadronization cross sections, detailed knowledge about the non-perturbative structure of the finite temperature quark propagator is absolutely necessary.

1.0.2 The results of this work

In this work we will make non-perturbative calculations of the finite temperature quark propagator within the Schwinger-Dyson (SD) approach in order to study confinement and dynamical mass generation. The SD approach starts from an infinite set of coupled integral equations for the n-point functions of the theory, with each n-point function being coupled to higher n-point functions. Figure 1.2 shows a table illustrating some of the common n-point functions, their diagrammatic representations, and the vacuum expectation values associated with them. The n-point functions are n-particle correlation functions much like those encountered in statistical mechanics. Due to the coupling to higher n-point functions there is no exact solution possible; however, by truncation of this system of equations we can achieve a closed system of non-perturbative equations for the finite temperature quark propagator. From the solutions obtained for the finite temperature quark propagator we can gain insight in the physics of deconfinement and dynamical mass generation. In addition, as mentioned above, these solutions are necessary ingredients in the calculation of finite temperature properties of the QGP itself in the thermal and hadronization stages.

We present here a method by which non-perturbative calculations of the finite temperature quark propagator can be made. As input, we model the gluon propagator. The model is chosen so that it reproduces the known high-energy behavior of the gluon propagator. The low-energy behavior of the gluon propagator is not known. Therefore, at this stage, we are left to model this regime. The chosen form models the

n	Common Name	Diagrammatic Representation	Expectation Value
2	Propagator	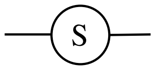	$< 0 \mid \phi\,\phi \mid 0 >$
3	Vertex Function	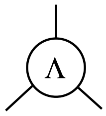	$< 0 \mid \phi\,\phi\,\phi \mid 0 >$
4	Scattering Matrix	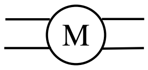	$< 0 \mid \phi\,\phi\,\phi\,\phi \mid 0 >$
n	*n*-point function	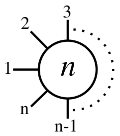	$< 0 \mid \underbrace{\phi\ \ldots\ \phi}_{n} \mid 0 >$

Figure 1.2: Common n-point functions, their diagrammatic representations, and the vacuum expectation values associated with each.

significant low-momentum enhancement of the gluon propagator expected from lattice and analytic studies [4, 5, 6]. We make no claim as to the quantitative accuracy of the model chosen, but do believe that it captures the qualitative features necessary for a description of the chiral and deconfinement phase transitions within QCD. We do, however, believe, that further refinement of the gluon propagator Ansatz will allow quantitive predictions using this technique.

We find that the low temperature quark propagator does not have a simple pole on the real $\underline{p}^2$ axis, but instead has a pair of complex conjugate poles. The possibility of having a complex pole in a propagator is not suprising. In fact, if we were to calculate the propagator for an unstable particle we would find just this. In the case of an unstable particle the imaginary part of the pole position is directly related to the lifetime of the unstable state. In the case of the quark, however, the interpretation is different. Since within pure QCD the quark is a fundamental particle, it is not possible for it to decay into anything else. In this case, the imaginary part of the pole position measures the decay of the probability of finding a colored state in the vacuum. If we were to place a quark somewhere, wait a short amount of time, and then try to annihilate the quark that was placed in the first place, we would find that the presence of the quark had induced dynamical pair generation in an attempt to screen this exposed color charge. After annihilating the original quark, the state that is left (the pairs that were produced from the vacuum) would not be the same vacuum state that we had started with, and therefore when the projection onto the vacuum is taken, the result will be very small and decreasing as a function of time. Since the probability of pair production is related to the ratio of the string tension[1] over the pair mass squared we should find that the imaginary part of the pole position should go to zero as the mass of the quark goes to infinity or the string tension goes to zero. This result is borne out by our calculations. In addition to obtaining a confining character we have also calculated the dynamical mass generated for the quark through gluon exchange. This dynamical mass is large compared to the bare mass of the quark due to the strong coupling nature of QCD.

As the temperature is increased, the dynamically generated portion of the quark mass decreases and the poles in the quark propagator move closer to the real $\underline{p}^2$ axis. At the critical temperature, T_c, we will show that the theory undergoes two second order phase transitions, the dynamically generated mass goes to zero and the poles move onto the real $\underline{p}^2$ axis. The vanishing of the dynamical mass corresponds to the chiral phase transition, and the movement of the poles onto the real $\underline{p}^2$ axis corresponds to the deconfinement phase transition, since a pole on the real $\underline{p}^2$ axis corresponds to a state which does not "decay". For zero bare mass quarks these phase transitions are coincident, but for larger quark masses chiral symmetry restoration happens at a lower temperature than deconfinement, with the separation being on the order of the quark mass. We have calculated the critical exponents for chiral and

[1]Within QCD the unscreened interquark potential increases linearly with quark separation. The slope of the potential is sometimes called the string constant.

deconfinement phase transitions and find that they are the same within the accuracy of the numerical solution with $\beta = 0.32 \pm .02$.

One of the ingredients in the solution of the SD equations is the vertex function. Typically, the vertex function is taken to be the bare vertex function of QCD; however, it is well-known that this approximation violates gauge invariance. In this work we have gone beyond the bare vertex, or rainbow, approximation by applying the finite temperature Ward-Takahashi (WT) identity. This identity relates the quark propagator to the quark-gluon vertex non-perturbatively and can be used to write the vertex function solely in terms of the propagator, thereby restoring gauge invariance and summing over a larger set of self-energy diagrams. We have made calculations with the bare and WT improved vertices which are shown to remove the gauge dependence of the results. Since previous calculations of the finite temperature quark propagator within this approach have used the bare vertex approximation [5] the results obtained were gauge dependent and thus unphysical.

The structure of this work is as follows: In Chapter 2, we provide a brief introduction to quantum field theory. In Chapter 3, we derive the Schwinger-Dyson equation at zero temperature and present results using different gluon propagator Ansätze and vertex approximations. In Chapter 4, we will extend the treatment to finite temperature and present results for the temperature dependence of the quark propagator, quark condensate, and critical exponents for the chiral and deconfinement phase transitions. In Chapter 5, we will present the conclusions and outlook.

Chapter 2

Quantum Field Theories

The starting point for functional treatments of quantum field theories is the specification of the generating functional for the theory. In general, the generating functional can be expressed as a path integral of the exponential of the action over all fields appearing therein, i.e.

$$Z[J_1,\ldots,J_n] \equiv e^{\frac{i}{\hbar}W[J_1,\ldots,J_n]} = \mathcal{N}\int \prod_{i=1}^{n} \mathcal{D}\Phi_i \, e^{\frac{i}{\hbar}S(\Phi_1,\ldots,\Phi_n)+\frac{i}{\hbar}\sum_{i=1}^{n}\int \mathrm{d}^4x\, J_i\Phi_i}\,, \tag{2.1}$$

where W is the generating functional for connected diagrams, Φ_i is a generalized field variable, J_i a classical source for that field, and $\mathcal{N}$ is a normalization constant which is irrelevant for physical observables [7, 8]. In this manuscript, we set $\hbar = c = 1$, but show $\hbar$ in the definition of the generating functional for the discussion in the next section.

The action is given by an integral of the Lagrangian density over space-time

$$S(\Phi_1,\ldots,\Phi_n) = \int \mathrm{d}^4x\, \mathcal{L}(\Phi_1,\ldots,\Phi_n)\,. \tag{2.2}$$

To completely specify the theory one needs to define the structure of the fields (i.e. scalar, vector, spinor, etc.), the symmetries that they obey (parity, charge, gauge, etc.), and the interaction terms which are consistent with these symmetries. In the following sections we outline the progression from the simplest scalar quantum field theory to the theory which is believed to govern quarks and gluons (QCD).

2.1 Scalar Quantum Field Theory

Let us consider the scalar Lagrangian

$$\mathcal{L}(x) = \frac{1}{2}\left(\partial_\mu\phi(x)\partial^\mu\phi(x) - M_o^2\phi^2(x)\right) + V(\phi(x))\,, \tag{2.3}$$

where

$$V(\phi(x)) = \sum_{n=2}^{\infty} a_n(x)\phi^n(x)\,, \tag{2.4}$$

is the most general interaction term possible and M_o is the bare, or classical, mass of the scalar particle. If we require invariance of the theory under $\phi \to -\phi$ (Z_2 invariance), then only even terms appear in the interaction sum,

$$V(\phi(x)) = \sum_{m=1}^{\infty} a_{2m}(x)\phi^{2m}(x)\,. \tag{2.5}$$

The path integral for any theory is defined by a limiting procedure in which spacetime is discretized and the lattice size is taken to zero so that the fields are distributed evenly over spacetime. For instance, the derivatives appearing the Lagrangian above (2.3) would be expressed as a finite difference

$$\partial_\mu\phi(x) \to \frac{\phi(x+\epsilon_\mu) - \phi(x)}{\epsilon_\mu}\,. \tag{2.6}$$

In this case, at each lattice point we place a one-component scalar field ϕ as shown in Figure (2.1). The path integral is computed by integrating over all possible spacetime lattice field configurations weighted by $i/\hbar$ times the exponential of the action. When the action associated with a particular field configuration is large compared to $\hbar$, the exponential oscillates wildly, so that the contribution from such

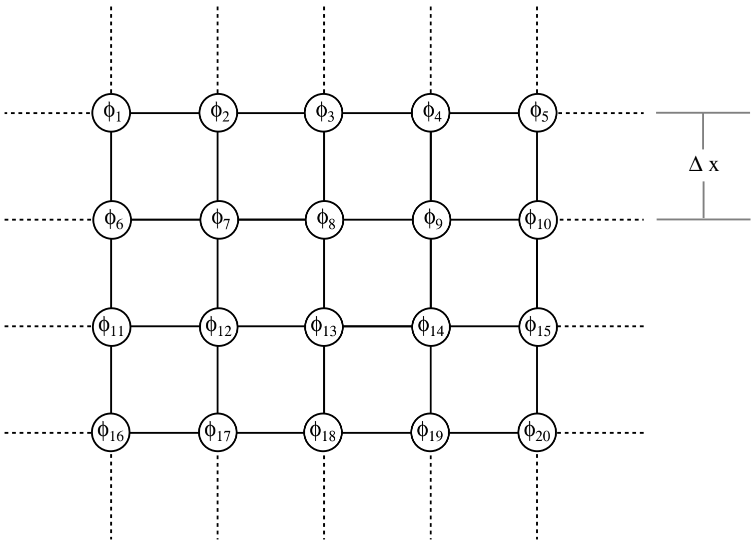

Figure 2.1: Schematic representation of a distribution of field variables at discrete spacetime points.

configurations is small compared to the contribution coming from configurations that minimize the classical action.[1]

In the classical limit, $\hbar \to 0$, only field configurations that minimize the action (classical field configurations) contribute to the path integral[2], and the free energy, W, is simply given by the bare action of the theory. However, if $\hbar$ is finite, field configurations other than the classical one contribute to the path integral.

When this is the case, the analytic evaluation of the path integral becomes difficult if interaction terms are non-Gaussian, i.e. $V(\phi)$ contains terms with $m > 1$. Methods to deal with this situation include the loop expansion, which is an expansion in $\hbar$ around the classical field configuration, and evaluating the path integral numerically using lattice quantum field theory [8, 9, 10].

Another way to deal with this problem is to avoid doing the path integral altogether by deriving relations between the moments, or n-point functions, of the path

[1]If one uses a Euclidean metric the factor of $i/\hbar$ becomes $-1/\hbar$. Within this metric it is more obvious that field configurations with large actions are suppressed.

[2]Minimization is sufficient since we can always add a constant term to the action which makes the field configuration of least action have $S = 0$.

integral (see Chapter 3) and solving those. This method yields an infinite hierarchy of equations for the n-point functions, so that the problem of having to perform the path integral over an infinite number of field configurations is transformed into solving an infinite set of coupled equations for the n-point functions. Through systematic extension of the level of truncation of this system of coupled equations (including higher and higher n-point functions), the usefulness of this transformation can be assessed. In practice, truncation of this system of equations has proved to be a successful [11, 12, 13] method for calculating hadronic observables (masses, lifetimes, scattering lengths, etc.), as well as offering some insight into how confinement may be realized in QCD. In Chapter 3, we will return to this topic in some detail. For now, though, we return to the discussion of the general properties of a scalar quantum field theory.

Quantum vacuum expectation values of field operators can be evaluated within the path integral formalism by weighting the exponential of the action by the operator in question, dividing by the generating functional, and then taking the limit that the external sources for the fields vanish. For a general operator $O(\phi)$

$$< 0\,|\,O(\phi)\,|\,0 >= \lim_{J\to 0} \frac{\int \mathcal{D}\phi\, O(\phi)\, e^{iS(\phi)+iJ\phi}}{Z[J]}\,. \tag{2.7}$$

For instance, if we were interested in the quantum expectation value of the product of two scalar fields then the corresponding expression would be

$$< 0\,|\,\phi(x)\phi(y)\,|\,0 >= \lim_{J\to 0} \frac{\int \mathcal{D}\phi\, \phi(x)\phi(y)\, e^{iS(\phi)+i\int \mathrm{d}^4x\, J\phi}}{Z[J]}\,. \tag{2.8}$$

This expectation value is called a two-point function because it involves fields at two points. Another way to write this quantity is to express it in terms of functional derivatives of the generating functional

$$\frac{\delta^2 Z}{\delta J(x)\delta J(y)} = -\int \mathcal{D}\phi\, \phi(x)\phi(y)\, e^{iS(\phi)+i\int \mathrm{d}^4x\, J\phi}\,, \tag{2.9}$$

so that

$$< 0 \,|\, \phi(x)\phi(y) \,|\, 0 >= - \lim_{J\to 0} \frac{1}{Z} \frac{\delta^2 Z}{\delta J(x) J(y)} \,. \tag{2.10}$$

These expressions bear a striking similarity to those encountered in statistical mechanics, and as a consequence much of the formalism used for the treatment of thermal statistical systems can be applied directly to the path integral formulation of quantum field theory.

The full n-point functions, $G_n[J]$, can be defined through the following relation

$$G_n[J] = \left(-i\frac{\delta}{\delta J}\right)^n Z[J] \,. \tag{2.11}$$

It is sometimes useful to express quantities in terms of the connected n-point functions G_n^c defined by

$$G_n^c[J] = \left(-i\frac{\delta}{\delta J}\right)^n W[J] \,. \tag{2.12}$$

A connected n-point function is the the n^{th} term in the cumulant expansion of the generating functional. In both cases physical quantities are given in the limit $J \to 0$.

With these definitions, we can begin to evaluate simple things in a scalar quantum field theory. To start we consider a free scalar field ($V(\phi) = 0$). In momentum space the generating functional for a free scalar field becomes

$$Z_o[J] = \int \mathcal{D}\phi \exp\left(i \int_x \frac{1}{2}\phi(k^2 - M_o^2)\phi + J\phi\right) \,. \tag{2.13}$$

Since, in this case, the Lagrangian is quadratic in ϕ, the path integral can be computed exactly, giving the following expressions for the free scalar generating functional and free energy

$$\begin{aligned} Z_o[J] &= \mathcal{N} \exp\left(-\frac{i}{2}\int_k J(k)(k^2 - M_o^2)^{-1} J(k)\right) \\ W_o[J] &= -\frac{\mathcal{N}'}{2}\int_k J(k)(k^2 - M_o^2)^{-1} J(k) \,. \end{aligned} \tag{2.14}$$

With this we can now write down all of the n-point functions of the theory exactly. Since we are primarily interested in propagators in this work, we will only evaluate the two-point function here. After performing some straightforward functional derivatives and taking $J \to 0$ we arrive at the following result

$$G_2^c(k) = \frac{1}{k^2 - M_o^2} = < 0 \,|\, \phi(k)\phi(k) \,|\, 0 > - < 0 \,|\, \phi(k) \,|\, 0 >< 0 \,|\, \phi(k) \,|\, 0 > \; . \tag{2.15}$$

This propagator is characteristic of a free particle propagator in that it has a simple pole at $k^2 = M_o^2$. Adding interactions to the action will change the position of this pole from the bare mass through dynamical mass generation. In order to compute the physical mass of the particle one has to "solve" the path integral including interactions and determine the position of the pole in the propagator.

2.2 Fermionic Field Theories

Fermionic fields can be described with four-component spinor fields, $\psi(x)$. The Lagrangian for a free fermion field is given by

$$\mathcal{L} = \bar{\psi}_i \left(i\gamma^\mu_{ij}\partial_\mu - M_o \right) \psi_j \, , \tag{2.16}$$

where $\bar{\psi} = \psi^\dagger \gamma_0$, and i and j are the spinor indices which run from $1 \to 4$ and are understood to be summed over. In four-dimensional Minkowski space the γ-matrices satisfy the anticommutation relations

$$\begin{aligned} \{\gamma_\mu, \gamma_\nu\} &\equiv \gamma_\mu\gamma_\nu + \gamma_\nu\gamma_\mu \\ &= 2g_{\mu\nu} \, , \end{aligned} \tag{2.17}$$

where $g_{\mu\nu}$ is the Minkowski space metric tensor. For contractions of vectors with γ-matrices we will use the notation $\gamma^\mu p_\mu = \not{p}$ and suppress spinor indices where they are straightforward.

Fermionic fields can be quantized using the path integral formalism in a similar manner to the scalar fields presented in the previous section . The key difference is that fermionic fields are anti-commuting and therefore the path integral has to be performed using anti-commuting fields. This can be done using Grassmann variables [8] which are anti-commuting numbers, instead of ordinary commuting numbers. Practically, this simply means that when reversing the order of fermionic fields we must take into account the minus sign that this induces.

In order to calculate the free fermion propagator we can repeat the calculation performed in the last section and obtain as the result

$$S(k) = \frac{1}{\not{k} - m}\,, \tag{2.18}$$

which when multiplied by $1 = (\not{k} + m)/(\not{k} + m)$ can be expressed as

$$\begin{aligned} S(k) &= \frac{\not{k}}{k^2 - M_o^2} + \frac{m}{k^2 - M_o^2} \\ &\equiv \sigma_v(k)\not{k} + \sigma_s(k)\,, \end{aligned} \tag{2.19}$$

where we have used the fact that $\not{k}\not{k} = k^2$. The second line in equation (2.19) explicitly shows that the fermion propagator has both vector and scalar pieces. Like the free scalar propagator, the free fermion propagator (2.19) has a simple pole located at $k^2 = M_o^2$.

2.3 Gauge Field Theories

Within the standard model of elementary particle physics, there are two basic types of interactions, the electroweak and the strong interaction. The electroweak interaction is the result of the unification of the electromagnetic and weak interactions and the strong interaction is the force that binds quarks into hadrons. These interactions have one common characteristic, they are all gauge field theories which are based on a local gauge[3] symmetry of the Lagrangian. In the next section, we will introduce the concept of local gauge and its consequences, using QED as an example.

2.3.1 QED

The Lagrangian density for a free fermion field

$$\mathcal{L} = i\bar{\psi}\partial\!\!\!/\psi - M_o\bar{\psi}\psi\,, \tag{2.20}$$

is invariant under global gauge transformations in which the fermion field ψ is transformed as

$$\begin{aligned} \psi &\rightarrow e^{i\alpha}\psi \\ \bar{\psi} &\rightarrow e^{-i\alpha}\bar{\psi}\,. \end{aligned} \tag{2.21}$$

Gauge transformations $U(\alpha) = e^{i\alpha}$ belong to the unitary abelian gauge group $U(1)$. The qualifier "abelian" means that the multiplication within the group is commutative, i.e.

$$U(\alpha_1)U(\alpha_2) = U(\alpha_2)U(\alpha_1)\,. \tag{2.22}$$

By Noether's theorem every continuous symmetry of the Lagrangian corresponds to a conserved quantity. For global gauge symmetry the conserved quantity is the local electromagnetic current [8].

We can extend this symmetry by requiring that the Lagrangian density be invariant under *local* gauge transformations since physical quantities can never depend on the local phase of the field, i.e.

$$U = e^{i\alpha(x)}\,, \tag{2.23}$$

[3] The name "gauge" symmetry stems from the invariance of the electromagnetic fields under certain transformations of the vector potential, $A(x) \rightarrow A(x) + \nabla\alpha(x)$, within Maxwellian electromagnetism. It can be translated as "phase" symmetry.

where the phase $\alpha(x)$ can now arbitrarily depend on space and time.

Under such a tranformation the second term in the free fermion Lagrangian density proportional to the free fermion mass is invariant; however, the first term containing the derivative is not:

$$\partial_\mu \psi \to U\psi + iU\psi\partial_\mu \alpha \,. \tag{2.24}$$

In order to enforce local gauge invariance one canonically introduces a vector field A_μ with transformation properties which ensure that the violating term is cancelled exactly. This can be done by replacing the ordinary derivative, ∂_μ, with a covariant derivative defined as

$$D_\mu \equiv \partial_\mu - ieA_\mu \,, \tag{2.25}$$

with the vector field A_μ transforming as

$$A_\mu \to A_\mu + \frac{1}{e}\partial_\mu \alpha \,. \tag{2.26}$$

With this addition the fermionic Lagrangian becomes

$$\mathcal{L} = i\bar{\psi}\partial\!\!\!/\psi - M_o\bar{\psi}\psi + e\bar{\psi}A\!\!\!/\psi \,. \tag{2.27}$$

To summarize, we have found that the requirement of local gauge invariance requires the introduction of a vector field, A_μ, the gauge field. If we wish to regard this new field as a physical field, we must add a kinetic energy for the field. Since this kinetic energy must be invariant under (2.26) we can only introduce this through the gauge invariant field strength tensor

$$F_{\mu\nu} = \partial_\mu A_\nu - \partial_\nu A_\mu \,. \tag{2.28}$$

With the gauge field kinetic energy added, the Lagrangian density becomes

$$\mathcal{L} = i\bar{\psi}\partial\!\!\!/\psi - M_o\bar{\psi}\psi + e\bar{\psi}A\!\!\!/\psi - \frac{1}{4}F_{\mu\nu}F^{\mu\nu} \,. \tag{2.29}$$

For generality we might also consider adding a mass for the gauge field, but a mass term, $1/2M_A^2 A_\mu A^\mu$, violates gauge invariance and is therefore forbidden. The Lagrangian (2.29) is the Lagrangian for pure QED with ψ representing the electron field and A_μ the photon field. With the photon field introduced, the solution for the full electron propagator is more difficult to compute; however, since the coupling constant in QED is small these quanitites can be computed in a perturbative expansion in e. Due to the existence of this perturbative expansion, QED has had unrivaled success as a theory of elementary particles, allowing calculation of atomic energy levels to incredible precision [8]. In the following section, we will discuss quantum chromodynamics (QCD) for which this perturbative expansion fails. It is for this reason that the theory of QCD is still not a successful calculational theory at low energies, even 25 years after its introduction into the standard model of elementary particle physics.

2.3.2 QCD

In the early 1970s particle physicists converged on a theory with local $SU(3)$ gauge invariance as the theory for quark interactions. The theory has been very successful in describing high-energy scattering data; however, little is known about how to describe mesons and hadrons in terms of their underlying quark and gluon degrees of freedom. As mentioned above, the main hurdle to the success of this theory has been the inapplicability of perturbation theory at low energies. At low energies, the QCD coupling constant becomes so large that quarks and gluons can no longer propagate freely, but are instead confined to the nuclear particles which they comprise.

The gauge group for this theory, $SU(3)$, is non-abelian. In general, a local $SU(3)$ gauge transformation can be expressed as an exponential of a contraction of a spacetime dependent phase vector and a vector containing the generators of the group

$$U = e^{igT_a\alpha_a(x)}\,, \tag{2.30}$$

where there are eight 3×3 matrices T_a.[4] These matrices do not commute, but instead obey the following commutation relation

$$[T_a, T_b] = if_{abc}T_c\,, \tag{2.31}$$

where f_{abc} is the completely antisymmetric structure constant for the gauge group. Starting from the free fermion Lagrangian density and requiring local $SU(3)$ gauge invariance leads to the introduction of a gauge field as in QED. Due to the non-abelian nature of $SU(3)$, however, the transformations of the gauge field are more complicated.

Minkowski Space

The QCD Lagrangian density can be written as a sum over three different contributions

$$\mathcal{L} = \mathcal{L}_{qg} + \mathcal{L}_{gh} + \mathcal{L}_{gf}\,. \tag{2.32}$$

The terms above represent the contributions from the quark and gluon fields, Fadeev-Popov ghost fields, and a gauge fixing term, respectively. Fadeev-Popov ghosts are not physical fields, but are mathematical consequences of removing gauge equivalent configurations from the path integral [8]. Ghosts only appear in the internal prts of Feynman diagrams, and, within the axial gauge, can be integrated out completely much like in QED. The three terms can be written in a general covariant gauge with N_f flavors and N_c colors as

$$\mathcal{L}_{qg} \;=\; \bar{q}_i\left(i\not{D}_{ij} - M_o\delta_{ab}\right)q_j - \frac{1}{4}G_a^{\mu\nu}G^a_{\mu\nu}$$

[4]For $SU(N)$ there are N^2-1 generators which are $N\times N$ matrices in the adjoint representation.

$$
\begin{aligned}
\mathcal{L}_{gh} &= \frac{1}{2}\eta_a^* \left(\delta_{ab}\Box^2 + g f_{abc} G_c^\mu \partial_\mu\right)\eta_b \\
\mathcal{L}_{gf} &= \frac{1}{2\alpha}\left(\partial^\mu G_\mu\right)\left(\partial^\nu G_\nu\right) ,
\end{aligned}
\tag{2.33}
$$

where q_i represent the quark fields with $i = 1, 2, 3$, $G_{a\mu}$ the gluon fields with $a = 1 \ldots 8$, and η_a the eight ghost fields. To keep things as general as possible we have introduced a $N_f \times N_f$ bare mass matrix for the quarks M_o, and an arbitrary covariant gauge fixing parameter α. In addition, we make the following definitions

$$
\begin{aligned}
\not{D}_{ij} &= \gamma^\mu D_{ij\mu} = \gamma^\mu(\partial_\mu + igG_\mu)_{ij} \\
G_{\mu\nu} &= \partial_\mu G_\nu - \partial_\nu G_\mu - ig\left[G_\mu, G_\nu\right] \\
G_\mu &= T_a G_{a\mu} ,
\end{aligned}
\tag{2.34}
$$

where the $N_c^2 - 1$ matrices, T_a, are the generators of SU(N_c).

Without the gauge fixing term this Lagrangian density is invariant under local SU(N_c) gauge transformations, $\alpha_a(x)$

$$
\begin{aligned}
q &\rightarrow e^{-igT_a\alpha_a(x)}q \\
G_{a\mu} &\rightarrow G_{a\mu} - f_{abc}\alpha_b(x)G_{c\mu} + \frac{1}{g}\partial_\mu\alpha_a(x) .
\end{aligned}
\tag{2.35}
$$

Two useful properties of the $SU(N)$ generators, T_a, are

$$
\begin{aligned}
\mathrm{Tr}\left[T_a T_b\right] &= \frac{1}{2}\,\delta_{ab} \\
\{T_a, T_b\} &= \frac{1}{3}\delta_{ab} + d_{abc}T_c ,
\end{aligned}
\tag{2.36}
$$

where d_{abc} are the completely symmetric structure constants of SU(N_c). Inserting the commutation relation (2.31) into the definition of $G_{\mu\nu}$ gives a more explicit form for the gluon field strength tensor, which allows one to see the origin of the three- and four-point gluon couplings which make non-abelian gauge theories so troublesome

$$
G_{a\mu\nu} = \partial_\mu G_{a\nu} - \partial_\nu G_{a\mu} + g f_{abc} G_{b\mu} G_{c\nu} . \tag{2.37}
$$

Euclidean Space

For performing numerical calculations it is advantageous to make a transformation to a Euclidean metric

$$
\begin{aligned}
x_o &\to -ix_4 \\
\partial_o &\to i\partial_4 \\
\gamma_o &\to \gamma_4 \\
\gamma_i &\to -i\gamma_i\,,
\end{aligned}
\tag{2.38}
$$

so that contractions of four-vectors simply become the sum of the products of the four components and the gamma matrices satisfy the anticommutation relation

$$
\{\gamma_\mu, \gamma_\nu\} = 2\delta_{\mu\nu}\,, \tag{2.39}
$$

characteristic of the four-dimensional rotation group [9]. Note here that G_μ transforms as a derivative, which can be seen by considering the case when G_μ is a pure gauge field configuration, $G_\mu = 1/g\,\partial_\mu\alpha(x)$.

Performing these substitutions yields the following expression for the Euclidean space generating functional for QCD

$$
Z[K,\bar{K},J] = \mathrm{e}^{-W} \equiv \mathcal{N}\int \mathcal{D}(q,\bar{q},G,\eta,\eta^*)\, e^{-S+\bar{q}K+\bar{K}q+J_\mu G^\mu}\,, \tag{2.40}
$$

with the Lagrangian density now given by the three terms

$$
\begin{aligned}
\mathcal{L}_{qg} &= \bar{q}\,(\not{D}+M_o)\,q + \frac{1}{4}G^a_{\mu\nu}G^a_{\mu\nu} \\
\mathcal{L}_{gh} &= \frac{1}{2}\eta^*_a\left(\delta_{ab}\nabla^2 + gf_{abc}G_{c\mu}\partial_\mu\right)\eta_b \\
\mathcal{L}_{gf} &= \frac{1}{2\alpha}\,(\partial_\mu G_\mu)\,(\partial_\nu G_\nu)\,,
\end{aligned}
\tag{2.41}
$$

in which we have dropped color indices where they are straightforward. It is useful to separate the interacting and non-interacting terms by writing $\mathcal{L} = \mathcal{L}_o + \mathcal{L}_I$. In momentum space the free or non-interacting piece can be written as

$$\begin{aligned}
\mathcal{L}_o &= \bar{q}\left(i\not{p} + M_o\right) q + \frac{1}{2} G_{a\mu}\left(\delta_{\mu\nu} p^2 - \left(1 - \frac{1}{\alpha}\right) p_\mu p_\nu\right) G_{a\nu} - \frac{1}{2}\eta_a^* p^2 \eta_a \\
\mathcal{L}_o &= \bar{q}\left(S_o(p)\right)^{-1} q + \frac{1}{2} G_{a\mu}\left(D_o^{\mu\nu}\right)^{-1} G_{a\nu} - \frac{1}{2}\eta_a^* p^2 \eta_a\,,
\end{aligned} \tag{2.42}$$

which defines the free quark and gluon propagators. Splitting the interaction terms into quark, gluon, and ghost field terms gives

$$\begin{aligned}
\mathcal{L}_{I,q} &= ig\bar{q}\not{G}q \\
\mathcal{L}_{I,g} &= \frac{1}{4} g^2 \left(f_{abc} G_{b\mu} G_{c\nu}\right)\left(f_{ade} G_{d\mu} G_{e\nu}\right) - \frac{i}{2} g f_{abc} G_{b\mu} G_{c\nu}\left(p_\mu G_{a\nu} - p_\nu G_{a\mu}\right) \\
\mathcal{L}_{I,gh} &= \frac{i}{2} g f_{abc} G_{c\mu} \eta_a^* p_\mu \eta_b\,.
\end{aligned} \tag{2.43}$$

We will work in Euclidean space by default in the rest of this thesis.

2.3.3 Analytic Properties of Euclidean Space Fermion and Vector Boson Propagators

Before making non-perturbative calculations of the fermion and vector boson propagators we have to specify the general forms of the propagators and the interpretation of their analytic properties. The free fermion propagator,

$$S_o(p) = \frac{1}{i\not{p} + M_o}\,, \tag{2.44}$$

has a simple pole at $p^2 = -M_o^2$ located on the negative real axis of the complex plane. When the fermion propagator is dressed, the position of this pole will change, and by determining the position of the pole in the fermion propagator we can determine its dressed mass. If the position of this pole has an imaginary part, this indicates that the particle in question is unstable with a lifetime inversely proportional to the imaginary part. In some cases the pole may split into a pair of complex conjugate poles. The presence of complex poles is one possible scenario for the confinement of quarks; however, great care must be taken to ensure that the presence of complex conjugate poles is not due to the analytical and numerical approximations used in the truncation and solution.

In general, the fermion propagator is a 4×4 matrix which can be expanded as

$$S^{-1}(p) = \sum_{n=1}^{\infty} A_n \not{p}^n + B(p^2) + \sum_{n=1}^{\infty} C_n \gamma_5^n + \sum_{n,m=1}^{\infty} D_{nm} \not{p}^n \gamma_5^m \,. \tag{2.45}$$

Using gamma matrix algebra it can be shown that $\not{p}\not{p} = p^2$ and that $\gamma_5\gamma_5 = I$; therefore, we can reduce the above expansion to

$$S^{-1}(p) = A(p^2)\not{p} + B(p^2) + C(p^2)\gamma_5 + D(p^2)\not{p}\gamma_5 \,. \tag{2.46}$$

We can further restrict the terms appearing in the general fermion propagator by requiring that the theory be invariant under parity transformations. Under parity the Dirac fields for the fermion transform as

$$P^\dagger \psi(x) P = \gamma_4 \psi(-\underline{\mathbf{x}}, x_4) \,. \tag{2.47}$$

In general there is an arbitrary phase that also appears, but this phase is irrelevant for this discussion and can therefore be discarded. It is also necessary to know that momentum vectors transform as

$$p \xrightarrow{\mathrm{P}} (-\underline{\mathbf{p}}, p_4) \,. \tag{2.48}$$

When the parity transformed fields and momenta are inserted into the fermionic Lagrangian density the inverse propagator becomes

$$S^{-1}(p) \xrightarrow{\mathrm{P}} \gamma_4 S^{-1}(-\underline{\mathbf{p}}, p_4)\gamma_4 \tag{2.49}$$

using $\{\gamma_\mu, \gamma_\nu\} = 2\delta_{\mu\nu}$, $\{\gamma_5, \gamma_\mu\} = 0$, and the fact that p^2 is unchanged under this transformation, the parity transformed fermion propagator becomes

$$S^{-1}(p) \xrightarrow{\mathrm{P}} A(p^2)\not{p} + B(p^2) - C(p^2)\gamma_5 - D(p^2)\not{p}\gamma_5\,, \tag{2.50}$$

showing that the terms proportional to γ_5 and $\gamma_5\not{p}$ pick up a minus sign and therefore cannot appear in a parity invariant theory such as pure QED or QCD. If we were also including the effects of the weak interaction, these terms would contribute since the weak interaction violates parity; however, this is not our goal here, so we can ignore the parity violating pieces of the electron and quark propagators.

Therefore, the full fermion propagator can always be written in either of the following forms

$$S(p) = \frac{1}{i\not{p}A(p^2) + B(p^2)} = \frac{Z(p^2)}{i\not{p} + M(p^2)} \tag{2.51}$$

or

$$\begin{aligned} S(p) &= \frac{-i\not{p}A(p^2) + B(p^2)}{A^2(p^2)p^2 + B^2(p^2)} \\ &= -i\not{p}\sigma_{\mathrm{v}}(p^2) + \sigma_{\mathrm{s}}(p^2)\,. \end{aligned} \tag{2.52}$$

For the free fermion propagator $A(p^2) = 1$ and $B(p^2) = M_o$ so that there is only one pole located at $s = -M_o^2$. As contributions from interactions modify the functions A and B, the position of this pole will change. As we will demonstrate, the Schwinger-Dyson equations for the fermion propagator can be transformed into a set of coupled integral equations for A and B allowing a non-perturbative determination of the singularity structure of the quark propagator.

The situation for the vector boson propagator is somewhat analogous. For now, we simply write down an expression for the most general photon/gluon propagator which satisfies gauge invariance [8]

$$D^{\mu\nu}(k) = [P_T^{\mu\nu}(k) + \alpha P_L^{\mu\nu}(k)]\,\frac{1}{k^2}\,, \tag{2.53}$$

where

$$P_T^{\mu\nu}(k) = \Delta_T(k)\left[\delta_{\mu\nu} - \frac{k^\mu k^\nu}{k^2}\right]$$

$$P_L^{\mu\nu}(k) = \frac{k^\mu k^\nu}{k^2}\,. \tag{2.54}$$

The transverse coefficient function, $\Delta(k)$, appearing above is defined through this relation and must be caculated.

2.4 Complex Poles and Particle Decay

In order to interpret the physical consequences of an imaginary component of the pole position we have to look at the configuration space propagator. For illustrative purposes we consider here a scalar particle, but the extension to fermions is straightforward.

2.4.1 Minkowski Space

First we perform the calculation in Minkowski space.

$$S(\underline{\mathbf{x}}, t) = \int_k e^{-i\underline{\mathbf{k}}\cdot\underline{\mathbf{x}}+ik_0t}\, S(k)\,. \tag{2.55}$$

Integrating over three-space we can define

$$\begin{aligned}\Delta(t) &\equiv \int d^3x\, S(\underline{\mathbf{x}}, t)\\ &= \int \frac{dk_0}{2\pi} S(k) e^{ik_ot}\,.\end{aligned} \tag{2.56}$$

When the momentum space propagator is taken to be bare, $S^{-1}(k) = k^2 - M_o^2$, the following result is obtained

$$\frac{\Delta(t)}{\Delta(t=0)} = e^{iM_ot}\,. \tag{2.57}$$

If, however, the position of the pole in the propagator is complex

$$S^{-1}(k) = (k - M_o - i\Gamma)(k + M_o + i\Gamma), \tag{2.58}$$

we would find instead that

$$\frac{\Delta(t)}{\Delta(t=0)} = e^{iM_o t} e^{-\Gamma t}. \tag{2.59}$$

Therefore, we see that if the position of the pole is complex, the probability of finding that state $\Delta(t)$ decays exponentially at a rate proportional to the imaginary component.

2.4.2 Euclidean Space

If we were to repeat this calculation in Euclidean space, we would find that when the pole position was real we would obtain an exponential decay of the form

$$\frac{\Delta(t)}{\Delta(t=0)} = e^{-M_o t}. \tag{2.60}$$

This quantity is used in lattice calculations to determine the masses of particles. If the pole position were complex we would obtain

$$\frac{\Delta(t)}{\Delta(t=0)} = e^{-M_o t} e^{-i\Gamma t}, \tag{2.61}$$

indicating that if we have an unstable particle, we should see oscillations in the Euclidean space correlation function as a function of Euclidean time. In the case of lattice simulations of QCD, oscillations of this type could be used as a signal for confinement.

One important point to note is that when propagtors containing complex poles like the ones obtained in this work are used in the solution for the quark bound states it can be shown that these particles have well-defined timelike poles and thus are not confined, i.e. hadronic states are observable physical states.

Chapter 3

Zero Temperature SD Equations

Within the path integral approach, the starting point for the derivation of the Schwinger-Dyson (SD) equations for QCD are the identities [14]

$$\int \mathcal{D}(q,\bar{q},G,\eta,\eta^*)\,\frac{\delta}{\delta q}\,e^{-S+\bar{q}K+\bar{K}q+J_\mu G_\mu}=0 \tag{3.1}$$

$$\int \mathcal{D}(q,\bar{q},G,\eta,\eta^*)\,\frac{\delta}{\delta G_\nu}\,e^{-S+\bar{q}K+\bar{K}q+J_\mu G_\mu}=0 \tag{3.2}$$

$$\int \mathcal{D}(q,\bar{q},G,\eta,\eta^*)\,\frac{\delta}{\delta \eta^*}\,e^{-S+\bar{q}K+\bar{K}q+J_\mu G_\mu}=0\,. \tag{3.3}$$

These identities will allow us to derive self-consistent relations for the quark, gluon, and ghost n-point functions, respectively. Since we assume that the fields go to zero at infinity, these identities are simply the fundamental rule of calculus in functional form, i.e. the integral of a derivative returns the function evaluated at the end points. In the following section, we will complete the derivation of the SD equation for the two-point function or propagator in the quark sector.

3.1 SD Equation for the Quark Propagator

Evaluating the left hand side of (3.1) gives the following functional differential equation

$$\left[S_o^{-1}(p)\frac{\delta}{\delta K}+ig\gamma_\mu\frac{\delta}{\delta J_\mu(p)}\frac{\delta}{\delta K}\right]Z=\bar{K}(p)Z\,. \tag{3.4}$$

Taking the functional derivative with respect to $\bar{K}(q)$ on both sides gives

$$\left[S_o^{-1}(p)\frac{\delta^2}{\delta\bar{K}(p)\delta K(q)}+ig\gamma_\mu\frac{\delta}{\delta J_\mu(p)}\frac{\delta^2}{\delta\bar{K}(p)\delta K(q)}\right]Z=\delta(q-p)Z+\bar{K}(p)\frac{\delta Z}{\delta\bar{K}(q)}\,. \tag{3.5}$$

The quark two-point function, $S(p,q)$, is given by

$$S(p,q) = Z^{-1}\frac{\delta^2 Z}{\delta\bar{K}(p)\delta K(q)} \tag{3.6}$$

so that, when rewritten in terms of $S(p,q)$, (3.5) becomes

$$\left[S_o^{-1}(p) + ig\gamma_\mu \frac{\delta}{\delta J_\mu(p)}\right] ZS(p,q) = \delta(q-p)Z + \bar{K}(p)\frac{\delta Z}{\delta\bar{K}(q)}\,. \tag{3.7}$$

Expanding the functional derivative with respect to $J_\mu(p)$ acting on $ZS(p,q)$ yields

$$\left[ZS_o^{-1}(p) + ig\gamma_\mu \frac{\delta Z}{\delta J_\mu(p)} + igZ\gamma_\mu \frac{\delta}{\delta J_\mu(p)}\right] S(p) = \delta(q-p)Z + \bar{K}(p)\frac{\delta Z}{\delta\bar{K}(q)}\,. \tag{3.8}$$

Dividing both sides by a factor of Z gives

$$\left[S_o^{-1}(p) + ig\gamma_\mu Z^{-1}\frac{\delta Z}{\delta J_\mu(p)} + ig\gamma_\mu \frac{\delta}{\delta J_\mu(p)}\right] S(p,q) = \delta(q-p) + \bar{K}(p)Z^{-1}\frac{\delta Z}{\delta\bar{K}(q)}\,. \tag{3.9}$$

The middle term appearing on the left hand side, $ig\gamma_\mu Z^{-1}\delta Z/\delta J_\mu$, is nothing more than the expectation value of the gluon field with source J. Since this expectation value vanishes as $J_\mu \to 0$ we can drop this term from the left side. In addition, we also take the limit that the classical quark source $\bar{K} \to 0$, leaving

$$\left[S_o^{-1}(p) + ig\gamma_\mu \frac{\delta}{\delta J_\mu(p)}\right] S(p,q) = \delta(p-q)\,. \tag{3.10}$$

3.1.1 Functional Definition of the Quark-Gluon Vertex

The second term on the left hand side of (3.10) can be rewritten in terms of the quark-gluon vertex function which is shown in Figure 3.1. Firstly, we use the chain rule for functional derivatives

$$\frac{\delta S(p,q)}{\delta J_\mu(p)} = \int_k \frac{\delta\!<\!G_\nu(k)\!>}{\delta J_\mu(p)}\frac{\delta S(p,q)}{\delta\!<\!G_\nu(k)\!>}\,, \tag{3.11}$$

where $\int_k = \int d^4k/(2\pi)^4$. To proceed further we introduce the Legendre transform of the generating functional for connected graphs with

$$\Gamma[Q,\bar{Q},\tilde{G}] \equiv W[J,K,\bar{K}] - \int_p \left(\bar{Q}(p)K(p) + \bar{K}(p)Q(p) + \tilde{G}_\mu(p)J_\mu(p)\right) , \tag{3.12}$$

from which the following relations can be derived

$$\begin{aligned}
\frac{\delta W}{\delta \bar{K}} &= Q = \langle q \rangle \\
\frac{\delta \Gamma}{\delta Q} &= -\bar{K} \\
\frac{\delta W}{\delta J_\mu} &= \tilde{G}_\mu = \langle G_\mu \rangle \\
\frac{\delta \Gamma}{\delta \tilde{G}_\mu} &= -J_\mu \\
\frac{\delta^2 W}{\delta \bar{K}(p)\delta K(q)} &= -\left(\frac{\delta^2 \Gamma}{\delta Q(p)\delta \bar{Q}(q)}\right)^{-1} \equiv -\Gamma_2^{-1}(p,q)\,.
\end{aligned} \tag{3.13}$$

The final relation above can be written in a more concise form as $S(p,q) = -\Gamma_2^{-1}(p,q)$. Inserting this into (3.11) gives

$$\frac{\delta S(p,q)}{\delta J_\mu(p)} = -\int_k \frac{\delta \tilde{G}_\nu(k)}{\delta J_\mu(p)} \frac{\delta \Gamma_2^{-1}(p,q)}{\delta \tilde{G}_\nu(k)}\,. \tag{3.14}$$

The functional derivative of an inverse can be determined using the identity

$$\frac{\delta}{\delta \tilde{G}}\left(\Gamma_2 \Gamma_2^{-1}\right) = 0\,, \tag{3.15}$$

which upon expansion gives

$$\frac{\delta \Gamma_2^{-1}(p,q)}{\delta \tilde{G}_\nu(k)} = -\int_{k_1,k_2} S(p,k_1)\frac{\delta \Gamma_2(k_1,k_2)}{\delta \tilde{G}_\nu(k)} S(k_2,q)\,. \tag{3.16}$$

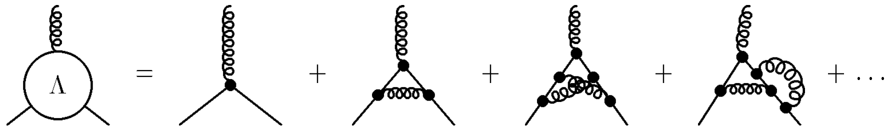

Figure 3.1: Diagrammatic expansion of the full vertex function showing a few of the lowest order diagrams which contribute.

Substituting this into (3.14) and using the fact that $\delta\tilde{G}_\nu(k)/\delta J_\mu(p) = D_{\mu\nu}(k,p)$, where $D_{\mu\nu}$ is the full gluon propagator, gives

$$\frac{\delta S(p,q)}{\delta J_\mu(p)} = \int_{k,k_1,k_2} S(k_1) D_{\mu\nu}(k,p) \frac{\delta\Gamma_2(k_1,k_2)}{\delta\tilde{G}_\nu(k)} S(k_2,q)\,. \tag{3.17}$$

At this point we can introduce the functional definition of the vertex function which is

$$ig\Lambda_\nu(p,q;k) = \frac{\delta\Gamma_2(p,q)}{\delta\tilde{G}_\nu(k)} = \frac{\delta}{\delta\tilde{G}_\nu(k)} \frac{\delta^2\Gamma}{\delta Q(p)\delta Q(q)}\,, \tag{3.18}$$

giving

$$ig\frac{\delta S(p,q)}{\delta J_\mu(p)} = -g^2 \int_{k,k_1,k_2} S(k_1) D_{\mu\nu}(k,p) \Lambda_\nu(k_1,k_2;k) S(k_2,q)\,. \tag{3.19}$$

In order to simplify the notation we define the quark self-energy function

$$\Sigma(q) \equiv g^2 \int_{k_1,k_2} \gamma_\mu S(k_1) D_{\mu\nu}(k_1,k_2) \Lambda_\nu(k_1,q;k_2)\,, \tag{3.20}$$

so that in the end we can rewrite (3.10) as

$$S_o^{-1}(p) S(p,q) - \int_k \Sigma(p,k) S(k,q) = \delta(p-q)\,. \tag{3.21}$$

After using momentum conservation and some minor rearrangement, the quark SD equation becomes

$$S(p) = S_o(p) + S_o(p)\Sigma(p)S(p)\,, \tag{3.22}$$

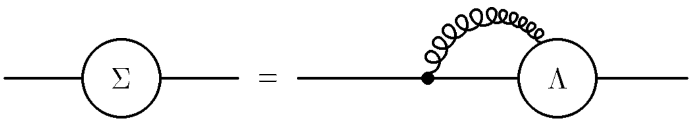

Figure 3.2: Diagrammatic representation of the Schwinger-Dyson equation for the quark self-energy

and the equation for the self-energy (3.20) with the color structure shown becomes

$$\Sigma(p)\mathbf{1} = g^2 \int_k (\gamma_\mu T^a)\,(S(k)\mathbf{1})\,(D_{\mu\nu}(p-k)\delta_{ab}\mathbf{1})\left(\Lambda_\nu(k,p;p-k)T^b\right)\,, \tag{3.23}$$

where $\mathbf{1}$ is a $N_c \times N_c$ unit color matrix. Using the fact that $\sum_a T^a T^a = \mathbf{1}(N_c^2-1)/2N_c$ we can factor out the identity matrix leaving the QCD Schwinger-Dyson equation[1]

$$\Sigma(p) = S^{-1}(p) - S_o^{-1}(p) = g^2\left(\frac{N_c^2-1}{2N_c}\right)\int_k \gamma_\mu S(k) D_{\mu\nu}(p-k)\Lambda_\nu(k,p;p-k)\,. \tag{3.24}$$

This equation is represented digrammatically in Figure 3.2.

3.1.2 Rainbow Approximation

There are two unknowns in the quark self-energy equation (3.24), the gluon propagator $D_{\mu\nu}$, and the quark-gluon vertex function Λ_ν. As a first approximation we set the vertex function equal to the bare vertex $\Lambda_\mu \to \gamma_\nu$. This approximation is known as the rainbow approximation because, when applied to the fermion self-energy, the graphs generated have nested gluon propagators which give the appearance of a rainbow (see Figure 3.3). The SD equation given this approximation becomes

$$S^{-1}(p) - S_o^{-1}(p) = \bar{g}^2 \int_k \gamma_\mu S(k) D_{\mu\nu}(p-k)\gamma_\nu\,, \tag{3.25}$$

[1] If we take $g^2(N_c^2-1)/(2N_c) \to e^2$ this equation is the same as the QED Schwinger-Dyson equation, therefore solutions to this equation offer insight into both QED and QCD, depending on the gauge propagator used.

where we have defined $\bar{g}^2 \equiv g^2(N_c^2-1)/2N_c$. Inserting the general forms of the gluon propagator (2.53) and the quark propagator (2.51) we can project out equations for the quantities $A(p)$ and $B(p)$ appearing in the general quark propagator. This is done by multiplying by $\not{p}$ and an identity matrix, respectively, and taking a trace yielding the following coupled integral equations

$$\begin{aligned} A(p^2) &= Z_2 + \frac{\bar{g}^2}{p^2}\int_k \left(\frac{A(k^2)}{A^2(k^2)k^2+B^2(k^2)}\right)\frac{1}{q^2}\left[\Delta_T(q)\left(p\cdot k + \frac{2(p\cdot q)(k\cdot q)}{q^2}\right)\right. \\ &\qquad \left. +\alpha\left(p\cdot k - \frac{2(p\cdot q)(k\cdot q)}{q^2}\right)\right] \\ B(p^2) &= M_o + \bar{g}^2\int_k \left(\frac{B(k^2)}{A^2(k^2)k^2+B^2(k^2)}\right)\frac{1}{q^2}\left[3\Delta_T(q)+\alpha\Delta_L(q)\right], \end{aligned} \tag{3.26}$$

where Z_2 is the bare field renormalization constant and $q = p - k$. In the Landau gauge, $\alpha = 0$, these equations reduce to

$$\begin{aligned} A(p^2) &= Z_2 + \frac{\bar{g}^2}{p^2}\int_k \left(\frac{A(k^2)}{A^2(k^2)k^2+B^2(k^2)}\right)\frac{1}{q^2}\left[\Delta_T(q)\left(p\cdot k + \frac{2(p\cdot q)(k\cdot q)}{q^2}\right)\right] \\ B(p^2) &= M_o + 3\bar{g}^2\int_k \left(\frac{B(k^2)}{A^2(k^2)k^2+B^2(k^2)}\right)\frac{\Delta_T(q)}{q^2}. \end{aligned} \tag{3.27}$$

Transforming to four-dimensional spherical coordinates, choosing p along the p_4 axis, and performing the trivial angular integrations gives

$$\begin{aligned} A(p^2) &= Z_2 + \frac{\bar{g}^2}{8\pi^3 p^2}\int_0^\infty k^2dk^2\left(\frac{A(k^2)}{A^2(k^2)k^2+B^2(k^2)}\right)\int_0^\pi \sin^2\beta d\beta \\ &\left(\frac{\Delta_T(p^2+k^2-2pk\cos\beta)}{p^2+k^2-2pk\cos\beta}\right)\left(pk\cos\beta + \frac{2\left[(p^2+k^2)(pk\cos\beta)-p^2k^2-(pk\cos\beta)^2\right]}{p^2+k^2-2pk\cos\beta}\right) \end{aligned} \tag{3.28}$$

$$\begin{aligned} B(p^2) &= M_o + \frac{3\bar{g}^2}{8\pi^3}\int_0^\infty k^2dk^2\left(\frac{B(k^2)}{A^2(k^2)k^2+B^2(k^2)}\right) \\ &\qquad \int_0^\pi \sin^2\beta d\beta\left(\frac{\Delta_T(p^2+k^2-2pk\cos\beta)}{p^2+k^2-2pk\cos\beta}\right). \end{aligned} \tag{3.29}$$

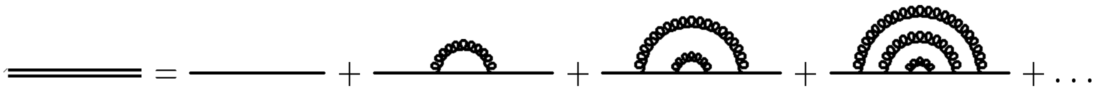

Figure 3.3: Diagrams contributing to the quark propagator within the quenched rainbow approximation.

3.1.3 Quenched Rainbow Approximation

In order to continue, we must specify the form of the gluon propagator. The lowest level approximation that can be made is to set the gluon propagator equal to its bare form, with $\Delta_T(q) = 1$ [15]. This approximation is called the quenched approximation because it ignores the dressing of the gluon propagator due to quark loops, i.e. vacuum production of quark pairs is quenched. In addition, this approximation also ignores gluon self-interactions which are generated by the nonlinear interaction terms in the QCD Lagrangian. Given this approximation, equations (3.28) and (3.29) become

$$A(x) = Z_2 + \frac{\bar{g}^2}{8\pi^2 p^2} \int_0^\infty y dy \left(\frac{A(y)}{A^2(y)y + B^2(y)} \right) K_A(x,y) \tag{3.30}$$

$$B(x) = M_o + \frac{3\bar{g}^2}{8\pi^2} \int_0^\infty y dy \left(\frac{B(y)}{A^2(y)y + B^2(y)} \right) K_B(x,y)\,, \tag{3.31}$$

with $x \equiv p^2$ and $y \equiv k^2$ and the integration kernels K_A and K_B given by

$$\begin{aligned} K_A(p^2,k^2) &= \frac{1}{\pi} \int_0^\pi \left(\frac{\sin^2\beta d\beta}{p^2 + k^2 - 2pk\cos\beta} \right) \\ &\quad \times \left(pk\cos\beta + \frac{2\left[(p^2+k^2)pk\cos\beta - p^2k^2 - (pk\cos\beta)^2\right]}{p^2+k^2-2pk\cos\beta} \right) \end{aligned} \tag{3.32}$$

$$\begin{aligned} &= I_1^1(p^2,k^2) + 2(p^2+k^2)I_2^1(p^2,k^2) \\ &\quad -2p^2k^2 I_2^0(p^2,k^2) - 2I_2^2(p^2,k^2) \end{aligned} \tag{3.33}$$

$$K_B(p^2,k^2) \;=\; \frac{1}{\pi}\int_0^{\pi}\left(\frac{\sin^2\beta d\beta}{p^2+k^2-2pk\cos\beta}\right) = I_1^0(p^2,k^2)\,, \tag{3.34}$$

where the integration formulas from Appendix B have beeen used. Applying the relations from Appendix B it can be shown that K_A vanishes for all p^2 and k^2, so that within the quenched bare vertex approximation the vector coefficient function $A(x) = Z_2$.

Solution on the positive real axis

For positive real x and y (p^2 and k^2) K_B can be simplified to

$$K_B(x,y) = \frac{1}{2\max(x,y)}\,, \tag{3.35}$$

so that the integral equation for $B(x)$ becomes

$$B(x) = M_o + \frac{3\bar{g}^2}{16\pi^2}\int_{\Lambda_{IR}^2}^{\Lambda_{UV}^2}\frac{y\,dy}{\max(x,y)}\left(\frac{B(y)}{(Z_2)^2y+B^2(y)}\right)\,, \tag{3.36}$$

where we have introduced infrared, Λ_{IR}, and ultraviolet, Λ_{UV}, cutoffs on the integration for numerical solution. This equation for $B(x)$ can be solved iteratively by choosing a seed function for $B(y)$ and iterating until the solution converges.

In Figure 3.4 we have plotted the dynamical mass function $B(p)$ in the zero bare mass limit (M_o=0) for real positive p obtained through iterative solution of the integral equation.

Analytical [16, 17, 18] solutions to this equation show that within the quenched rainbow approximation with zero bare mass, $M_o = 0$, there exists a critical coupling $\lambda_c = 3g_c^2/16\pi^2 = 1/4$. Below this coupling the trivial $B = 0$ solution is obtained, preserving chiral symmetry, while above it, a non-trivial solution for B is obtained, signaling dynamical chiral symmetry breaking.

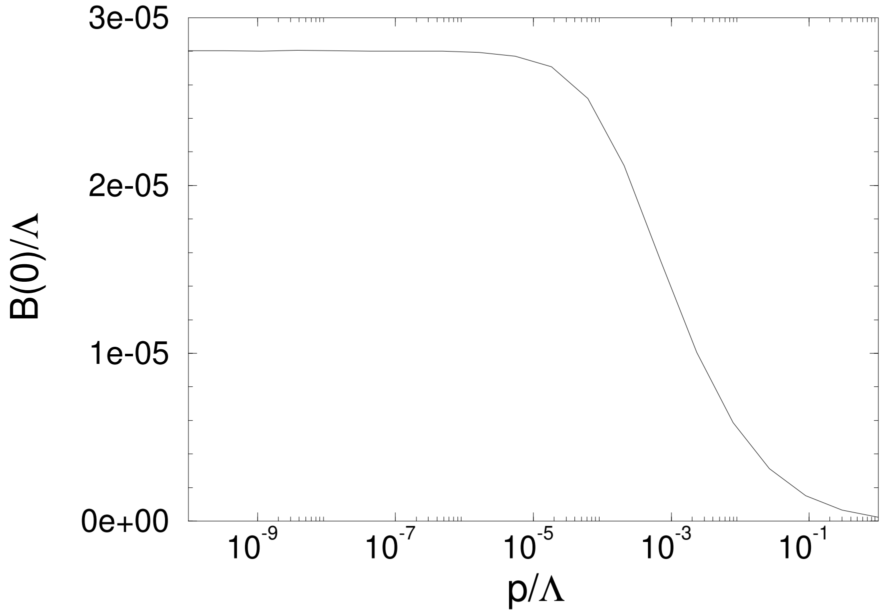

Figure 3.4: Mass function $B(p)/\Lambda$ vs. p/Λ within the quenched bare vertex approximation. ($M_o = 0$; $\Lambda = 10^5$; $\bar{g}^2 = 15 > g_c^2$; $\alpha = 0$).

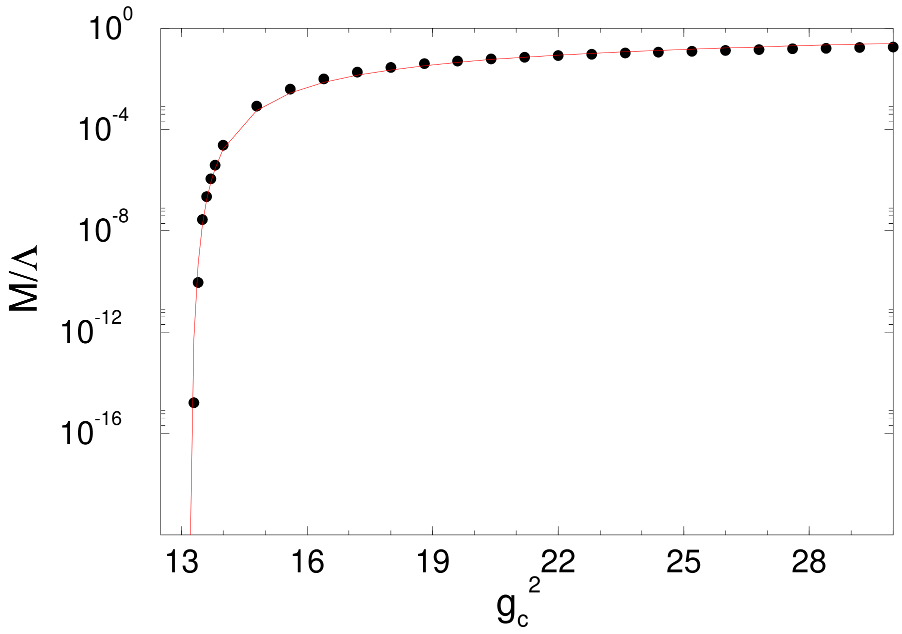

Figure 3.5: Mass $B(0)$ vs. $\bar{g}^2$ within the quenched bare vertex approximation. Data points ($\bullet$) are the results of an iterative solution of (3.36) and the solid line ($-$) is the curve fit to extract the critical coupling g_c^2 =13.15 $\pm$ 0.04. ($M_o = 0$; $\Lambda^2 = 10^5$; $\bar{g}^2 = 15 > g_c^2$; $\alpha = 0$).

To check the numerics we have computed the dynamical mass close to the critical coupling and compared that with the form predicted by the analytic work of Miransky [16, 17, 18], who found that in the Landau gauge as $g^2 \to g^2_{c+}$,

$$\frac{M}{\Lambda} = \exp\left[\frac{-\pi}{\sqrt{g^2/g_c^2 - 1}} + \ln 4\right] . \tag{3.37}$$

Therefore, we made a fit of the data shown in Figure 3.5 to the form

$$\frac{M}{\Lambda} = \exp\left[\frac{-A}{\sqrt{g^2/C - 1}} + B\right] , \tag{3.38}$$

which gave us the following results

$$A = 3.11,\ B = 1.47,\ C = 13.15\,, \tag{3.39}$$

which indicate agreement with theoretical predictions for the zero temperature critical coupling. This result gives us confidence in the numerical method and provides a zero temperature result that we can check the limits of the finite temperature codes against.

Solution in the entire complex plane

Since the integration in (3.36) is along the positive real axis, the argument of $B(y)$ is always real. Therefore a solution along the positive real axis allows us to map out the solution in the entire complex plane. If the kernel K_B had singularities for complex arguments, then we would have to deal with this complication, but since in this case it does not, we can plug in any complex x and the solution of B along the positive real axis, achieved through iterative solution, and solve for $B(x)$.

Equation (3.36) for complex argument $x = x_R + x_I$ and scalar coefficient function

$B(x) = B_R(x) + B_I(x)$ can be written as

$$B_R(x) = M_o + \frac{3\bar{g}^2}{32\pi^2(x_R^2 + x_I^2)} \int_{\Lambda_{IR}^2}^{\Lambda_{UV}^2} dy \left(\frac{B(y)\left[x_R(x_R + y - \mathcal{U}) + x_I(\mathcal{V} - x_I)\right]}{(Z_2)^2 y + B^2(y)} \right)$$

$$B_I(x) = -\frac{3\bar{g}^2}{32\pi^2(x_R^2 + x_I^2)} \int_{\Lambda_{IR}^2}^{\Lambda_{UV}^2} dy \left(\frac{B(y)\left[x_I(x_R + y - \mathcal{U}) + x_R(\mathcal{V} - x_I)\right]}{(Z_2)^2 y + B^2(y)} \right), \tag{3.40}$$

where $\mathcal{U} = \mathrm{Re}\left[\sqrt{(x_R + ix_I - y)^2}\right]$ and $\mathcal{V} = \mathrm{Im}\left[\sqrt{(x_R + ix_I - y)^2}\right]$.

Once $B(y)$ is obtained on the real-axis, these equations specify the real and imaginary parts of B everywhere. With this, a determination of the pole structure of the quark propagator within this approximation can be made by finding the zeros of $x + B^2(x)$. These zeros indicate the position of the poles in the propagator. Within this approximation we find that the only pole present is on the negative real axis, predicting that there should be a physically observable particle, the electron. For more information on the singularity structure of the electron propagator see reference [19].

3.1.4 Modeling Confinement

To truly solve the Schwinger-Dyson equations for the quark propagator we must also solve the coupled equations for the gluon propagator and all of the higher n-point functions. Short of this we can propose analytic forms for the gluon propagator and study the resulting quark propagators. At zero-temperature there has been much work along these lines [11, 20, 21, 15, 22, 23, 24, 25].

Since perturbative renormalization group studies are not reliable below $p^2 \sim 1$ GeV^2 the low energy running of the coupling constant must be determined in a different manner. Results from non-perturbative lattice and analytic studies suggest that the gluon propagator is significantly enhanced for small spacelike-k^2 [4, 5, 6]. Traditional potential analysis suggests that the gluon propagator behaves like $1/q^4$

for small q and studies have been performed with this assumption or regularizations of this form [26, 6, 27, 28]. When modeling confinement we will instead use a parameterization which is a regularized version of $1/q^4$ plus a perturbative piece

$$\frac{\bar{g}^2 \Delta_T(q)}{q^2} = 4\pi^2 \left[4\pi^2 m_t^2 \delta^4(q) + \frac{d}{q^2} \right] , \tag{3.41}$$

where $d = 12/(33-2N_f)$. The number of flavors chosen should be appropriate for the energies considered and can even be made momentum dependent to model the effects of particle thresholds. This parameterization contains two pieces: a delta function which models long-range effects like confinement through an integrable infrared singularity, and a perturbative piece which ensures that the large-q^2 limit is correct up to $\ln[q^2]$ corrections [29]. The $\ln[q^2]$ were included in the studies of [30, 27, 28], but we ignore them here for simplicity, since it is the confining delta function which we are primarily interested in. The parameter m_t can be interpreted as the energy scale which marks the transition between the perturbative and non-perturbative regimes. In a calculation using a similar parameterization, C.D. Roberts and M.R. Frank [11] have fixed this quantity by fitting to a set of pion observables (f_π, N_π, scattering lengths, etc.) and find $m_t = 0.69\,\mathrm{GeV}$. Once this parameter is fixed, the resulting quark propagator can be used to make a host of predictions about meson data.

In the next section we will review the solution [21, 20] obtained with only the first piece of (3.41).

Delta function singularity

Ignoring the perturbative piece of our model gluon propagator (3.41) amounts to neglecting asymptotic freedom; however, if we are interested in studying how confinement may be realized, the delta function alone provides an interesting analytically solvable model [21, 20]. We consider here the choice

$$\bar{g}^2 \Delta_T(q) = m_t^2 \, q^2 \, (2\pi)^4 \, \delta^4(q) \,. \tag{3.42}$$

When inserted into the rainbow SD equation (3.27), the integral equations for A and B reduce to a set of non-linear algebraic equations

$$A(x) = Z_2 + D \left(\frac{A(x)}{A^2(x)x + B^2(x)} \right) \tag{3.43}$$

$$B(x) = M_o + 2D \left(\frac{B(x)}{A^2(x)x + B^2(x)} \right) , \tag{3.44}$$

with $D = 3/2 \, m_t^2$. When $M_o = 0$, this system of equations has two solutions. The first, trivial, solution has $B = 0$, and the second has the following form ($Z \equiv 1/A$, $M \equiv B/A$)

$$Z(x) = \frac{1}{2} \tag{3.45}$$

$$M(x) = \sqrt{\frac{1}{2}D - x} \qquad ; \; x \leq \frac{1}{2}D \tag{3.46}$$

$$Z(x) = \frac{x}{2D} \left(\sqrt{1 + \frac{4D}{x}} - 1 \right) \tag{3.47}$$

$$M(x) = \pm i \sqrt{x - \frac{1}{2}D} \qquad ; \; x > \frac{1}{2}D \,, \tag{3.48}$$

where the $\pm$ on the last term indicates the ambiguity introduced by the square root cut.

The fact that there are no singularities on the real-p^2 axis means that the quark within this model can never be on mass shell and can therefore never be an asymptotic particle state. The quark within this model does have a dynamical mass function however, which affects the dynamics of hadronic bound states. Note that there is no critical coupling for dynamical mass generation or confinement within this model.

Delta function plus perturbative piece

When the full model gluon propagator (3.41) is used, an analytic solution is no longer possible and numerical techniques must be used. The equations for the scalar and vector coefficient functions (3.29) become

$$
\begin{aligned}
A(p^2) &= Z_2 + \frac{3m_t^2}{2}\left(\frac{A(p^2)}{A^2(p^2)p^2 + B^2(p^2)}\right) + \\
&\qquad \frac{\bar{g}^2}{4\pi^2 p^2}\int_0^\infty k^3 dk \left(\frac{A(k^2)}{A^2(k^2)k^2 + B^2(k^2)}\right) K_A(p,k) \\
B(p^2) &= M_o + 3m_t^2\left(\frac{B(p^2)}{A^2(p^2)p^2 + B^2(p^2)}\right) + \\
&\qquad \frac{3\bar{g}^2}{4\pi^2}\int_0^\infty k^3 dk \left(\frac{B(k^2)}{A^2(k^2)k^2 + B^2(k^2)}\right) K_B(p,k)\,, \qquad (3.49)
\end{aligned}
$$

where K_A and K_B are the kernels from the quenched rainbow approximation (Section 3.1.3). The iterative solution to these coupled equations is convergent for positive p^2 with no critical coupling for dynamical mass generation. A plot of B for positive p^2 is shown in Figure 3.6.

In orer to determine the presence or absence of poles we must affect a solution for negative p^2. For negative p^2 the system of equations as written in (3.49) is not convergent and some manipulation is necessary in order to obtain a convergent system of equations. To see how to proceed we examine the equation

$$
B_{i+1}(p^2) = 3m_t^2\left(\frac{B_i(p^2)}{p^2 + B_i^2(p^2)}\right)\,. \qquad (3.50)
$$

This equation has two fixed points

$$
\begin{aligned}
B_1^*(p^2) &= 0 \\
B_2^*(p^2) &= \sqrt{3m_t^2 - p^2}\,. \qquad (3.51)
\end{aligned}
$$

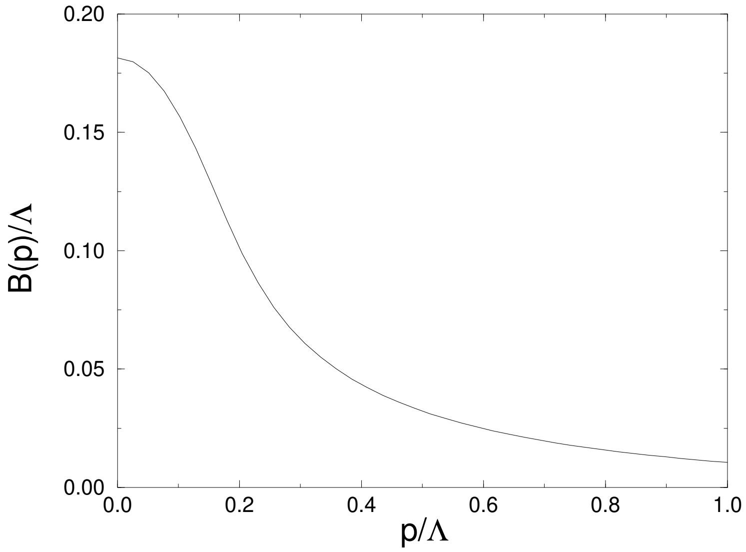

Figure 3.6: p dependence of the scalar coefficient function obtained with a confining gluon propagator ($M_o = 0$, $\Lambda = 10^5$; $\bar{g}^2 = 20 > g_c^2$).

Analysis of the stability of these fixed points shows that for $p^2 > 0$ the non-trivial solution, B_2^*, is a stable fixed point, while for $p^2 < 0$ this solution is unstable. Therefore, in order to solve (3.50) for $p^2 < 0$ we will have to transform this into a stable fixed point. One way to do this is to iterate using the inverse of the function appearing on the right hand side of (3.50). In its most general form (3.50) can be written as

$$\underline{\mathbf{x}} = f(\underline{\mathbf{x}})\,, \tag{3.52}$$

which, if we apply the the function $f^{-1}()$ to both sides, can be rewritten as

$$\underline{\mathbf{x}} = f^{-1}(\underline{\mathbf{x}})\,. \tag{3.53}$$

The benefit of using the inverse instead of the function itself is that the previously unstable fixed point will now be stable. For (3.50) performing this transformation yields

$$B_{i+1}(p^2) = \frac{3m_t^2}{2B_i} \pm \sqrt{\left(\frac{3m_t^2}{2B_i}\right)^2 - p^2}\,. \tag{3.54}$$

Choosing + above yields an equation which is convergent to the non-trivial fixed point with positive B, while choosing $-$ above yields an equation which is convergent to the solution with $B < 0$. Therefore, for negative p^2 we can still solve (3.50) iteratively, we just use the inverse of the function.

When the perturbative pieces are added it is still possible to transform the equations into an iteratively convergent form. Consider the equation for the coefficient function B in (3.49) with $A = 1$ for simplicity.

$$
\begin{aligned}
B(p^2) &= M_o + 3m_t^2 \left(\frac{B(p^2)}{p^2 + B^2(p^2)} \right) + \\
&\qquad \frac{3\bar{g}^2}{4\pi^2} \int_0^\infty k^3 dk \left(\frac{B(k^2)}{k^2 + B^2(k^2)} \right) K_B(p,k) \,. \qquad (3.55)
\end{aligned}
$$

This equation can be written in general terms as

$$
\underline{\mathbf{x}} = f(\underline{\mathbf{x}}) + \mathbf{A} \cdot g(\underline{\mathbf{x}}) \,, \tag{3.56}
$$

where $\mathbf{A}$ is a matrix which represents the integration, or it can be rewritten as

$$
f^{-1}(f(\underline{\mathbf{x}})) = f(\underline{\mathbf{x}}) + \mathbf{A} \cdot g(f^{-1}(f(\underline{\mathbf{x}}))) \,. \tag{3.57}
$$

Defining $\underline{\mathbf{y}} = f(\underline{\mathbf{x}})$ we can get an equation for $\underline{\mathbf{y}}$

$$
f^{-1}(\underline{\mathbf{y}}) = \underline{\mathbf{y}} + \mathbf{A} \cdot g(f^{-1}(\underline{\mathbf{y}})) \,, \tag{3.58}
$$

which upon rearrangement yields

$$
\underline{\mathbf{y}} = f^{-1}(\underline{\mathbf{y}}) - \mathbf{A} \cdot g(f^{-1}(\underline{\mathbf{y}})) \,. \tag{3.59}
$$

In this way we can solve for $\underline{\mathbf{y}}$ and in the end apply $f^{-1}()$ to obtain $\underline{\mathbf{x}}$. This method can be generalized to the full set of equations (3.49) and is the method employed in the solution of these equations for negative p^2. Note, however, that this method works in this case because the $\underline{\mathbf{x}}$ dependence of $\mathbf{A}$ is simple. In general, other tricks

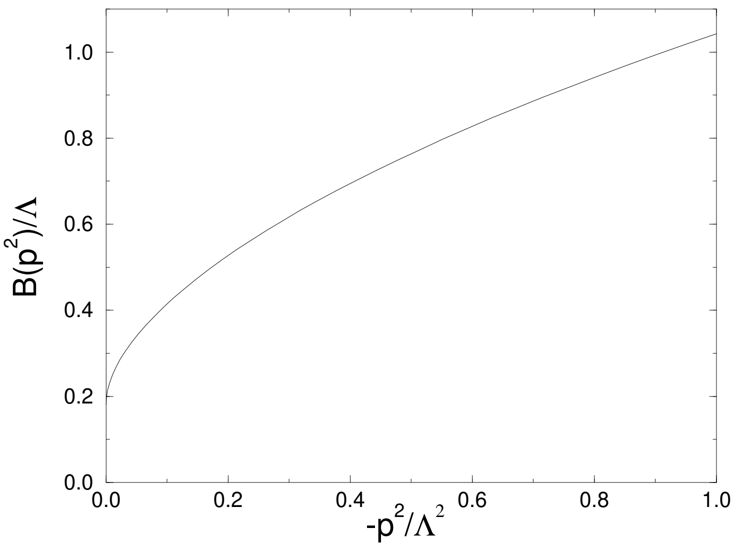

Figure 3.7: p^2 dependence of the scalar coefficient function obtained with a confining gluon propagator for negative (timelike) p^2 ($M_o = 0$, $\Lambda = 10^5$; $\bar{g}^2 = 20 > g_c^2$).

may be necessary. In Figure 3.7 we have plotted $B(p^2)$ for negative p^2. For all m_t^2 and $\bar{g}^2$ this solution gives no pole on the negative p^2 axis and hence is a good candidate for a confining model.

3.1.5 Improving upon the rainbow approximation

One of the major problems with the rainbow approximation is that the bare vertex used does not satisfy gauge invariance as manifest through the Slavnov-Taylor (ST) identities [29, 8, 14, 31, 32]

$$\begin{aligned}(p-q)_\nu \Lambda_\nu(p,q;p-q)[1+b(q^2)] &= \\ &[gT^a - B^a(p,q;p-q)]S^{-1}(p) - S^{-1}(q)[gT^a - B^a(p,q;p-q)]\,, \quad (3.60)\end{aligned}$$

where $a = 1 \ldots N_c^2 - 1$ is the color index, $b(k^2)$ is the ghost self-energy, and B^a is the ghost-quark scattering kernel. The ghost self-energy and ghost-quark scattering kernel are shown diagrammatically in Figure 3.8.

This identity ensures that the vertex function, Λ_ν, and the fermion propagator,

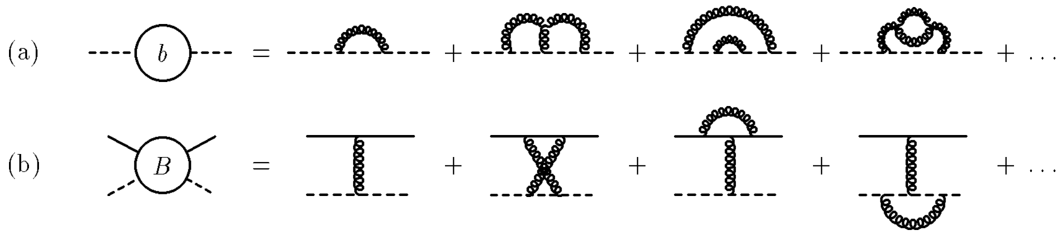

Figure 3.8: (a) Low order diagrams contributing to the ghost self-energy. (b) Low order diagrams contributing to the ghost-quark scattering kernel.

S, are related in such a way that physical quantities do not depend on the choice of gauge. By dressing the propagator and vertex functions in this self-consistent manner, a larger class of diagrams is included in the Schwinger-Dyson summation. Unfortunately, it is difficult to tell exactly which diagrams are included. In future work we will address this question in greater depth. For now, however, it is sufficient to know that the bare vertex violates gauge invariance and that a vertex that is consistent with gauge invariance will provide a systematic improvement. If the results were to depend on the choice of gauge then this would imply that one gauge is preferred over another since at some point we have to match experiment. Since one of the founding tenets of gauge field theory is that physical quantities can not depend on the choice of gauge we must do everything we can to remove gauge dependence of our results.

With the ghost particles included, this identity is difficult to implement; however, for QED, or QCD in which the ghost fields are ignored, this identity reduces to the abelian version of the ST identities, the Ward-Takahashi (WT) identity

$$i(p-q)_\nu \Lambda_\nu(p,q;p-q) = S^{-1}(p) - S^{-1}(q)\,. \tag{3.61}$$

In the limit of vanishing momentum transfer this identity reduces to the simpler

Ward identity

$$i\Lambda_\nu(p,p;0) = \frac{\partial S^{-1}(p)}{\partial p_\nu}\,. \tag{3.62}$$

The bare vertex $\Lambda_\nu = \gamma_\nu$ satisfies the WT identity if the bare propagator is used in (3.61); however, if the propagator is dressed without properly dressing the vertex function as well, this identity is violated. In the following section we will derive the Ward-Takahashi identity at zero temperature and show how this identity can be used to constrain the longitudinal component of the vertex function.

The Zero Temperature Ward-Takahashi Identity

Apart from the gauge fixing term, the QCD/QED Lagrangian density (2.41) is invariant under local $SU(N_c)/U(1)$ gauge transformations (2.35)/(2.23). However, with this term included it is not. This violation should not appear in physical quantities, therefore the generating functional (partition function) for the theory must remain invariant under gauge transformations [14]. Actually this condition is too strong. All that we really have to require is that functional derivations with repect to the sources are invariant when the sources are removed; however, for the derivation below it is sufficient to require the stronger condition that the generating functional itself be gauge invariant since in the end we take functional derivatives and take the sources to zero. This requirement leads to relations between the n-point functions of the theory that guarantee that gauge invariance of physical quantities is always maintained.

Consider performing an infinitesimal abelian gauge transformation

$$\begin{aligned} G_\mu^{'} &= G_\mu + \partial_\mu \Lambda \\ q^{'} &= q - ig\Lambda q \\ \bar{q}^{'} &= \bar{q} + ig\Lambda \bar{q}\,. \end{aligned} \tag{3.63}$$

When inserted into the expression for the partition function (2.40) and ghost terms are ignored, the integrand of Z picks up a factor

$$Z^{'} = \exp\left[\int_x -\frac{1}{\alpha}\partial_\mu G_\mu \nabla^2\Lambda - \frac{1}{2\alpha}(\nabla^2\Lambda)^2 + ig\bar{q}K\Lambda - ig\bar{K}q\Lambda + J_\mu\partial_\mu\Lambda\right] Z\,, \qquad (3.64)$$

where the exponential is understood to be in the integrand of the path integral. To first order in Λ this expression gives

$$\begin{aligned} Z^{'} &= Z + \mathbf{S}Z \\ \mathbf{S} &= \int_x \left[-\frac{1}{\alpha}\partial_\mu G_\mu \nabla^2\Lambda + ig\bar{q}K\Lambda - ig\bar{K}q\Lambda + J_\mu\partial_\mu\Lambda\right]\,, \end{aligned} \qquad (3.65)$$

so that if the generating functional is to remain invariant under this gauge transformation ($Z^{'} = Z$) the operator $\mathbf{S}$ acting on Z must give zero, i.e.

$$\int_x \left[-\frac{1}{\alpha}\partial_\mu G_\mu \nabla^2\Lambda + ig\bar{q}K\Lambda - ig\bar{K}q\Lambda + J_\mu\partial_\mu\Lambda\right] Z = 0\,. \qquad (3.66)$$

After integrating by parts this expression becomes

$$\int_x \left[-\frac{1}{\alpha}\nabla^2\partial_\mu G_\mu + ig(\bar{q}K - \bar{K}q) - \partial_\mu J_\mu\right] \Lambda Z = 0\,. \qquad (3.67)$$

Since Λ is an arbitrary function this implies that

$$\left[-\frac{1}{\alpha}\nabla^2\partial_\mu G_\mu + ig(\bar{q}K - \bar{K}q) - \partial_\mu J_\mu\right] Z = 0\,. \qquad (3.68)$$

Replacing the fields appearing in the operator $\mathbf{S}$ with the appropriate functional derivatives (3.13) and transforming to momentum space gives the following functional differential equation

$$\left[\frac{i}{\alpha}k^2 k_\mu \frac{\delta}{\delta J_\mu} + ig(K\frac{\delta}{\delta K} - \bar{K}\frac{\delta}{\delta \bar{K}}) - ik_\mu J_\mu\right] Z = 0\,, \qquad (3.69)$$

which, using the relation $Z = \exp(-W)$, can be turned into an equation for the generating functional for connected graphs W

$$\left[\frac{i}{\alpha}k^2 k_\mu \frac{\delta}{\delta J_\mu} + ig(K\frac{\delta}{\delta K} - \bar{K}\frac{\delta}{\delta \bar{K}}) - ik_\mu J_\mu\right] W = 0\,. \tag{3.70}$$

Using the relations (3.13) again allows us to express this as a functional differential equation for the effective action, Γ

$$\frac{i}{\alpha}k^2 k_\mu \tilde{G}_\mu(k) + ig(Q(k)\frac{\delta\Gamma}{\delta Q(k)} - \bar{Q}(k)\frac{\delta\Gamma}{\delta\bar{Q}(k)}) - ik_\mu \frac{\delta\Gamma}{\delta\tilde{G}_\mu(k)} = 0\,. \tag{3.71}$$

Applying the operator $\delta^2/\delta Q(p_1)\delta\bar{Q}(p_2)$ and setting $\tilde{G}_\mu = Q = \bar{Q} = 0$ reduces this expression to

$$ig\left(\frac{\delta^2\Gamma}{\delta Q(p_1)\bar{Q}(p_1)} - \frac{\delta^2\Gamma}{\delta Q(p_2)\bar{Q}(p_2)}\right) - i(p_1 - p_2)_\mu \frac{\delta^3\Gamma}{\delta\tilde{G}_\mu(p_1 - p_2)\delta Q(p_1)\bar{Q}(p_1)} = 0\,, \tag{3.72}$$

which, when expressed in term of propagators and vertex functions (equations (3.13) and (3.18)), gives the familiar Ward-Takahashi identity

$$i(p-k)_\nu \Lambda_\nu(p,k;p-k) = S^{-1}(p) - S^{-1}(k)\,. \tag{3.73}$$

The limit of zero momentum transfer can be determined by dividing both sides by $(p-k)_\mu$ and taking the limit as $(p-k)_\mu \to 0$ giving the Ward Identity

$$i\Lambda_\mu(p,p;0) = \frac{\partial S^{-1}(p)}{\partial p_\mu}\,. \tag{3.74}$$

Therefore we see that, as a consequence of gauge invariance, there is a non-perturbative relation between the dressed quark propagator and the dressed quark-gluon vertex. In the next section, we will determine exactly to what extent the Ward and Ward-Takahashi identities constrain the dressed quark-gluon vertex function.

Ball-Chiu Vertex

The consequences of the zero temperature Ward-Takahashi identity for the QED vertex function were first worked out by Ball and Chiu [33, 34]. We will present a quick derivation of the result here for comparison with the finite temperature case. To begin we insert the most general form of the quark-gluon vertex function

$$\begin{aligned}\Lambda_\nu(p,k;p-k) &= \Lambda^L_\nu(p,k;p-k) + \Lambda^T_\nu(p,k;p-k) \\ &= (p+k)_\nu \left[a(p^2,k^2)(\not p + \not k) + b(p^2,k^2)\right] \\ &\qquad + c(p^2,k^2)\gamma_\nu + \Lambda^T_\nu(p,k;p-k)\,, \end{aligned} \tag{3.75}$$

and quark propagator (2.51) into the Ward-Takahashi identity (3.73), giving

$$\begin{aligned} i(p^2-k^2)\left[a(p^2,k^2)(\not p + \not k) + b(p^2,k^2)\right] + ic(p^2,k^2)(\not p - \not k) &= \\ i\not p A(p^2) - i\not k A(k^2) + B(p^2) - B(k^2)\,, \end{aligned} \tag{3.76}$$

which upon rearrangement becomes

$$\begin{aligned} \Big((p^2-k^2)a(p^2,k^2) + c(p^2,k^2)\Big)\, i\not p \quad &+ \quad \Big((p^2-k^2)a(p^2,k^2) - c(p^2,k^2)\Big)\, i\not k \\ i(p^2-k^2)b(p^2,k^2) \quad &= \quad i\not p A(p^2) - i\not k A(k^2) + B(p^2) - B(k^2)\,. \end{aligned} \tag{3.77}$$

Matching terms on the left and right hand sides fixes the functions a, b, and c uniquely with

$$\begin{aligned} a(p^2,k^2) &= \frac{1}{2}\left(\frac{A(p^2)-A(k^2)}{p^2-k^2}\right) \\ b(p^2,k^2) &= \frac{1}{i}\left(\frac{B(p^2)-B(k^2)}{p^2-k^2}\right) \\ c(p^2,k^2) &= \frac{1}{2}(A(p^2)+A(k^2))\,, \end{aligned} \tag{3.78}$$

so that the expression for the general form of the vertex function (3.75) becomes

$$\Lambda_\nu(p,k;p-k) = \frac{(p+k)_\nu}{p^2-k^2}\left[\frac{1}{2}\left(A(p^2)-A(k^2)\right)(\not p+\not k)+\frac{1}{i}\left(B(p^2)-B(k^2)\right)\right]+ \frac{\gamma_\nu}{2}(A(p^2)+A(k^2))+\Lambda^T_\nu(p,k;p-k)\,, \tag{3.79}$$

with the transverse piece given by

$$\Lambda^T_\nu(p,k;q)=\sum_{i=1}^{8}\tau^i(p^2,k^2,q^2)T^i_\nu(p,k)\,. \tag{3.80}$$

The basis for this decomposition is the set of eight transverse vectors which span the space specified by $q_\mu T^i_\mu(p,k)=0, q\equiv p-k$. These vectors are [33]

$$T^1_\nu(p,k) = k_\nu(p\cdot q)-p_\mu(k\cdot q) \tag{3.81}$$

$$T^2_\nu(p,k) = (\not p+\not k)T^1_\nu \tag{3.82}$$

$$T^3_\nu(p,k) = q^2\gamma_\nu - q_\nu\not q \tag{3.83}$$

$$T^4_\nu(p,k) = k_\mu p_\lambda\sigma_{\mu\lambda}T^1_\nu \tag{3.84}$$

$$T^5_\nu(p,k) = \sigma_{\nu\mu}q_\mu \tag{3.85}$$

$$T^6_\nu(p,k) = \gamma_\nu(p^2-k^2)-(p+k)_\nu\not q \tag{3.86}$$

$$T^7_\nu(p,k) = (p^2-k^2)[\gamma_\nu(\not p+\not k)-(p+k)_\nu]+(p+k)_\nu k_\mu p_\lambda\sigma_{\mu\lambda} \tag{3.87}$$

$$T^8_\nu(p,k) = -\gamma_\nu k_\lambda p_\mu\sigma_{\lambda\nu}-k_\nu\not p-p_\nu\not k\,. \tag{3.88}$$

The Ward-Takahashi identity only constrains the longitudinal part of Λ_ν, leaving the functions τ^i undetermined. Recently, Curtis and Pennington [13] examined the result of requiring multiplicative renormalizability for the quark propagator and vertex. The conclusion of the authors was that only the basis vector T^6_ν contributed to the transverse component (i.e. $\tau_i=0$ for $i\neq 6$) with

$$\tau^6(p^2,k^2,q^2)=\frac{A(p^2)-A(k^2)}{2d(p,k)}\,, \tag{3.89}$$

where $d(p,k)$ is a symmetric, singularity-free function with the limiting behavior $\lim_{p^2 \gg k^2} d(p,k) = p^2$.

To fix $d(k,p)$ Curtis and Pennington generalized the solution obtained with massless fermions to fermions with dynamically generated masses, giving

$$d(p,k) = \frac{(p^2-k^2)^2 + \left[M^2(p^2)+M^2(k^2)\right]^2}{p^2+k^2} \tag{3.90}$$

Studies using this vertex have shown that it does reduce the gauge dependence of the results, however, a residual dependence remains [35]. Further improvements are being researched [36, 37]. We will not include this term in this work since the finite temperature extension is non-trivial. We will instead simply use the Ball-Chiu vertex function.

3.1.6 Schwinger-Dyson equations with the Ball-Chiu vertex function

When the most general form for the vertex function,

$$\Lambda_\nu(p,k;p-k) = (p+k)_\nu \left[a(p^2,k^2)(\not{p}+\not{k}) + b(p^2,k^2)\right] + c(p^2,k^2)\gamma_\nu\,, \tag{3.91}$$

is inserted into the Schwinger-Dyson equation (3.24), the coupled equations for the coefficient functions are of course changed from the rainbow approximation result (Section 3.1.3). In the Landau gauge ($\alpha = 0$) the equations become

$$\begin{aligned} A(p^2) \;\; = \;\; & Z_2 + \frac{\bar{g}^2}{p^2}\int_k \left(\frac{1}{A^2(k^2)k^2+B^2(k^2)}\right)\frac{1}{q^2}\Big[\Delta_T(q)\Big(p\cdot k\,\Big(c(p^2,k^2)A(k^2)+ \\ & ib(p^2,k^2)B(k^2)+(p^2+k^2)a(p^2,k^2)\Big)\Big) - ip^2 b(b^2,k^2)B(k^2)- \\ & 2k^2p^2a(p^2,k^2)A(k^2)+ \\ & \frac{\left(2A(k^2)c(p^2,k^2)+ib(p^2,k^2)B(k^2)+(p^2+k^2)a(p^2,k^2)A(k^2)\right)(p\cdot q)(k\cdot q)}{q^2}+ \end{aligned}$$

$$\left.\left.\frac{\left(k^2 a(p^2,k^2)A(k^2)+ib(p^2,k^2)B(k^2)\right)(p\cdot q)^2}{q^2}\right)\right]$$

$$\begin{aligned}
B(p^2) &= M_o+\bar{g}^2\int_k\left(\frac{B(k^2)}{A^2(k^2)k^2+B^2(k^2)}\right)\frac{1}{q^2}\Big[\Delta_T(q)\Big(3c(p^2,k^2)B(k^2)+\\
&\quad (k^2+p^2)a(p^2,k^2)B(k^2)+\Big(2a(p^2,k^2)B(k^2)-ib(p^2,k^2)A(k^2)\Big)\,p\cdot k+\\
&\quad k^2a(p^2,k^2)B(k^2)-ik^2b(p^2,k^2)A(k^2)+\\
&\quad \frac{\left(2ib(p^2,k^2)A(k^2)-2a(p^2,k^2)B(k^2)\right)(p\cdot q)(k\cdot q)}{q^2}-\\
&\quad \frac{a(p^2,k^2)B(k^2)(p\cdot q)^2}{q^2}+\\
&\quad \left.\left.\frac{\left(2ib(p^2,k^2)A(k^2)-a(p^2,k^2)B(k^2)\right)(k\cdot q)^2}{q^2}\right)\right]\,. \qquad (3.92)
\end{aligned}$$

If we are using the Ball-Chiu vertex, we substitute the expressions for $a(p^2,k^2)$, $b(p^2,k^2)$, $c(p^2,k^2)$ obtained in the previous section (3.78) into these equations prior to numerical solution. It can be explictly verified that in the rainbow limit,

$$\begin{aligned}
a(p^2,k^2)=b(p^2,k^2) &= 0\\
c(p^2,k^2) &= 1\,, \qquad (3.93)
\end{aligned}$$

the rainbow approximation SD equations (3.26) are reproduced.

Quenched approximation

When the full Ball-Chiu vertex (3.78) is used within the quenched approximation ($\Delta_T = 1$), and the trivial angular integrations are performed, one finds that the vector coefficient function $A(p^2)$ is no longer simply equal to its bare value, Z_2, but instead must be coupled to the equation for $B(p^2)$.

With the addition of the new vertex terms, we find that the dynamical mass generation is enhanced as seen in Figure 3.9, and that the critical coupling of the

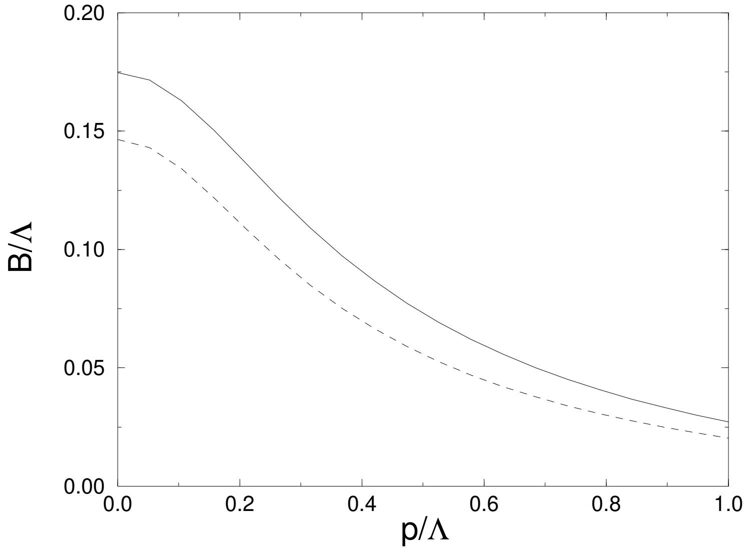

Figure 3.9: Comparison between the vector coefficient functions obtained using the rainbow approximation (dashed line) and the full Ball-Chiu vertex (solid line). ($M_o = 0$, $Z_2 = 1$, $\Lambda = 10^5$; $\bar{g}^2 = 20 > g_c^2$).

Gauge (α)	g_c^2
Landau (0)	$13.15 \pm .05$
Feynman (1)	$22.35 \pm .05$
Yennie (3)	$27.62 \pm .05$

Table 3.1: The critical coupling for dynamical mass generation within the rainbow approximation for three different covariant gauges, Landau ($\alpha = 0$), Feynman ($\alpha = 1$), and Yennie ($\alpha = 3$) gauges.

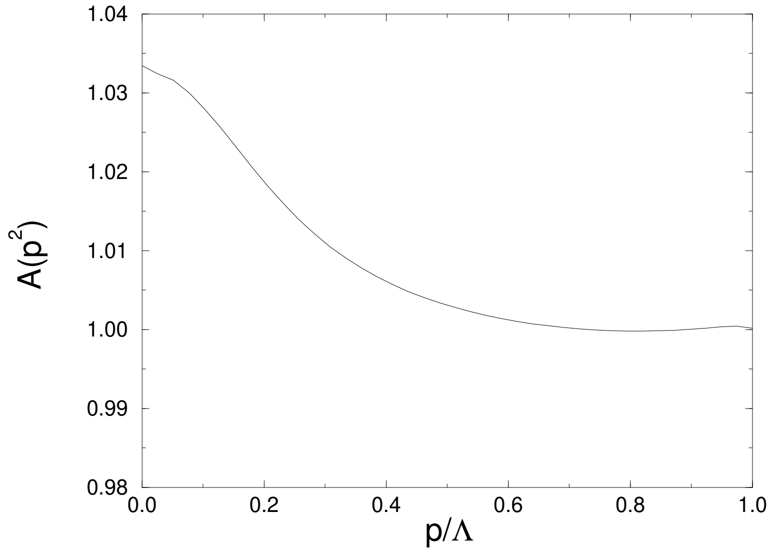

Figure 3.10: Plot showing the p dependence of the vector coefficient function, $A(p^2)$, with the full Ball-Chiu vertex and a quenched gluon propagator. ($M_o = 0$, $Z_2 = 1$, $\Lambda = 10^5$; $\bar{g}^2 = 20 > g_c^2$).

theory is lowered from $g_c^{\text{rainbow}} = 13.15$ to $g_c^{\text{bc}} = 12.22$ in the Landau gauge. We have shown the p dependence of the vector coefficient function in Figure 3.10.

We have also measured the dependence of the critical coupling for dynamical mass generation on the covariant gauge parameter α and find that within the rainbow approximation there is significant variation in the critical couplings for different gauges. We list in Table 3.1 the critical couplings computed for the Landau ($\alpha = 0$), Feynman ($\alpha = 1$), and Yennie ($\alpha = 3$) gauges within the rainbow approximation. When the full Ball-Chiu vertex is used the gauge variation of the critical coupling is almost entirely removed, as can be seen in Table 3.2. This is a very important result since we have shown that by improving the vertex function through the application of the WT identity we can produce physically relevant results, i.e. ones which do not depend on the choice of gauge.

Gauge (α)	g_c^2
Landau (0)	$12.22 \pm .05$
Feynman (1)	$12.15 \pm .05$
Yennie (3)	$12.12 \pm .05$

Table 3.2: The critical coupling for dynamical mass generation with the full Ball-Chiu vertex for three different covariant gauges, Landau ($\alpha = 0$), Feynman ($\alpha = 1$), and Yennie ($\alpha = 3$) gauges.

Delta function gluon propagator

If we model the gluon propagator by a delta function [20]

$$\bar{g}^2 \Delta_T(q) = m_t^2\, q^2\, (2\pi)^4\, \delta^4(q) \tag{3.94}$$

and insert this into the right hand side of (3.92) the following coupled equations result

$$\begin{aligned}
A(p^2) &= Z_2 + 3m_t^2 (A^2(p^2)p^2 + B^2(p^2))^{-1} \times \\
&\qquad \left(\frac{1}{2}c(p^2,p^2)A(p^2) - \frac{i}{2}b(p^2,p^2)B(p^2) - p^2 a(p^2,p^2)A(p^2)\right) \\
B(p^2) &= M_o + 3m_t^2 (A^2(p^2)p^2 + B^2(p^2))^{-1} \times \\
&\qquad \left(c(p^2,p^2)B(p^2) + p^2 a(p^2,p^2)B(p^2) - \frac{i}{2}p^2 b(p^2,p^2)A(p^2)\right)
\end{aligned} \tag{3.95}$$

In the limit that $p^2 \to k^2$ two of the Ball-Chiu vertex coefficient functions (3.78) become derivatives with respect to p^2 and the other becomes simply $A(p^2)$,

$$\begin{aligned}
a(p^2,p^2) &= \frac{1}{2}\frac{\partial A(p^2)}{\partial p^2} \\
b(p^2,p^2) &= \frac{1}{i}\frac{\partial B(p^2)}{\partial p^2} \\
c(p^2,p^2) &= A(p^2)\,,
\end{aligned} \tag{3.96}$$

so that the equations (3.95) become coupled differential equations, as opposed to the coupled algebraic equations obtained within the rainbow approximation

$$
\begin{aligned}
A(s) &= Z_2 + \frac{3m_t^2}{2(A^2(s)+B^2(s))}\left(A^2(s) - sA(s)A'(s) - B(s)B'(s)\right) \\
B(s) &= M_o + \frac{3m_t^2}{2(A^2(s)+B^2(s))}\left(2A(s)B(s) + sB(s)A'(s) - sA(s)B'(s)\right)
\end{aligned} \tag{3.97}
$$

with $s \equiv p^2$ and the boundary conditions $A(\infty) = Z_2$ and $B(\infty = M_o)$.

The solution to these equations [20] yields a propagator which has no singularities for real p^2, and therefore the confining character of the delta function gluon propagator is maintained even after vertex improvement. However, the nature of the solution is quite different. In the case of the rainbow approximation, the solution for $B^2(p^2)$ grows linearly for negative p^2 and hence there is never a point at which $p^2 + B^2(p^2) = 0$. In the case of the Ball-Chiu vertex the absence of poles is due to a delicate cancellation between the zeros of the numerator and denominator of the quark propagator [20].

To summarize, the confining character of the delta function gluon propagator is maintained under vertex improvement; however, the method in which the poles are eliminated is quite different, showing that the quark-gluon vertex function can have a significant quantitative effect on Schwinger-Dyson based studies of QCD.

Chapter 4

Finite Temperature SD Equations

In the previous chapter we derived and solved the Schwinger-Dyson equations at zero temperature. It is desirable to carry out this same program at finite temperature because it is widely believed that at finite temperature, QCD undergoes a phase transition from the low-temperature phase with confined quarks and gluons and chiral symmetry breaking, to a high-temperature phase in which quarks and gluons are no longer confined and chiral symmetry is restored (in the zero bare mass limit). The main tool for the theoretical investigation of non-perturbative finite temperature QCD has been lattice gauge simulations [9, 10]. However, the results produced from these studies are limited to small lattice sizes due to the numerical complexity of lattice simulations. Another possible approach is to solve truncations of the finite temperature Schwinger-Dyson (FTSD) hierarchy to obtain information about the phase structure of QED, QCD, and other field theories [38, 39, 40, 41, 42].

In the following section we will note the differences between the zero and finite temperature field theory and the consequences of these differences.

4.1 Finite Temperature Formalism

At finite temperature the Green's function must be thermally averaged [43] so that

$$G_{\pm}(x,y;\tau,0) = Z^{-1}\mathrm{Tr}\left[\hat{\rho}T_{\pm}\left[\hat{\phi}(x,\tau)\hat{\phi}(y,0)\right]\right] , \tag{4.1}$$

where $\hat{\rho} = \exp(-H/k_B T)$ is the density matrix and $T_{\pm}$ is the imaginary time ordering operator

$$T_{\pm}\left[\hat{\phi}(\tau_1)\hat{\phi}(\tau_2)\right] = \hat{\phi}(\tau_1)\hat{\phi}(\tau_2)\theta(\tau_1-\tau_2) \pm \hat{\phi}(\tau_2)\hat{\phi}(\tau_1)\theta(\tau_2-\tau_1) . \tag{4.2}$$

The plus and minus signs above correspond to the cases of bosonic and fermionic fields, respectively. In keeping with convention, we set the Boltzmann constant $k_B = 1$ and define $\beta = 1/T$. Using the form (4.1) for the Green's function we can show

$$
\begin{aligned}
G_\pm(x,y;\tau,0) &= Z^{-1}\mathrm{Tr}\left[\mathrm{e}^{-\beta H}T_\pm\left[\hat{\phi}(x,\tau)\hat{\phi}(y,0)\right]\right] \\
&= Z^{-1}T_\pm\left[\mathrm{Tr}\left[\mathrm{e}^{-\beta H}\hat{\phi}(x,\tau)\hat{\phi}(y,0)\right]\right] \\
&= Z^{-1}T_\pm\left[\mathrm{Tr}\left[\hat{\phi}(y,0)\mathrm{e}^{-\beta H}\hat{\phi}(x,\tau)\right]\right] \\
&= Z^{-1}T_\pm\left[\mathrm{Tr}\left[\mathrm{e}^{-\beta H}\mathrm{e}^{\beta H}\hat{\phi}(y,0)\mathrm{e}^{-\beta H}\hat{\phi}(x,\tau)\right]\right] \\
&= Z^{-1}T_\pm\left[\mathrm{Tr}\left[\mathrm{e}^{-\beta H}\hat{\phi}(y,\beta)\hat{\phi}(x,\tau)\right]\right] \\
&= \pm\, Z^{-1}\mathrm{Tr}\left[\hat{\rho}T_\pm\left[\hat{\phi}(x,\tau)\hat{\phi}(y,\beta)\right]\right] \\
&= \pm\, G_\pm(x,y;\tau,\beta)\,,
\end{aligned}
\tag{4.3}
$$

that the fields must be either periodic in the case of bosons, $\phi(y,0) = \phi(y,\beta)$, or anti-periodic in the case of fermions, $\phi(y,0) = -\phi(y,\beta)$. Due to this periodicity the Fourier transform of ϕ becomes discrete so that an integral over the fourth component of the Euclidean four vector becomes an infinite sum over the Matsubara frequencies ω_m [43]

$$
\int \frac{dk_4}{2\pi} f(\mathbf{k},k_4) \to \frac{1}{\beta}\sum_{m=-\infty}^{m=\infty} f(\mathbf{k},\omega_m)\,, \tag{4.4}
$$

where $\omega_m = 2\pi m T$ for bosons and $\omega_m = (2m+1)\pi T$ for fermions.

Within the path integral formalism this constraint is implemented by restricting the path integral to periodic (or anti-periodic) field configurations with period β

$$
Z[J_\mu,K,\bar{K}] = \mathrm{e}^{-W} \equiv \mathcal{N}\int_- \mathcal{D}(q,\bar{q})\int_+ \mathcal{D}(G,\eta,\eta^*)\, e^{-S[q,\bar{q},G_\mu]+\bar{q}K+\bar{K}q+J_\mu G_\mu} \tag{4.5}
$$

$$
S[q,\bar{q},G_\mu] = \int_0^\beta dx_4 \int d^3\mathbf{x}\,\mathcal{L}(q,\bar{q},G_\mu)\,, \tag{4.6}
$$

where the plus and minus signs on the integrations indicate periodic and anti-periodic constraints respectively.

4.2 Finite Temperature SD Equations

The finite temperature Schwinger-Dyson equation for the electron and quark propagators can be obtained from their zero temperature counterparts (3.24) simply by including the dependence on the heat bath four-velocity, u, and discretizing the k_4 integration, i.e.

$$\begin{aligned}\Sigma(p, p\cdot u) &= S^{-1}(p, p\cdot u) - S_o^{-1}(p, p\cdot u) \\ &= g^2\left(\frac{N_c^2-1}{2N_c}\right)\int_k \gamma_\mu S(k, k\cdot u)D_{\mu\nu}(p-k, (p-k)\cdot u) \\ &\qquad \times \Lambda_\nu(k, k\cdot u, p, p\cdot u; p-k, (p-k)\cdot u)\,, \qquad (4.7)\end{aligned}$$

where now $\int_k = 1/\beta \sum_m \int d^3k/(2\pi)^3$.

4.2.1 Finite temperature quark and gluon propagators

When written in covariant form, the most general finite temperature quark propagator is

$$S^{-1}(p,u) = iA(p^2, p\cdot u)\not{p} + B(p^2, p\cdot u) + iC(p^2, p\cdot u)\not{u}\,. \qquad (4.8)$$

There has been some debate about whether a tensor term proportional to $\sigma_{\mu\nu}$ should also appear [38, 39, 44, 45]; however, the recent studies of Rusnak and Furnstahl [46] have ruled out the appearance of such a term through the application of $\mathcal{PT}$ (parity and time) invariance.

When making calculations we fix the reference frame by specifying the medium four-velocity u. If we choose our reference frame to be the rest frame of the heat bath, then $u = (0,0,0,1)$, so that (4.8) reduces to

$$S^{-1}(p,\omega_n) = iA(p^2,\omega_n)\not{p} + B(p^2,\omega_n) + iC(p^2,\omega_n)\gamma_4\,. \tag{4.9}$$

For now we continue to work with the covariant form (4.8) and wait to specify the frame until the end of the derivation. Using $\not{p}\not{p} = p^2$, $\not{u}\not{u} = 1$, and $\not{p}\not{u} + \not{u}\not{p} = 2u\cdot p$ we can express the general form of the finite temperature quark propagator (4.8) as

$$S(p,p\cdot u) = \frac{-iA(p^2,p{\cdot}u)\not{p} + B(p^2,p{\cdot}u) - iC(p^2,p{\cdot}u)\not{u}}{A^2p^2 + 2ACp\cdot u + B^2 + C^2}\,. \tag{4.10}$$

A commonly used approximation [38, 39] is to neglect the contribution coming from both A and C; however, perturbative expansions indicate that C contributes significantly [47], and recent studies show that pion observables are quantitatively sensitive to the presence of these terms and so they should not be neglected [40].

The self-energy appearing on the left of (4.7) can be expressed as a sum of three terms

$$\Sigma(p,p\cdot u) = \Sigma_A(p,p\cdot u)\not{p} + \Sigma_B(p,p\cdot u) + \Sigma_C(p,p\cdot u)\not{u} \tag{4.11}$$

where $\Sigma_A = A - Z_2$, $\Sigma_B = B - M_o$, $\Sigma_C = C$.

The gluon propagator at finite temperature has the general form

$$D^{\mu\nu}(q,q\cdot u) = \frac{\Delta_{3T}(q,q\cdot u)}{q^2}P^{\mu\nu}_{3T} + \frac{\Delta_{3L}(q,q\cdot u)}{q^2}P^{\mu\nu}_{3L} + \frac{\alpha}{q^2}P^{\mu\nu}_{4L}\,, \tag{4.12}$$

where $P^{\mu\nu}_{4L}$ is the four dimensional longitudinal projector (2.54), $q^2 = q_1^2 + q_2^2 + q_3^2 + q_4^2$, and $P^{\mu\nu}_{3T}$ and $P^{\mu\nu}_{3L}$ are three dimensionally transverse and longitudinal projectors, respectively. These three dimensional projectors are both four-dimensionally transverse and are given by [43]

$$P^{00}_{3T} \;=\; P^{0i}_{3T} = P^{i0}_{3T} = 0$$

$$
\begin{aligned}
P_{3T}^{ij} &= \delta_{ij} + \frac{q_i q_j}{\underline{\mathrm{q}}^2} \qquad (i,j = 1,2,3) \\
P_{3L}^{\mu\nu} &= P_{4T}^{\mu\nu} - P_{3T}^{\mu\nu} \,,
\end{aligned}
\tag{4.13}
$$

where $\underline{\mathrm{q}}^2 = q_1^2 + q_2^2 + q_3^2$.

Zero Temperature Limit

In the zero temperature limit Lorentz invariance is restored therefore

$$
\begin{aligned}
&\lim_{T\to 0} \qquad C \to 0 \\
&\lim_{T\to 0} \qquad \Delta_{3T} \to \Delta_{3L} \,,
\end{aligned}
\tag{4.14}
$$

and the coefficient functions become functions of only p^2. In this limit the finite temperature quark and gluon propagators revert to their zero temperature forms (2.52,2.54).

4.2.2 Finite Temperature Rainbow Approximation

Taking the quark-gluon vertex to be bare gives the following equation for the quark self-energy

$$
\begin{aligned}
\Sigma(p, p\cdot u) &= S^{-1}(p, p\cdot u) - S_o^{-1}(p, p\cdot u) \\
&= g^2 \left(\frac{N_c^2 - 1}{2N_c}\right) \int_k \gamma_\mu S(k, k\cdot u) D_{\mu\nu}(p-k, (p-k)\cdot u)\gamma_\nu \,.
\end{aligned}
\tag{4.15}
$$

Inserting the general forms of the finite temperature quark and gluon propagators obtained in the last section and setting the gauge parameter $\alpha = 0$ (Landau gauge) gives

$$\Sigma(p,p\cdot u) \;=\; g^2\left(\frac{N_c^2-1}{2N_c}\right)\int_k \frac{\gamma_\mu}{q^2}\,[(iA\not{p}-iC\not{u}+B)(\Delta_{3T}-\Delta_{3L})P_{3T}^{\mu\nu}+ (iA\not{p}-iC\not{u}+B)\Delta_{3L}P_{4T}^{\mu\nu}]\,\gamma_\nu/(A^2p^2+2ACp\cdot u+B^2+C^2)\,. \tag{4.16}$$

Taking traces of (4.16) with $-i\not{p}$, $-i\not{u}$, and 1 gives the three coupled integral equations

$$\begin{aligned}
1/4\ \mathrm{Tr}[\,-i\not{p}\,\Sigma(p,p\cdot u)\,] &= p^2\Sigma_A+p\cdot u\,\Sigma_C \\
&= g^2\left(\frac{N_c^2-1}{2N_c}\right)\int_k\left(\frac{1}{q^2(A^2k^2+2ACk\cdot u+B^2+C^2)}\right) \\
&\quad \Bigg[A\Delta_{3L}\left(p\cdot k+\frac{2(k\cdot q)(p\cdot q)}{q^2}\right)+ \\
&\quad C\Delta_{3L}\left(p\cdot u+\frac{2(p\cdot q)(q\cdot u)}{q^2}\right)+ \\
&\quad A(\Delta_{3T}-\Delta_{3L})\left(2(p\cdot k-\underline{\mathbf{p}}\cdot\underline{\mathbf{k}})+\frac{2(\underline{\mathbf{k}}\cdot\underline{\mathbf{q}})(\underline{\mathbf{p}}\cdot\underline{\mathbf{q}})}{\underline{\mathrm{q}}^2}\right)+ \\
&\quad C(\Delta_{3T}-\Delta_{3L})\left(2(p\cdot u-\underline{\mathbf{p}}\cdot\underline{\mathbf{u}})+\frac{2(\underline{\mathbf{p}}\cdot\underline{\mathbf{q}})(\underline{\mathbf{q}}\cdot\underline{\mathbf{u}})}{\underline{\mathrm{q}}^2}\right)\Bigg]\,, \\
1/4\ \mathrm{Tr}[\,-i\not{u}\,\Sigma(p,p\cdot u)\,] &= p\cdot u\,\Sigma_A+u^2\Sigma_C \\
&= g^2\left(\frac{N_c^2-1}{2N_c}\right)\int_k\left(\frac{1}{q^2(A^2k^2+2ACk\cdot u+B^2+C^2)}\right) \\
&\quad \Bigg[A\Delta_{3L}\left(k\cdot u+\frac{2(k\cdot q)(u\cdot q)}{q^2}\right)+ \\
&\quad C\Delta_{3L}\left(\underline{\mathrm{u}}^2+\frac{2(q\cdot u)(q\cdot u)}{q^2}\right)+ \\
&\quad A(\Delta_{3T}-\Delta_{3L})\left(2(u\cdot k-\underline{\mathbf{u}}\cdot\underline{\mathbf{k}})+\frac{2(\underline{\mathbf{k}}\cdot\underline{\mathbf{q}})(\underline{\mathbf{u}}\cdot\underline{\mathbf{q}})}{\underline{\mathrm{q}}^2}\right)+
\end{aligned}$$

$$C(\Delta_{3T}-\Delta_{3L})\left(2(u\cdot u-\underline{\mathbf{u}}\cdot\underline{\mathbf{u}})+\frac{2(\underline{\mathbf{q}}\cdot\underline{\mathbf{u}})(\underline{\mathbf{q}}\cdot\underline{\mathbf{u}})}{\underline{\mathrm{q}}^2}\right)\Bigg]\,,$$

$$\begin{aligned}1/4\ \mathrm{Tr}[\,1\,\Sigma(p,p\cdot u)\,] &= \Sigma_B \\ &= g^2\left(\frac{N_c^2-1}{2N_c}\right)\int_k\left(\frac{B\,(\Delta_{3L}+2\Delta_{3T})}{q^2(A^2k^2+2ACk\cdot u+B^2+C^2)}\right)\,.\end{aligned} \tag{4.17}$$

If we make the following definitions

$$\begin{aligned}\mathcal{A} &\equiv \mathrm{Tr}[\,-i\not{p}\,\Sigma(p,p\cdot u)\,] \\ \mathcal{B} &\equiv \mathrm{Tr}[\,\mathbf{1}\,\Sigma(p,p\cdot u)\,] \\ \mathcal{C} &\equiv \mathrm{Tr}[\,-i\not{u}\,\Sigma(p,p\cdot u)\,]\,,\end{aligned} \tag{4.18}$$

then the equations for $\Sigma_{A,B,C}$ can be written as

$$\begin{aligned}\Sigma_A &= (\mathcal{A}-(p\cdot u)\,\mathcal{C})\,/\underline{\mathrm{p}}^2 \\ \Sigma_B &= \mathcal{B} \\ \Sigma_C &= \left(p^2\mathcal{C}-(p\cdot u)\,\mathcal{A}\right)/\underline{\mathrm{p}}^2\,.\end{aligned} \tag{4.19}$$

At this point, we can verify whether these equations have the right zero temperature limit. In the zero temperature limit, Σ_C must vanish, which, via (4.19), requires that

$$\lim_{T\to 0} p^2\mathcal{C}\to(p\cdot u)\mathcal{A}\,. \tag{4.20}$$

This limit can be explicitly verified by fixing $u=(0,0,0,1)$ and taking the zero temperature limit in equations (4.17). Therefore, the set of equations (4.19) has the correct zero temperature rainbow limit and can be used to determine the temperature dependence of the quark or electron propagator.

When the angular integrals in (4.17) are performed the equations for $\Sigma_{A,B,C}$ become of the form

$$\mathcal{A} = \frac{\bar{g}^2T}{(2\pi)^2}\sum_{m=-\infty}^{\infty}\int_0^\infty \underline{\mathrm{k}}^2d\underline{\mathrm{k}}\left(\frac{K_A(\underline{\mathrm{p}},\omega_n,\underline{\mathrm{k}},\omega_m;A,C)}{A^2(\underline{\mathrm{k}}^2+\omega_m^2)+2AC\omega_m+B^2+C^2}\right)$$

$$\mathcal{B} = \frac{\bar{g}^2 T}{(2\pi)^2} \sum_{m=-\infty}^{\infty} \int_0^\infty \underline{\mathrm{k}}^2 d\underline{\mathrm{k}} \left(\frac{K_B(\underline{\mathrm{p}}, \omega_n, \underline{\mathrm{k}}, \omega_m; B)}{A^2(\underline{\mathrm{k}}^2 + \omega_m^2) + 2AC\omega_m + B^2 + C^2} \right)$$

$$\mathcal{C} = \frac{\bar{g}^2 T}{(2\pi)^2} \sum_{m=-\infty}^{\infty} \int_0^\infty \underline{\mathrm{k}}^2 d\underline{\mathrm{k}} \left(\frac{K_C(\underline{\mathrm{p}}, \omega_n, \underline{\mathrm{k}}, \omega_m; A, C)}{A^2(\underline{\mathrm{k}}^2 + \omega_m^2) + 2AC\omega_m + B^2 + C^2} \right), \quad (4.21)$$

where K_A, K_B, and K_C are the integration kernels which depend on the form of Δ_{3L} and Δ_{3T}. Once these two functions are specified, the exact form of these kernels can be calculated. In the following sections we will examine the results obtained using different gauge boson propagators.

4.2.3 Finite Temperature Quenched Rainbow Approximation

When the gluon or photon propagator is taken to be bare ($\Delta_{3L} = \Delta_{3T} = 1 = \Delta_{4T}$) the kernels in equations (4.21) become

$$\begin{aligned} K_A(\underline{\mathrm{p}}, \omega_n, \underline{\mathrm{k}}, \omega_m; A, C) &= A(k, \omega_m) \Big[\omega_n \omega_m J_1^0(\underline{\mathrm{p}}, \underline{\mathrm{k}})_{nm} + \underline{\mathrm{p}}\underline{\mathrm{k}} J_1^1(\underline{\mathrm{p}}, \underline{\mathrm{k}})_{nm} + \\ & 2 \left(\omega_n \omega_m (\omega_n - \omega_m)^2 + (\omega_m \underline{\mathrm{p}}^2 - \omega_n \underline{\mathrm{k}}^2)(\omega_n - \omega_m) - \underline{\mathrm{p}}^2 \underline{\mathrm{k}}^2 \right) J_2^0(\underline{\mathrm{p}}, \underline{\mathrm{k}})_{nm} + \\ & 2\underline{\mathrm{p}}\underline{\mathrm{k}} \left(\underline{\mathrm{p}}^2 + \underline{\mathrm{k}}^2 + (\omega_n - \omega_m)^2 \right) J_2^1(\underline{\mathrm{p}}, \underline{\mathrm{k}})_{nm} - 2\underline{\mathrm{p}}^2 \underline{\mathrm{k}}^2 J_2^2(\underline{\mathrm{p}}, \underline{\mathrm{k}})_{nm} \Big] + \\ & C(k, \omega_m) \Big[\omega_n J_1^0(\underline{\mathrm{p}}, \underline{\mathrm{k}})_{nm} + 2 \left(\omega_n (\omega_n - \omega_m)^2 + \underline{\mathrm{p}}^2 (\omega_n - \omega_m) \right) J_2^0(\underline{\mathrm{p}}, \underline{\mathrm{k}})_{nm} - \\ & 2\underline{\mathrm{p}}\underline{\mathrm{k}} (\omega_n - \omega_m) J_2^1(\underline{\mathrm{p}}, \underline{\mathrm{k}})_{nm} \Big] \end{aligned}$$

$$K_B(\underline{\mathrm{p}}, \omega_n, \underline{\mathrm{k}}, \omega_m; B) = 3B(k, \omega_m) J_1^0(\underline{\mathrm{p}}, \underline{\mathrm{k}})_{nm}$$

$$\begin{aligned} K_C(\underline{\mathrm{p}}, \omega_n, \underline{\mathrm{k}}, \omega_m; A, C) &= A(k, \omega_m) \Big[\omega_m J_1^0(\underline{\mathrm{p}}, \underline{\mathrm{k}})_{nm} - \\ & 2 \left(\underline{\mathrm{k}}^2 - \omega_m (\omega_n - \omega_m) \right) (\omega_n - \omega_m) J_2^0(\underline{\mathrm{p}}, \underline{\mathrm{k}})_{nm} + 2\underline{\mathrm{p}}\underline{\mathrm{k}} J_2^1(\underline{\mathrm{p}}, \underline{\mathrm{k}})_{nm} \Big] + \\ & C(k, \omega_m) \left[J_1^0(\underline{\mathrm{p}}, \underline{\mathrm{k}})_{nm} + 2(\omega_n - \omega_m)^2 J_2^0(\underline{\mathrm{p}}, \underline{\mathrm{k}})_{nm} \right], \end{aligned} \quad (4.22)$$

where the integratals in Appendix C have been used. With the kernels evaluated we can now solve for the coefficient functions A, B, and C. For comparison, however, we will first examine the scalar approximation.

Scalar Approximation

If we ignore the contributions coming from the field renormalizations A and C by fixing $A = Z_2 = 1$ and $C = 0$, we are left with a single integral equation for the scalar coefficient B

$$\begin{aligned} B(\underline{\mathrm{p}}, \omega_n) &= M_o + \frac{3\bar{g}^2 T}{8\pi^2 \underline{\mathrm{p}}} \sum_{m=-M}^{M} \int_{\kappa}^{\Lambda} \underline{\mathrm{k}}^2 d\underline{\mathrm{k}} \left(\frac{B(k, \omega_m)}{\underline{\mathrm{k}}^2 + \omega_m^2 + B^2 + C^2)} \right) \\ &\times \ln \left[\frac{\underline{\mathrm{p}}^2 \underline{\mathrm{k}}^2 + (\omega_n - \omega_m)^2 + 2\underline{\mathrm{p}}\underline{\mathrm{k}}}{\underline{\mathrm{p}}^2 \underline{\mathrm{k}}^2 + (\omega_n - \omega_m)^2 - 2\underline{\mathrm{p}}\underline{\mathrm{k}}} \right], \end{aligned} \tag{4.23}$$

where M is the largest Matsubara mode, κ is an infrared cutoff, and Λ is an ultraviolet cutoff. The largest Matsubara mode M is set such that $\omega_M \approx \Lambda$ and therefore is not a free parameter.

This equation, like its zero temperature counterpart (3.36), can be solved iteratively by evaluating the integrals using Gaussian quadratures and performing the Matsubara sums numerically. The temperature dependence of the scalar coefficient function is shown in Figure 4.1. In this Figure we see that the mass is relatively unchanged until just prior to the critical temperature for chiral symmetry restoration, at which point it undergoes a very sharp transition into the symmetric phase. In fact, the way in which the transition occurs for a finite number of iterations suggests that the if we were to take the number of iterations in infinity, then there would be a discontinuity in $B(0, m = 0)$, i.e. the chiral phase transition is first order within quenched QED/QCD. In this plot we have shown the results of two levels of iteration to illustrate that larger number of iterations are necessary when approaching the critical temperature; however, for this set of equations the point at which the lines in Figure 4.1 intersect is independent of the number of iterations performed (beyond a minimal set) and allows us to identify the critical temperature from two low-iteration runs. Note here that the jumps seen in B as a function of T seen in Figures 4.1 and Figure 4.3 are a result of the finiteness of the UV cuttoff. The requirement that $\omega_{n_{max}} \sim \Lambda$ leads to the fact that as the temperature increase less modes are be included in the Matsubara sum. If the UV cutoff, Λ, were significantly larger, then these jumps would be minimal, and as $\Lambda \to \infty$ these discontinuities would be removed completely. We are unable to take Λ very large due to the computer time needed to compute the Matsubara sums.

We have measured the temperature dependence of the critical coupling for dynamical mass generation within the scalar approximation and have found that it increases with temperature as shown in Figure 4.2.

Including the Field Renormalizations

When the coupling of the equation for the scalar coefficient function, B, to the vector coefficient terms, A and C, is taken into account, the qualitative features of the results remain the same, the critical coupling increases with temperature, and for any finite coupling there exists a critical temperature above which chiral symmetry is restored. However, the quantitative results for the dependence of the critical coupling on the temperature are affected significantly; the temperature dependence of A, B, and C are shown in Figure 4.4. In the next figure, Figure 4.5, we have plotted the temperature dependence of the critical coupling for comparison with the scalar approximation, Figure 4.2.

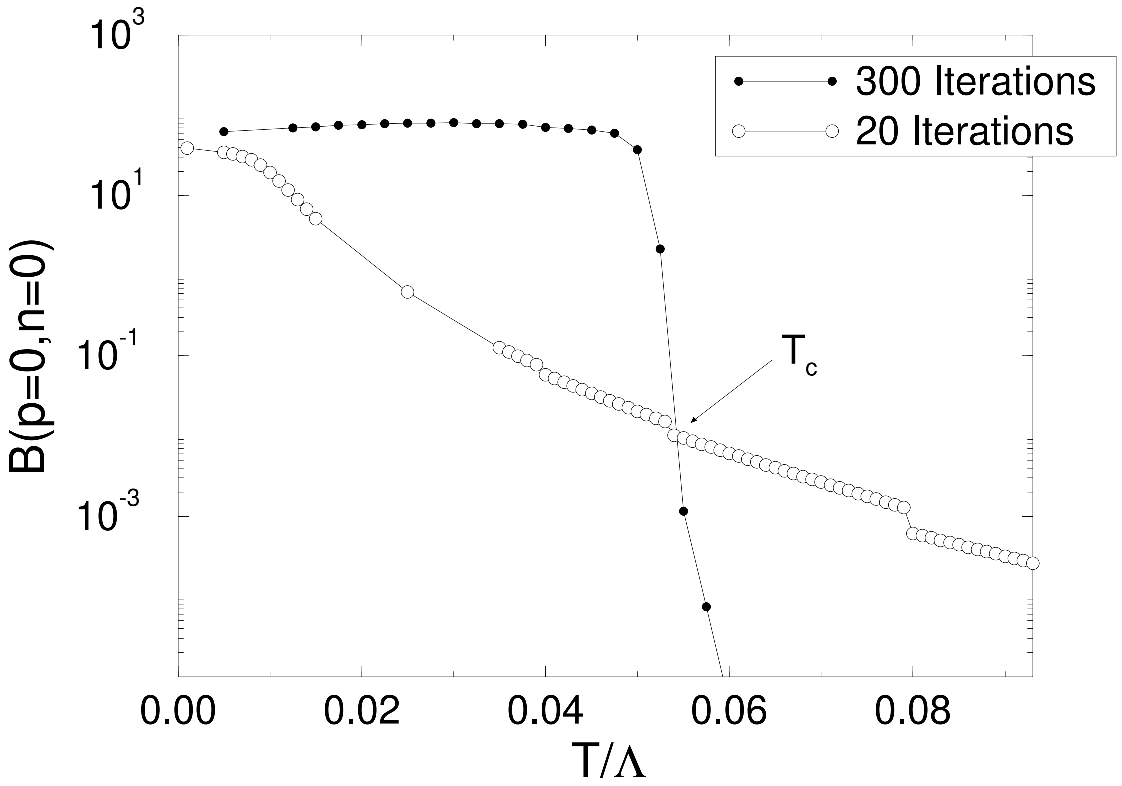

Figure 4.1: $B(\underline{p} = 0, n = 0)$ as a function of T/Λ showing the chiral symmetry restoration temperature $T_c(g^2 = 20\,, \Lambda = 1000)$.

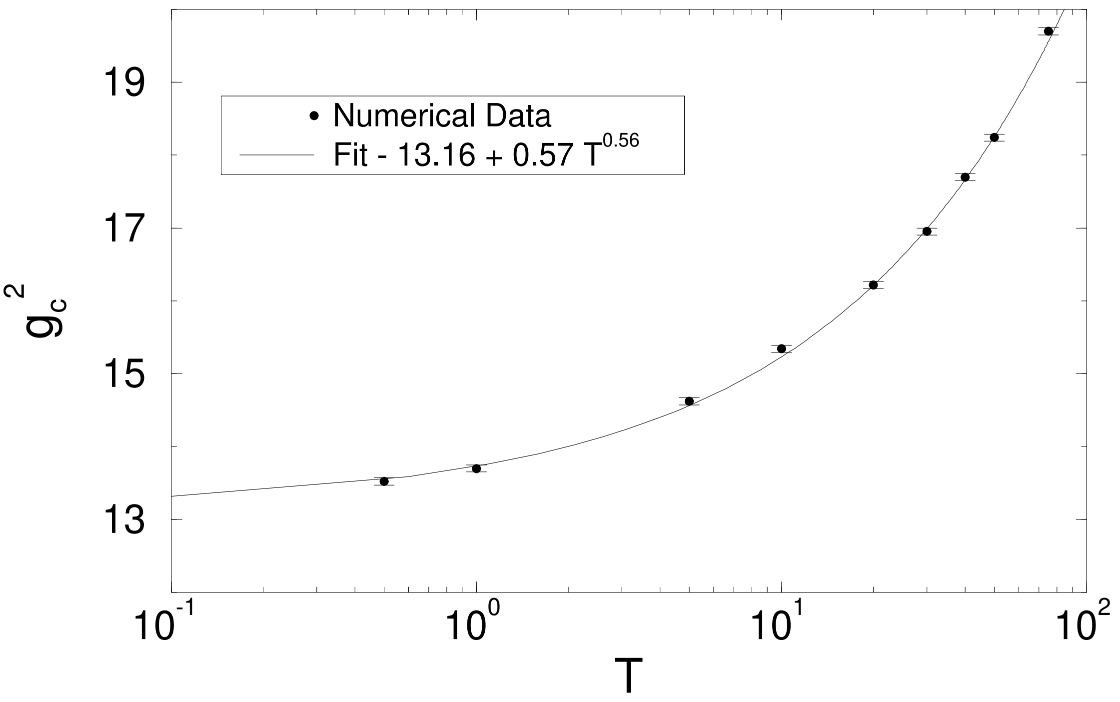

Figure 4.2: Critical coupling $\bar{g}_c^2$ as a function of temperature along with fit of the form $g_c(T) = A + BT^C$ within the scalar approximation($\Lambda = 1000$).

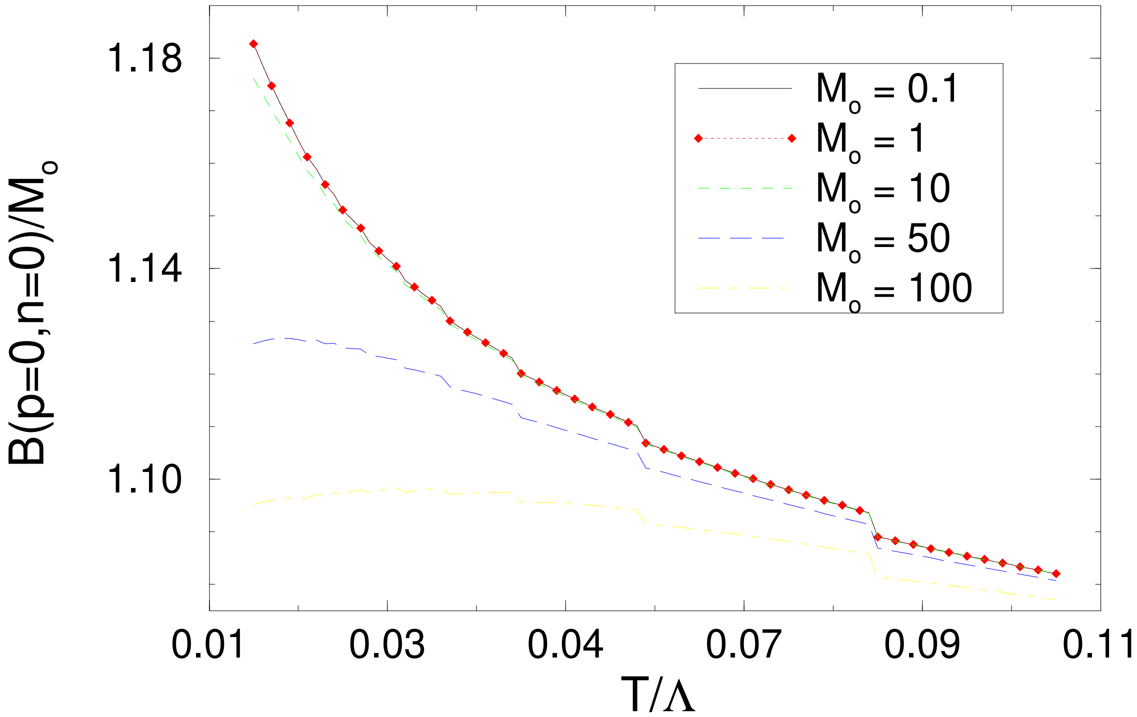

Figure 4.3: Plot of $B(\underline{\mathrm{p}} = 0, n = 0)$ vs. T/Λ showing the dependence of the weak-coupling ($\bar{g}^2 = 0.01$) solution on the bare mass M_o of the fermion. ($\Lambda = 1000$).

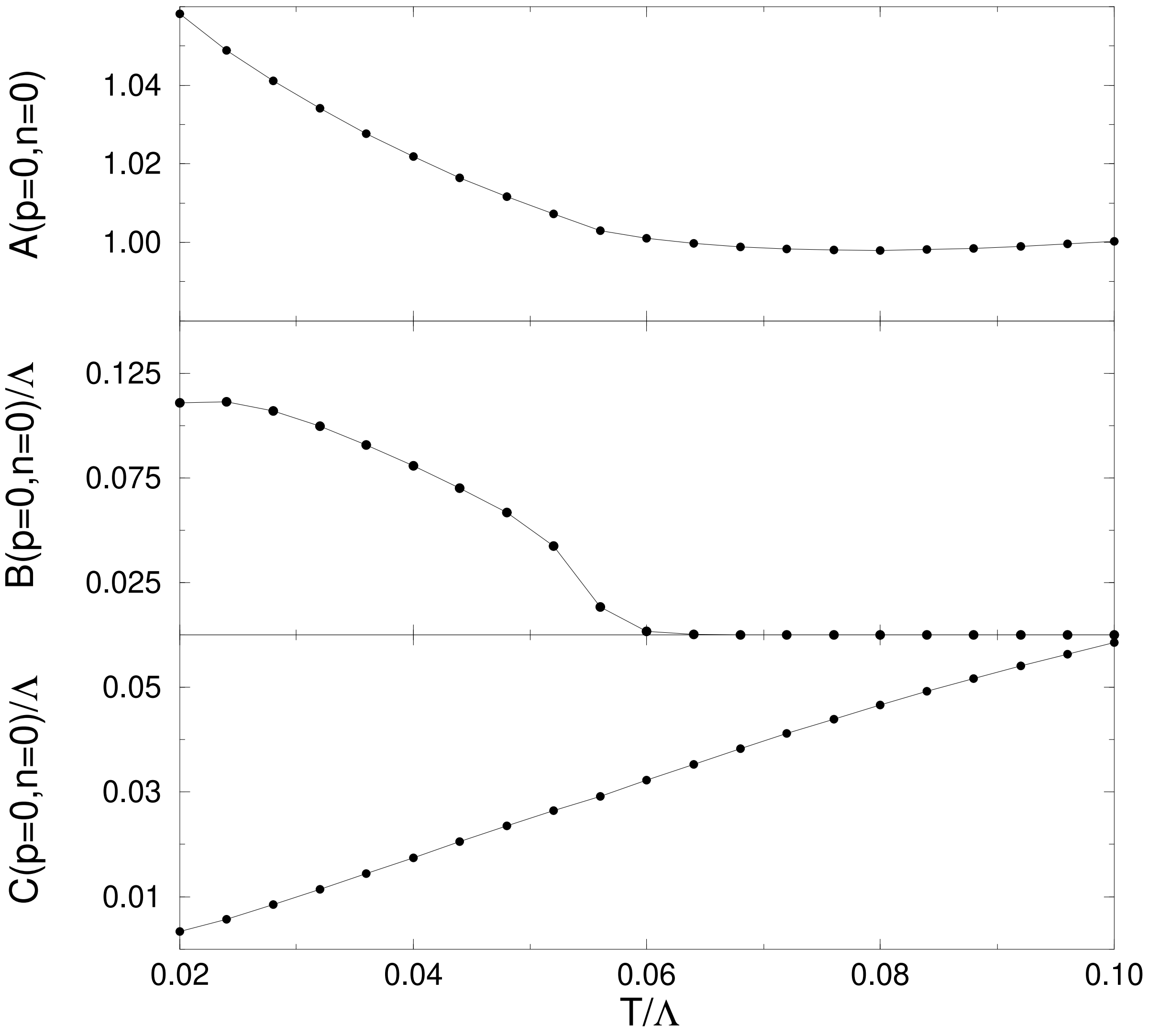

Figure 4.4: Temperature dependence of the coefficient functions A, B, and C within the finite temperature rainbow approximation ($M_o = 0$, $\bar{g}^2 = 25$, $\Lambda = 1000$).

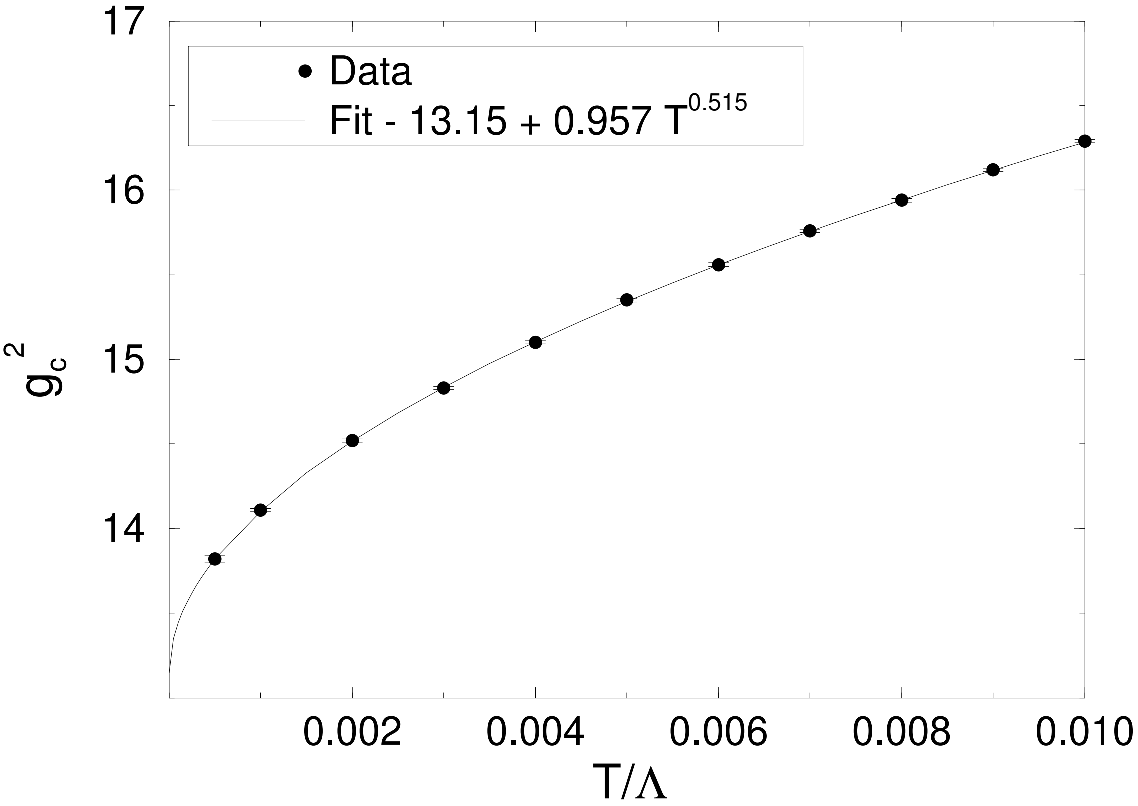

Figure 4.5: Critical coupling g_c^2 as a function of temperature along with fit of the form $g_c(T) = A + BT^C$ including the effects of the field renormalizations ($\Lambda = 1000$).

4.2.4 The Finite Temperature Vertex Function

As was the case at zero temperature, at finite temperature the rainbow approximation violates gauge invariance because of inconsistent dressing of the propagator and vertex functions. We found in Chapter 2 that at zero temperature vertex improvement greatly reduces the gauge dependence of the critical coupling. It can be shown that the gauge dependence of other physical quantities (quark condensate, hadronic observables, etc.) is reduced and therefore it is crucial to properly dress the vertex function if we wish to calculate these quantities. In addition, we will see below that the vertex function strongly affects the critical temperature for deconfinement/chiral symmetry restoration and therefore should not be ignored. To determine the necessary vertex improvements we can apply the finite temperature Ward-Takahashi identity (FTWT) in order to constrain the coefficient functions appearing in the finite temperature vertex function. The method for doing this is the same as in the zero temperature case (Section 3.1.5) since the FTWT identity is virtually identical to its zero temperature counterpart, with the only difference being the discretization of p_4.

The most general form for the finite temperature quark-gluon vertex function is

$$\begin{aligned}\Lambda_\nu(p,k;p-k) &= \Lambda^L_\nu(p,k;p-k) + \Lambda^T_\nu(p,k;p-k) \\ &= (p+k)_\nu\left[a(p,k,u)(\not p+\not k) + b(p,k,u) + c(p,k,u)\not u\right] \\ &\quad + d(p,k,u)\gamma_\nu + u_\nu\left[e(p,k,u)(\not p+\not k) + f(p,k,u) + g(p,k,u)\not u\right] \\ &\quad + \Lambda^T_\nu(p,k;p-k)\,, \end{aligned} \tag{4.24}$$

where $a \ldots g$ are functions of $p^2, k^2, p{\cdot}u$, and $k{\cdot}u$, and the vector u is the four velocity of the heat bath.[1] Recalling that the general form for the finite temperature quark

[1] Conventionally one chooses the Lorentz frame to be the rest frame of the heat bath so that $u = (0,0,0,1)$.

propagator is

$$S^{-1}(p,u) = iA(p^2,p\cdot u)\not{p} + B(p^2,p\cdot u) + iC(p^2,p\cdot u)\not{u}\,, \tag{4.25}$$

we can insert these expressions into the Ward-Takahashi identity (3.73), which gives the following four equations

$$\begin{aligned}
A(p^2,p\cdot u) - A(k^2,k\cdot u) &= 2(p^2-k^2)a(p,k,u) + 2u\cdot(p-k)e(p,k,u) && (4.26)\\
A(p^2,p\cdot u) + A(k^2,k\cdot u) &= 2d(p,k,u) && (4.27)\\
B(p^2,p\cdot u) - B(k^2,k\cdot u) &= i(p^2-k^2)b(p,k,u) + iu\cdot(p-k)f(p,k,u) && (4.28)\\
C(p^2,p\cdot u) - C(k^2,k\cdot u) &= (p^2-k^2)c(p,k,u) + u\cdot(p-k)g(p,k,u)\,. && (4.29)
\end{aligned}$$

After a moment of reflection, it becomes clear that we have four equations and seven unknowns, which is not enough to solve for all of the coefficient functions that appear in the finite temperature vertex function; however, we can posit a one-parameter solution which satisfies the Ward-Takahashi identity at finite temperature:

$$\begin{aligned}
a(p,k,u) &= \bar{a}\,\frac{A(p^2,p\cdot u) - A(k^2,k\cdot u)}{2(p^2-k^2)} && (4.30)\\
b(p,k,u) &= \bar{a}\,\frac{B(p^2,p\cdot u) - B(k^2,k\cdot u)}{i(p^2-k^2)} && (4.31)\\
c(p,k,u) &= \bar{a}\,\frac{C(p^2,p\cdot u) - C(k^2,k\cdot u)}{(p^2-k^2)} && (4.32)\\
d(p,k,u) &= \frac{1}{2}\Big(A(p^2,p\cdot u) + A(k^2,k\cdot u)\Big) && (4.33)\\
e(p,k,u) &= (1-\bar{a})\frac{A(p^2,p\cdot u) - A(k^2,k\cdot u)}{2u\cdot(p-k)} && (4.34)\\
f(p,k,u) &= (1-\bar{a})\frac{B(p^2,p\cdot u) - B(k^2,k\cdot u)}{iu\cdot(p-k)} && (4.35)\\
g(p,k,u) &= (1-\bar{a})\frac{C(p^2,p\cdot u) - C(k^2,k\cdot u)}{u\cdot(p-k)}\,. && (4.36)
\end{aligned}$$

Looking at the solutions for e, f, and g we see that unless $\bar{a} = 1$ these coefficient functions are divergent for $n = m, p \neq k$. Therefore, by requiring all of the coefficient functions to be finite, we can constrain the finite temperature vertex completely with

$$a(p,k,u) = \frac{A(p^2, p\cdot u) - A(k^2, k\cdot u)}{2(p^2 - k^2)} \tag{4.37}$$

$$b(p,k,u) = \frac{B(p^2, p\cdot u) - B(k^2, k\cdot u)}{i(p^2 - k^2)} \tag{4.38}$$

$$c(p,k,u) = \frac{C(p^2, p\cdot u) - C(k^2, k\cdot u)}{(p^2 - k^2)} \tag{4.39}$$

$$d(p,k,u) = \frac{1}{2}\Big(A(p^2, p\cdot u) + A(k^2, k\cdot u)\Big) \tag{4.40}$$

Improving the Vertex Within the Quenched Approximation

As a first pass we consider using the following vertex function within the quenched approximation

$$\Lambda_\nu(p,k,\omega_n,\omega_m) = \frac{1}{2}\left[A(p,\omega_n) + A(k,\omega_m)\right]\gamma_\nu \tag{4.41}$$

in order to determine the extent to which this improvement affects the finite temperature behavior of the fermion propagator.

This improvement is straightforward to implement, since it merely introduces a factor of $1/2\,(A(p,\omega_n) + A(k,\omega_m))$ to the right hand sides of (4.21).

The qualitative results of this improvement are that A and C are practically unchanged, while the dynamical mass B is enhanced for low temperature. In addition, the critical temperature for chiral symmetry restoration is lowered. Figure (4.6) shows a comparison between the rainbow and improved vertex (4.41) solutions. Calling this vertex function an "improvement" may be a misnomer since it is unknown whether this improves aggreement with experiment. We call it an improvement here, because it includes a large subset of diagrams in the self-energy summation.

4.2.5 Modeling Confinement at Finite Temperature

As in Section 3.1.4 on modeling confinement at zero temperature, at finite temperature we will model the confining part of the gluon propagator by a delta function (3.41) and add a perturbative piece which reproduces the high energy results up to logarithmic corrections. First, we investigate the result of having only a delta function gluon propagator (constant in space) at non-zero temperature.

Delta Function Gluon Propagator

In this section we will examine the finite temperature quark propagator obtained when the gluon propagator is a constant in space and time

$$\bar{g}^2\Delta_{3T}(q,\omega_n) = \bar{g}^2\Delta_{3L}(q,\omega_n) = m_t^2\, q^2\, \frac{(2\pi)^3}{T}\, \delta^3(q)\delta_{n0}\,. \tag{4.42}$$

Rainbow Approximation

When inserted into the rainbow SD (4.17) the following system of equations is obtained ($Z_1 = 1/A, Z_2 = C/A, M = B/A$)[2]

$$\begin{aligned} Z_1 + \frac{5}{3}m_t^2 Z_1^2/(p^2+2Z_2\omega_n+M^2+Z_2^2) &= 1 \\ M_o + 3m_t^2 M Z_1^2/(p^2+2Z_2\omega_n+M^2+Z_2^2) &= M \\ m_t^2 Z_1^2(Z_2-\frac{2}{3}\omega_n)/(p^2+2Z_2\omega_n+M^2+Z_2^2) &= Z_2\,. \end{aligned} \tag{4.43}$$

When $M_o = 0$ the solutions to this system of equations give a quark propagator that

[2]We have used $\int d^3k\delta^3(\underline{\mathbf{q}})f(p-q)(\underline{\mathbf{p}}\cdot\underline{\mathbf{q}})^2/\underline{\mathrm{q}}^2 = \underline{\mathrm{p}}^2 f(p)/3$.

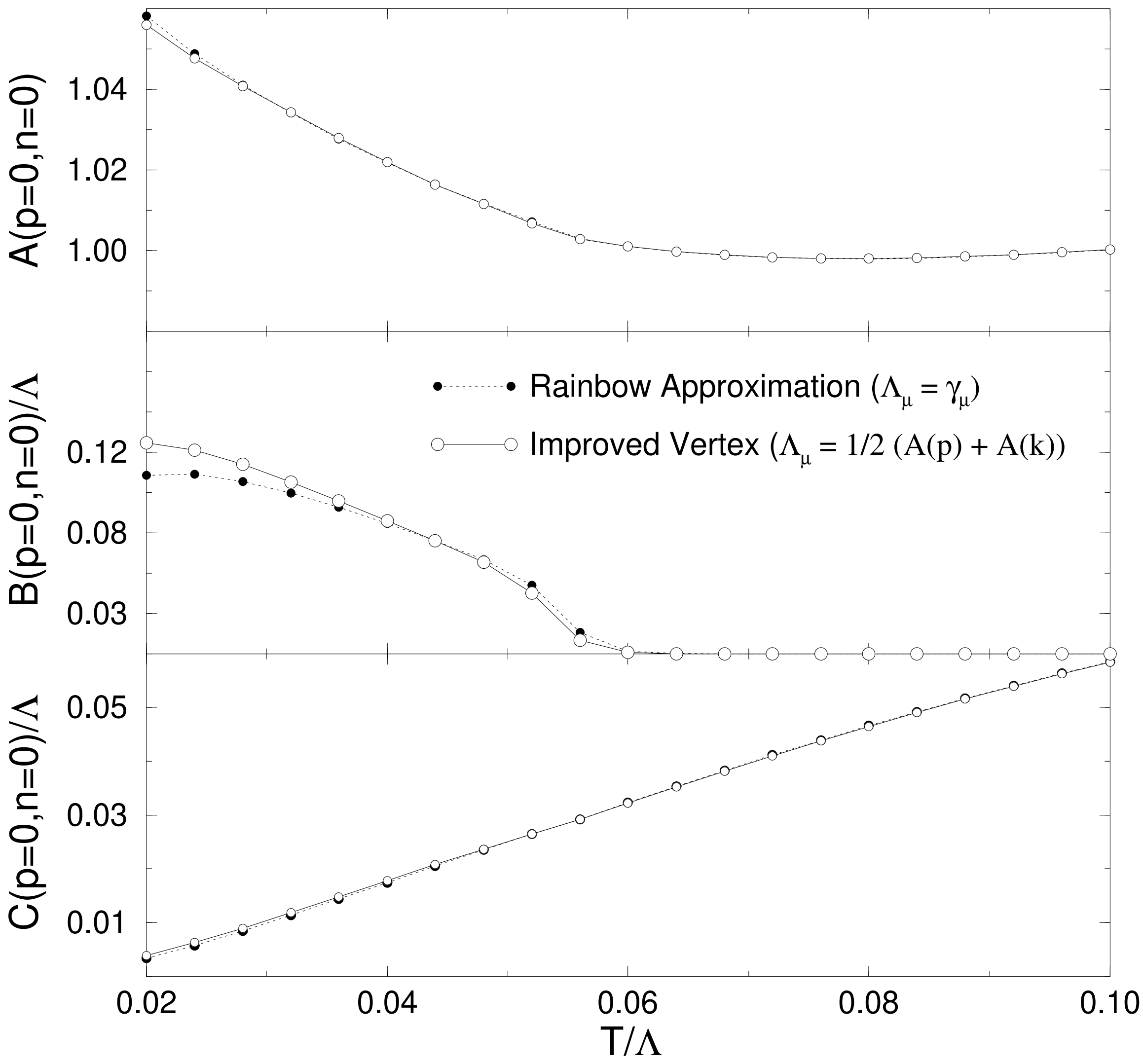

Figure 4.6: Temperature dependence of the coefficient functions A, B, and C with an improved vertex $\Lambda_\nu(p,k,\omega_n,\omega_m) = \frac{1}{2}\left[A(p,\omega_n) + A(k,\omega_m)\right]\gamma_\nu$. Rainbow approximation results are shown for comparison ($M_o = 0$, $\bar{g}^2 = 25$, $\Lambda = 1000$).

is free from singularities for $T > T_c$. The key difference with the zero temperature case is that the cut line now extends from $\underline{\mathrm{p}}^2 = 16/27\, m_t^2 - 4/9\, \omega_n^2 \to \infty$.

$$
\begin{aligned}
Z_1(\underline{\mathrm{p}}^2, \omega_n) &= \frac{4}{9} \\
Z_2(\underline{\mathrm{p}}^2, \omega_n) &= -\frac{\omega_n}{3} \\
M(\underline{\mathrm{p}}^2, \omega_n) &= \sqrt{\frac{16}{27} m_t^2 - \underline{\mathrm{p}}^2 - \frac{4}{9}\omega_n^2} \qquad ;\ \underline{\mathrm{p}}^2 \leq \frac{16}{27} m_t^2 - \frac{4}{9}\omega_n^2 \,.
\end{aligned} \tag{4.44}
$$

The solutions for $\underline{\mathrm{p}}^2 > 16/27\, m_t^2 - 4/9\, \omega_n^2$ have $M = 0$ and Z_1 and Z_2 non-zero; however, due to the algebraic complexity we do not list them here but instead show the $\underline{\mathrm{p}}^2$ dependence of Z_1 and Z_2 in Figure 4.7.

The key result of this calculation is that for $\omega_n^2 > 4/3\, m_t^2$ there is no solution with $M \neq 0$ signaling the restoration of chiral symmetry. In addition, when the bare mass is zero the restoration of chiral symmetry coincides with the appearance of a pole at $p^2 = 0$ signaling the deconfinement of the quark in this model. Therefore, within this simple analytic model we achieve chiral symmetry restoration and deconfinement in a straightforward manner in each Matsubara mode at a temperature given by

$$
T_c(n) = \sqrt{\frac{4}{3}} \frac{m_t}{\mid (2n+1) \mid \pi} \,, \tag{4.45}
$$

which for the $n = 0$ mode gives $T_c(0) = \sqrt{4/3}\, m_t/\pi$. Using the value for $m_t = 0.69$ GeV determined at zero temperature by Roberts and Frank [11] we get $T_c(n = 0) = 254\,\mathrm{MeV}$. This value for m_t was determined using a sum of a delta function and a perturbative piece, and so is not directly applicable in this case, but should provide an order of magnitude estimate for the deconfinement and chiral symmetry restoration critical temperature.

In addition, we can calculate the critical exponent for chiral symmetry restoration in this model. Defining our order parameter to be

$$\begin{aligned}
\chi(T) \equiv M(0, n=0) &= \sqrt{\frac{16}{27} m_t^2 - \frac{1}{3}(2\pi T)^2} \\
&\propto \sqrt{T_c^2 - T^2} \\
&\propto |T_c - T|^{\beta}, \qquad (4.46)
\end{aligned}$$

we can see that within this simple model the chiral phase transition is second order with $\beta = 1/2$.

When $M_o \neq 0$ analytic solution is not possible; however, through numerical solution we find that the deconfinement transition and vanishing of dynamical mass generation occur at a higher temperature and are no longer coincident. We find that the difference between the chiral phase transition temperature T_c^{χ} (signaled by the vanishing of the dynamically generated mass) and the deconfinement phase transition temperature $T_c^{\rm dc}$ is approximately M_o, with the chiral transition happening prior to the deconfinement transition, i.e.

$$T_c^{\rm dc} - T_c^{\chi} \approx M_o\,. \qquad (4.47)$$

As was the case with the zero temperature solution, the system of equations (4.43) is not convergent for all $\underline{\mathrm{p}}^2$ and T; therefore, we have to use the techniques described in the zero temperature section 3.1.4. At finite temperature, this technique becomes more difficult to apply since for a fixed $\underline{\mathrm{p}}^2$ one has to switch the iteration from the function to the inverse function depending on the index of the mode, n. Once implemented, however, the solution produces a convergent answer for all $\underline{\mathrm{p}}^2$ and n.

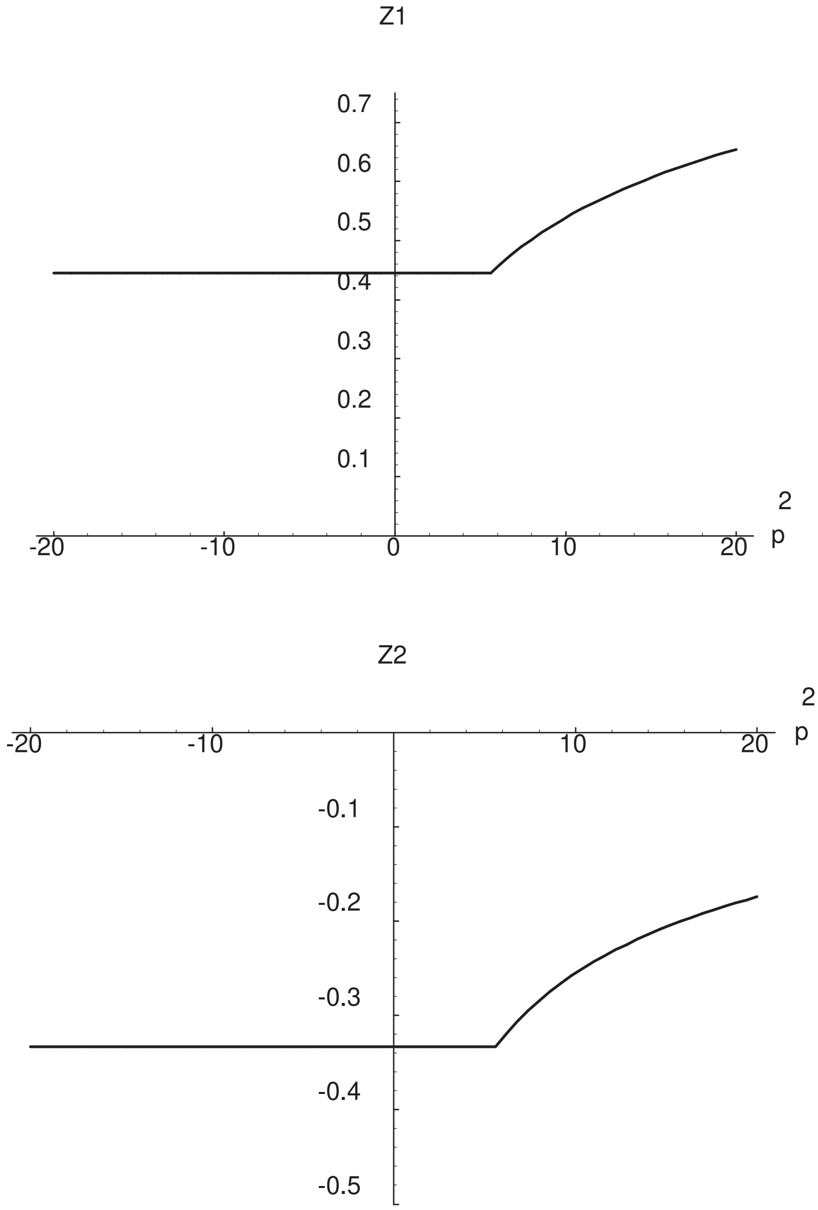

Figure 4.7: Vector coefficient functions Z_1 and Z_2 as a function of $\underline{\mathrm{p}}^2$ obtained using a delta function gluon propagator at finite temperature. ($m_t^2 = 10$, $\omega_n = 1$, $\Lambda = 1000$).

Rainbow Approximation + Vertex Improvement

First we consider the vertex improvement

$$\Lambda_\nu = \frac{1}{2}\left[A(p^2;\omega_n) + A(k^2;\omega_m)\right]\gamma_\nu\,, \tag{4.48}$$

in conjuction with the delta function gluon propagator. When inserted into the FTSD equation (4.21), the following system of equations is obtained

$$\begin{aligned} Z_1 + \frac{5}{3}m_t^2 Z_1/(p^2 + 2Z_2\omega_n + M^2 + Z_2^2) &= 1 \\ M_o + 3m_t^2 M Z_1/(p^2 + 2Z_2\omega_n + M^2 + Z_2^2) &= M \\ m_t^2 Z_1(Z_2 - \frac{2}{3}\omega_n)/(p^2 + 2Z_2\omega_n + M^2 + Z_2^2) &= Z_2\,. \end{aligned} \tag{4.49}$$

This system of equations is analytically solvable for $M_o = 0$ with a non-trivial solution given by

$$\begin{aligned} Z_1(\underline{p}^2,\omega_n) &= \frac{4}{9} \\ Z_2(\underline{p}^2,\omega_n) &= -\frac{\omega_n}{3} \\ M(\underline{p}^2,\omega_n) &= \sqrt{\frac{4}{3}m_t^2 - \underline{p}^2 - \frac{4}{9}\omega_n^2} \qquad ;\ \underline{p}^2 <= \frac{4}{3}m_t^2 - \frac{4}{9}\omega_n^2\,. \end{aligned} \tag{4.50}$$

Which shows that when $M_o = 0$ the vertex improvement increases the critical temperature considerably, with T_c now given by

$$T_c = \frac{\sqrt{3}m_t}{\pi} \tag{4.51}$$

which, using the value $M_t = 0.69\,\mathrm{GeV}$, gives $T_c = 380\,\mathrm{MeV}$. Therefore, the finite temperature vertex function used has a significant effect on the phase transition temperature and must be treated carefully in FTSD solutions. Note that with this vertex improvement the critical exponent remains $\beta = 1/2$.

Full Finite Temperature Ball-Chiu Vertex

When the finite temperature Ball-Chiu vertex function (4.40) is used, the system of algebraic equations becomes a system of differential equations

$$\begin{aligned}\Sigma_A &= m_t^2(A^2p^2+2AC\omega_n+B^2+C^2)^{-1}\left[\frac{5}{3}A^2+\left(\omega_n^2+\frac{\omega_n^4}{\underline{\mathrm{p}}^2}-\frac{4}{3}\underline{\mathrm{p}}^2\right)AA'+\right.\\ &\quad\left(2\frac{\omega_n^3}{\underline{\mathrm{p}}^2}-\frac{10}{3}\omega_n\right)CA'+\left(\frac{\omega_n^2}{\underline{\mathrm{p}}^2}-\frac{4}{3}\right)BB'+\\ &\quad\left.\left(\frac{2}{3}\omega_n+\frac{\omega_n^3}{\underline{\mathrm{p}}^2}\right)AC'+\left(\frac{\omega_n^2}{\underline{\mathrm{p}}^2}-\frac{4}{3}\right)CC'\right] \end{aligned} \tag{4.52}$$

$$\begin{aligned}\Sigma_B &= m_t^2(A^2p^2+2AC\omega_n+B^2+C^2)^{-1}\left[3AB+\left(\frac{4}{3}\underline{\mathrm{p}}^2+\omega_n^2\right)\left(BA'-AB'\right)+\right.\\ &\quad\left.2\omega_n\left(BC'-CB'\right)\right] \end{aligned} \tag{4.53}$$

$$\begin{aligned}\Sigma_C &= m_t^2(A^2p^2+2AC\omega_n+B^2+C^2)^{-1}\left[-\frac{2}{3}\omega_nA^2+AC-\right.\\ &\quad\left(\frac{2}{3}\underline{\mathrm{p}}^2\omega_n+2\omega_n^3+\frac{\omega_n^5}{\underline{\mathrm{p}}^2}\right)AA'+\left(\frac{4}{3}\underline{\mathrm{p}}^2+\frac{\omega_n^2}{3}-2\frac{\omega_n^4}{\underline{\mathrm{p}}^2}\right)CA'-\\ &\quad\left(\frac{2}{3}\omega_n+\frac{\omega_n^3}{\underline{\mathrm{p}}^2}\right)BB'-\left(\frac{4}{3}\underline{\mathrm{p}}^2+\frac{5}{3}\omega_n^2+\frac{\omega_n^4}{\underline{\mathrm{p}}^2}\right)AC'-\\ &\quad\left.\left(\frac{2}{3}\omega_n+\frac{\omega_n^3}{\underline{\mathrm{p}}^2}\right)CC'\right], \end{aligned} \tag{4.54}$$

with the boundary conditions

$$\begin{aligned} A(\underline{\mathrm{p}}=\infty,n) &= Z\\ B(\underline{\mathrm{p}}=\infty,n) &= M_o\\ C(\underline{\mathrm{p}}=\infty,n) &= 0\,. \end{aligned} \tag{4.55}$$

Solution of this system of differential equations yields a propagator that is free from singularities on the negative $\underline{\mathrm{p}}^2$ axis and exhibits dynamical chiral symmetry breaking up to a critical temperature, at which point the dynamically generated mass goes to zero, and a pole appears in the propagator. We have measured the critical exponent for the chiral transition and find that $\beta = 0.34 \pm .02$. This value is agreement with current lattice calculations [10].

Delta Function plus Perturbative Piece

We will now examine the consequences of adding an additional piece to the delta function, which reproduces the correct high energy behavior of the quark propagator. We choose the following parameterization

$$\frac{\bar{g}^2 \Delta_{3L}(q, \omega_n)}{\underline{q}^2 + \omega_n^2} = \frac{\bar{g}^2 \Delta_{3T}(q, \omega_n)}{\underline{q}^2 + \omega_n^2} = m_t^2 \, \frac{(2\pi)^3}{T} \, \delta^3(q) \delta_{n0} + \frac{4\pi^2 d}{\underline{q}^2 + \omega_n^2} \,, \tag{4.56}$$

where $d = 12/(33 - 2N_f)$. This parameterization is a straightforward extension of the zero temperature one and introduces no new parameters. In order to solve the FTSD equation with the model gluon propagator, we have to use the method described in the zero temperature section on confinement (3.1.4) and automatically detect which version of the equation yields a convergent iterative solution.

Rainbow Approximation

The solutions obtained for the coefficient functions A, B, and C using the full model gluon propagator and $\Lambda_\nu = \gamma_\nu$ are shown in Figure (4.8). For this solution we set the bare mass to be $M_o = 0.001\Lambda$. From this plot we see that the coefficient functions A and C are affected strongly by the introduction of the delta function singularity (for comparison see Figure 4.4).

In Figure 4.9 we show the temperature dependence of the coefficient functions. This Figure shows that, using the model gluon propagator (4.56), the dynamically generated mass vanishes at T increases. As $T \to \Lambda$ the B approaches the bare mass,

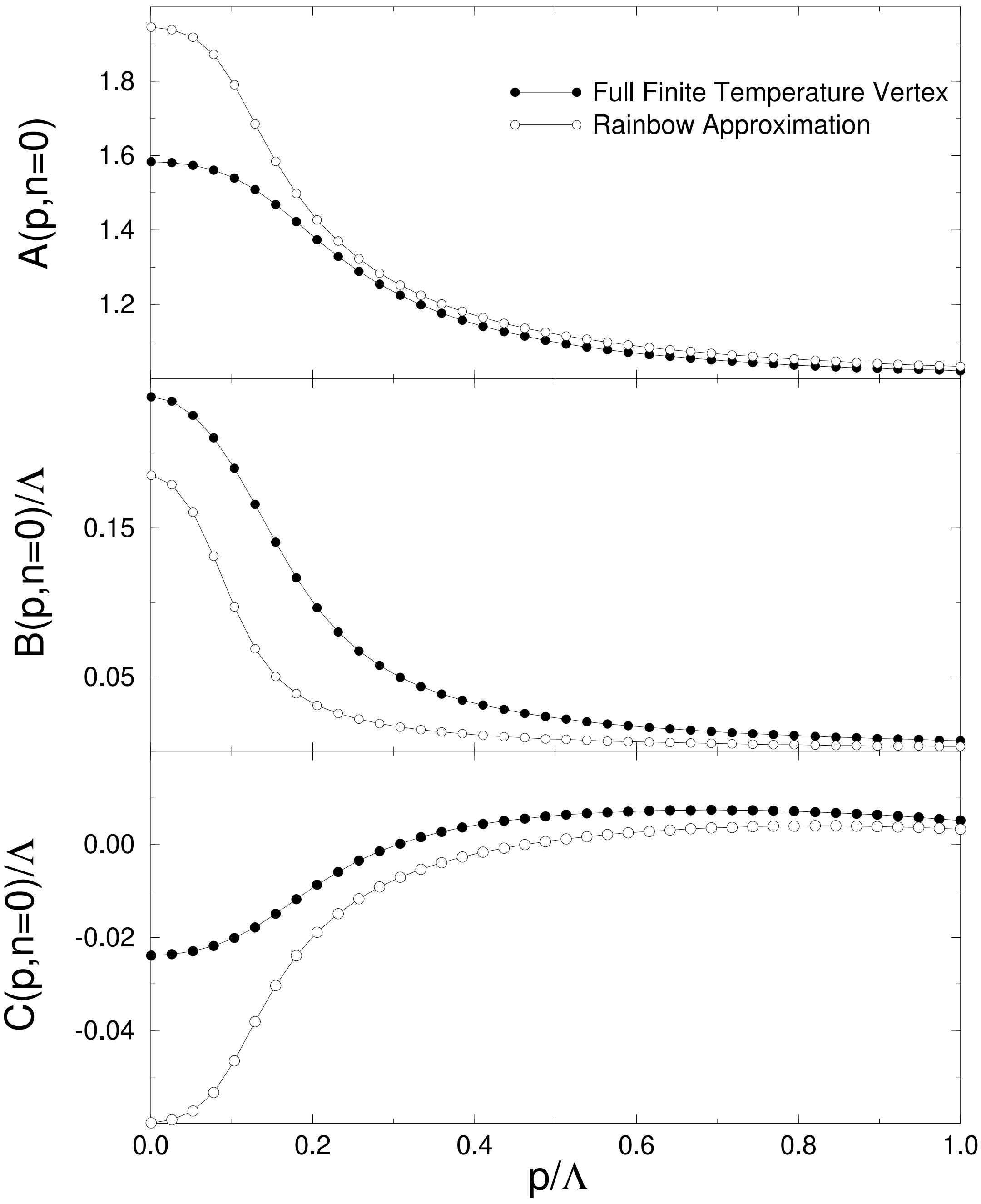

Figure 4.8: Coefficient functions A, B, and C as a function of $\underline{\mathrm{p}}$ using a confining gluon propagator plus (○) the rainbow approximation ($\alpha = 0$) and (•) the full finite temperature Ball-Chiu vertex ($m_t^2 = 138$, $\bar{g} = 17.546$, $T = 20$, $M_o = 1$, $\Lambda = 1000$).

M_o. We have measured the critical exponent in this case and find $\beta = 0.32 \pm .02$. We have also measured the position of the poles in the quark propagator as a function of temperature and find that there is a pair of complex conjugate poles in the quark propagator as alluded to in earlier sections. As the temperature increases these poles move closer to the real axis and for temperatures above the critical temperature the two poles coalesce into one pole on the real negative p^2 axis. This is shown in Figure 4.10.

Full Finite Temperature Ball-Chiu Vertex

The solutions obtained for the coefficient functions A, B, and C using the full model gluon propagator and the full finite temperature Ball-Chiu vertex are shown in Figure (4.8) along with the rainbow approximation results for comparison. From this Figure we see that the vertex function has a significant effect on the infrared properties of all of the coefficient functions and therefore consistently dressed vertices should be used in SD based studies of QCD.

In Figure 4.9 we show the temperature dependence of the coefficient functions using the full finite temperature Ball-Chiu vertex. As with the rainbow approxmiation, the dynamically generated mass vanishes at T increases. As $T \to \Lambda$ the B approaches the bare mass, M_o. We have measured the critical exponent in this case and find $\beta = 0.32 \pm .02$ showing that the critical exponent is not affected, within the accuracy of the measurement, by the introduction of the improved vertex; however, the critical temperature is affected significantly. We have also measured the position of the poles in the quark propagator as a function of temperature using this vertex. The complex conjugate poles found using the rainbow approximation remain after vertex improvement as shown in Figure 4.11.

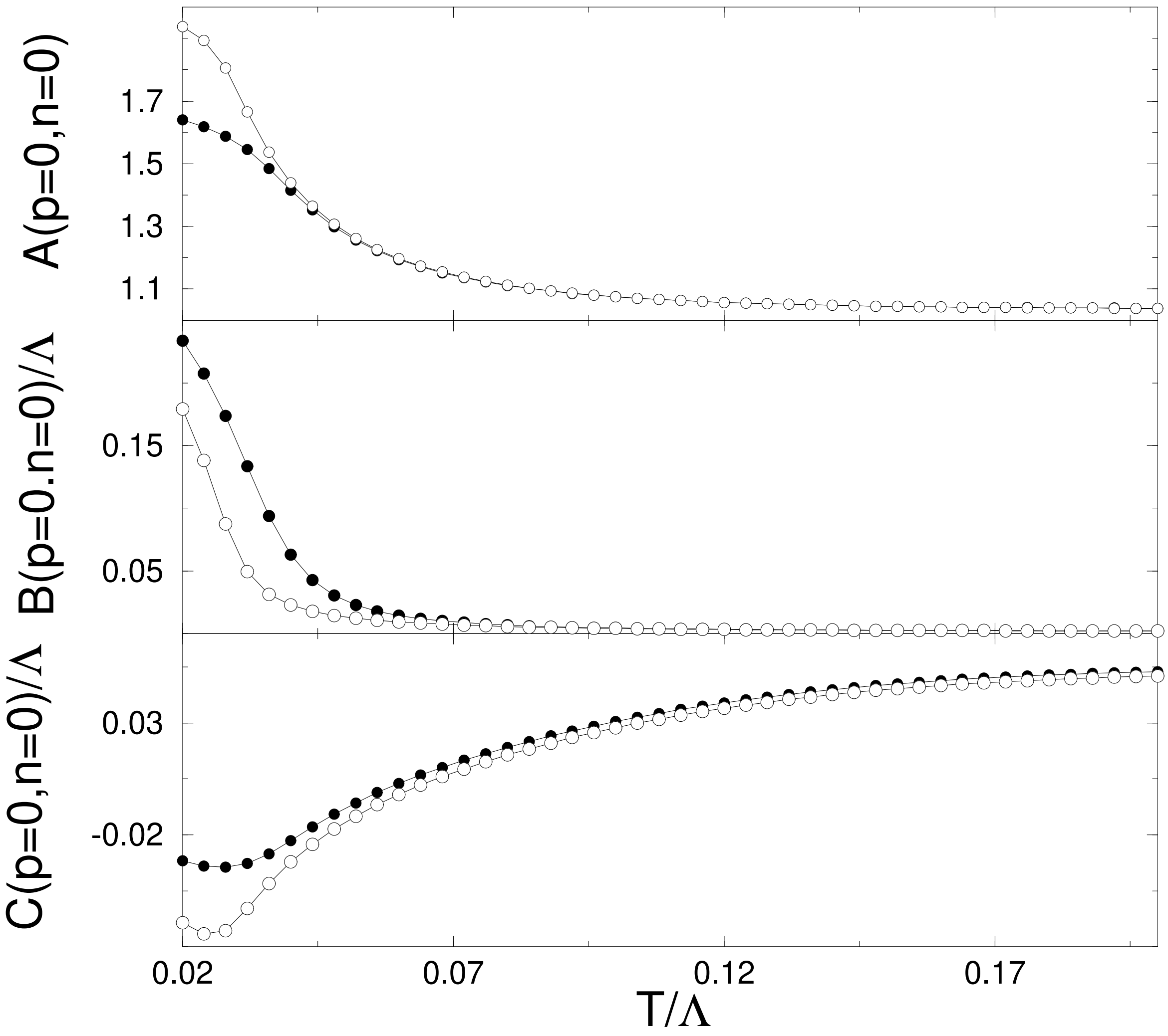

Figure 4.9: Coefficient functions A, B, and C at zero three-momentum and lowest Matsubara mode as a function of T using a confining gluon propagator plus ($\circ$) the rainbow approximation and ($\bullet$) the full finite temperature Ball-Chiu vertex ($m_t^2 = 138$, $\bar{g} = 17.546$, $M_o = 1$, $\Lambda = 1000$).

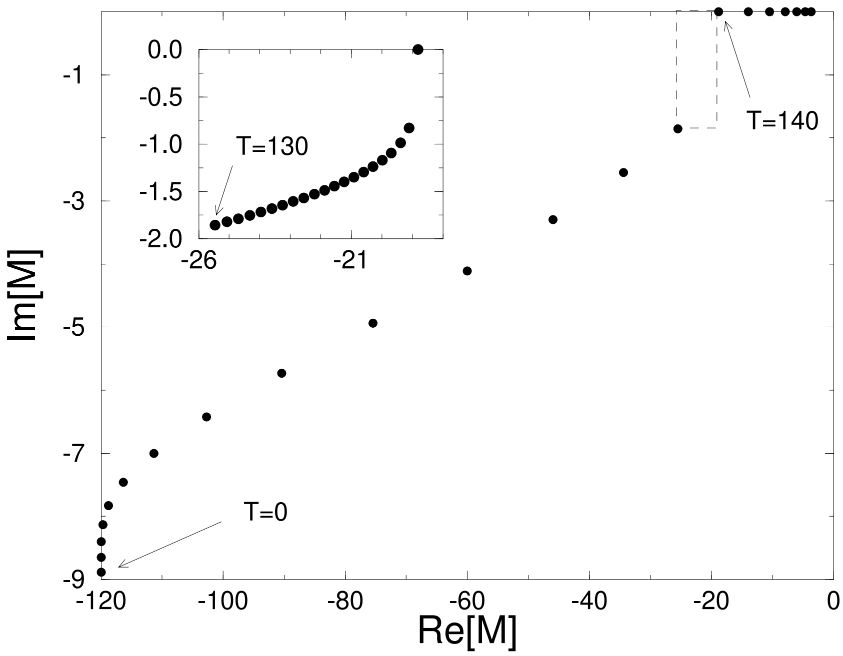

Figure 4.10: Temperature dependence of the poles in the quark propagator obtained using a confining gluon propagator and rainbow approximation for the vertex function. T is in MeV and data points ($\bullet$) are in 0.5 MeV intervals in the inset and 10 MeV intervals outside ($m_t^2 = 60$, $\bar{g} = 17.546$, $\Lambda = 1000$).

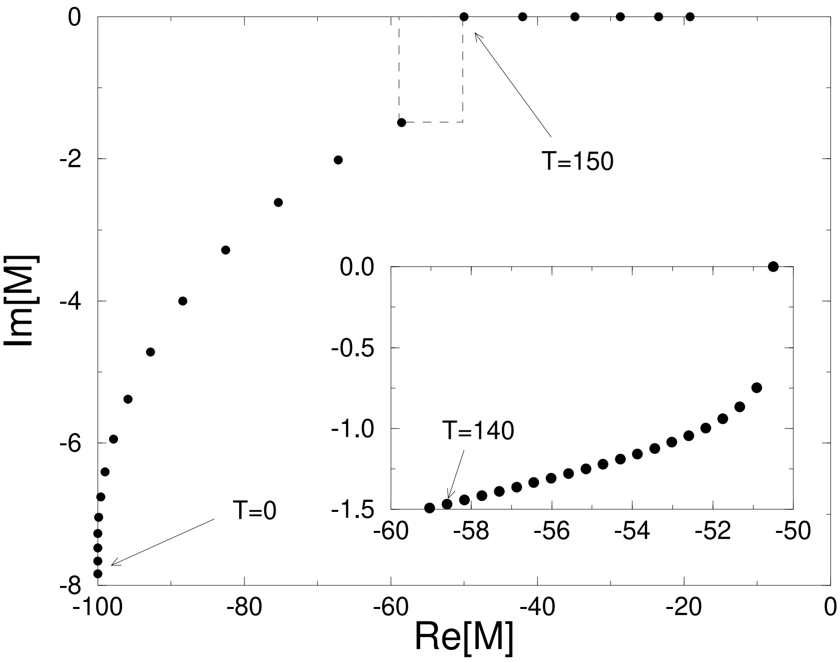

Figure 4.11: Temperature dependence of the poles in the quark propagator obtained using a confining gluon propagator and the finite temperature Ball-Chiu vertex function. T is in MeV and data points ($\bullet$) are in 0.5 MeV intervals in the inset and 10 MeV intervals outside ($m_t^2 = 60$, $\bar{g} = 17.346$, $\Lambda = 1000$).

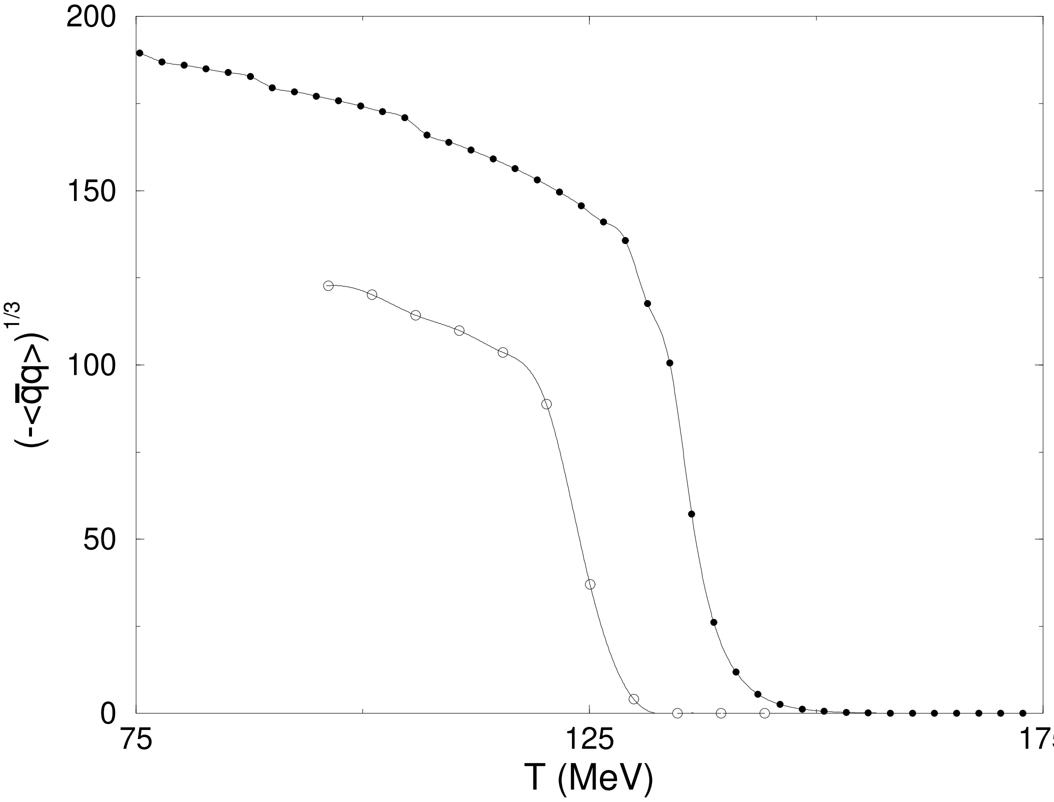

Figure 4.12: Quark condensate $(-<\bar{q}q>)^{\frac{1}{3}}$ as a function of temperature with the rainbow vertex ($\circ$) and the full finite temperature Ball-Chiu vertex ($\bullet$) ($m_t^2 = 138$, $\bar{g} = 17.546$, $M_o = 1$, $\Lambda = 1000$) [Note: The experimental zero temperature value is $(-<\bar{q}q>)^{\frac{1}{3}} = 225 \pm 25$ MeV].

Temperature Dependence of the Quark Condensate

The quark condensate defined through

$$<\bar{q}q>\equiv<0\,|\,\bar{q}q\,|\,0>= -\lim_{x\to 0^+} \mathrm{Tr}\,[S(x) - S^o(x)] \tag{4.57}$$

can be written in terms of an integral involving the coefficient functions A, B, and C

$$<\bar{q}q>= -12\int_k \left(\frac{B(k^2,\omega_m)}{A^2p^2 + 2AC\omega_m + B^2 + C^2} - \frac{M_o}{p^2+M_o^2}\right) . \tag{4.58}$$

In Figure 4.12 we plot the temperature dependence of the quark condensate within the rainbow approximation and with the full finite temperature Ball-Chiu vertex.

Again, the magnitude of the condensate and the critical temperature depend sensitively on the vertex used demonstrating that proper treatment of the finite temperature vertex function is necessary.

Chapter 5

Conclusions

In this thesis we have made calculations of the finite temperature quark propagator using several different gluon propagator Ansätze and quark-gluon vertex functions. The results of the calculations are applicable to strong coupling QED as well as QCD. In strong coupling QED, we have shown that the critical coupling for dynamical mass generation increases with temperature so that for a fixed coupling constant, $g > g_c(T = 0)$ there is always a critical temperature for chiral symmetry restoration. Our numerical calculations indicate that within this model the chiral phase transition is first order.

When modeling QCD, we have used a gluon propagator which includes a sum of a delta function, which models the infrared enhancement seen in lattice and SD studies of the gluon propagator, and a perturbative piece which models the short range interaction. The results using this Ansatz are that at low temperature there is significant dynamical mass generation with no critical coupling strength and that the propagator has complex conjugate poles indicative of an "unstable" particle. As the temperature is increased, the dynamical mass and imaginary part of the propagator pole position go to zero in a continuous manner with approximately the same critical exponent, $\beta = 0.32 \pm 0.02$. We have extended previous calculations by going beyond the bare vertex, or rainbow approximation, through application of the finite temperature Ward-Takahashi identity which allows us to write the vertex function in terms of the quark propagator. Improvement of the vertex function is crucial in order to obtain gauge invariant results. Results obtained using the bare vertex approximation are gauge dependent and therefore cannot be directly compared

Figure 5.1: Diagrammatic representation of the Bethe-Salpeter equation (SD equation of the quark four-point function). M is the four-point function, S is the full propagator (two-point function) and V is the two-particle irreducible scattering kernel.

to experiment. In addition, our results indicate that the vertex function used can have a significant quantitative effect (10% or more depending on the model) on the critical temperature, and therefore should be treating properly when calculating finite temperature quantities within a Schwinger-Dyson based approach to QCD.

There are several questions that remain to be answered at the level of the two-point function. The first concerns the importance of the transverse parts of the vertex function. This piece has been ignored in this work and could have an effect on the results obtained (critical temperature, exponents, etc.). There has been recent work [36] on deriving Ward-Takahashi identities for the transverse parts of the vertex function. Secondly, we would like study different gluon propagator Ansätze in order to determine what features are necessary to achieve a quark propagator with complex conjugate poles. Lastly, it is desirable to solve the SD equation for the gluon and ghost propagators in conjunction with quark equation in order to remove the uncertainty in the inputs of this treatment.

Once these questions have been addressed we can begin make calculations of finite temperature quark bound state properties. By solving the SD equations for higher n-point functions we should be able to calculate hadron masses and wavefunctions at finite temperature. In order to determine meson masses at finite temperature one must solve the Schwinger-Dyson equation for the quark four-point function which is conventionally called the Bethe-Salpeter (BS) equation. The inhomogeneous BS equation is represented diagrammatically in Figure 5.1.

It is possible that there are poles in the four-point function much like the poles encountered in the quark propagator. These poles correspond to bound states and the residues of these poles correspond to the bound state wavefunction [14]. The zero temperature solution of the BS equation using confined quark propagators has had much success in the calculation of mesonic observables [11]. The finite temperature extension, apart from the extra terms which will appear in the spinor decomposition, is straightforward. Through solution of the finite temperature BS equation, both the masses and wavefunctions of the mesonic bound states can be calculated.

The next n-point function of interest is the six-point function. Non-perturbative solutions of the homogenous six-point function SD equation, conventionally called the Fadeev equation, will allow the calculation of finite temperature baryon masses and wavefunctions. Once the BS and Fadeev equations have been solved at finite temperature, then calculations of hadronization cross sections for both mesons and baryons can be made assuming that the amplitudes factorize near the transistion temperature. This assumption may prove to be invalid and calculation of even higher n-point functions may be necessary; however, the only way to determine if this is the case is to proceed systematically up the chain of n-point functions and compare with the data which will soon be coming out of RHIC and LHC.

Appendix A

Numerical Methods

A.1 Numerical Evaluation of Integrals

In evaluating the integrals we split the integration region into an integral from 0 to p and one from p to Λ and evaluate each using Gauss-Legendre quadratures [48].

$$
\begin{aligned}
f(p) &= \int_0^\Lambda dk\, g(p,k) = \int_0^p dk\, g(p,k) + \int_p^\Lambda dk\, g(p,k) \\
&= \sum_{i=1}^{N} w_i^1 g(p,k_i^1) + \sum_{i=1}^{N} w_i^2 g(p,k_i^2)\,,
\end{aligned}
\tag{A.1}
$$

where we $(\underline{\mathbf{x}}^1, \underline{\mathbf{w}}^1)$ and $(\underline{\mathbf{x}}^2, \underline{\mathbf{w}}^2)$ are the weights and grid points returned by `gauleg` routine. By splitting the integration in this way, we avoid problems which may be encountered in the integration kernels at $p = k$. We discretize p on an evenly spaced grid with approximately 100 points. Typically we choose on the order of 100 Gauss-Legendre quadrature points for the integrations. Since the grids for p and k are different we must interpolate the coefficient functions. We choose linear interpolation because this can be applied uniformly over the entire domain of integration and is the most computationally efficient method.

A.2 Iteration of the Integral Equations

The SD equations are solved through iteration of the numerical integration. We choose a seed function, integrate, and then repeat the process until convergence is seen. Our convergence criteria is that the integrated sum of all of the coefficient functions changes by less that 10^{-8} during an iteration. When attempting solution near the critical coupling or critical temperature more iteration steps are necessary. Below the critical temperature the result will continue to decrease to zero until the machine precision is reached. In order to save computer time, we measure the slope of the percentage change in the sum of the coefficient functions as a function of iteration. If after a minimal number of iterations this slope is increasing or zero, we stop the iteration process.

The codes ran on a Cray T90 supercomputer at the North Carolina Supercomputing Center and were vertorizable up to $\sim$ 600 MFlops.

Appendix B

Four Dimensional Integrals

In four dimensional Euclidean space we can use spherical coordinates, so that the integration measure can be expressed as

$$\begin{aligned}\int_k f(p,k) &= \int \frac{d^4k}{(2\pi)^4} f(k) \\ &= \frac{1}{(2\pi)^4} \int_0^L k^3 dk \int_0^\pi \sin^2\beta d\beta \int_0^\pi \sin\theta d\theta \int_0^{2\pi} d\phi\, f(p,k)\,, \qquad \text{(B.1)}\end{aligned}$$

where p is an external variable not dependent on k. In most cases, the dependence of f on the angles θ and ϕ can be removed by choosing the axes properly, and the integration over these variables can be performed, leaving

$$\int_k f(p,k) = \frac{1}{(2\pi)^3} \int_0^L k^2 dk^2 \int_0^\pi \sin^2\beta d\beta f(p^2,k^2,pk\cos\beta)\,. \qquad \text{(B.2)}$$

The angular integrals that are encountered can be evaluated using the relation

$$\begin{aligned}\int_0^\pi \frac{\sin^2\beta d\beta}{a+b\cos\beta} &= \frac{i}{8}\oint \frac{(t-1/t)^2 dt}{bt^2/2+at+b/2} \\ &= -\frac{\pi}{4}\left(\mathrm{Res}(t=0) + \mathrm{Res}\left(t = \frac{-a+\sqrt{a^2-b^2}}{b}\right)\right) \\ &= \frac{\pi}{b^2}\left(a - \sqrt{a^2-b^2}\right)\,, \qquad \text{(B.3)}\end{aligned}$$

which leads to the following results

$$\begin{aligned}I_1^0(p^2,k^2) &\equiv \frac{1}{\pi}\int_0^\pi \frac{\sin^2\beta d\beta}{p^2+k^2-2pk\cos\beta} \\ &= \frac{1}{4p^2k^2}\left(p^2+k^2-\sqrt{(p^2-k^2)}\right) \qquad \text{(B.4)}\end{aligned}$$

$$
\begin{aligned}
I_2^0(p^2,k^2) &\equiv \frac{1}{\pi}\int_0^\pi \frac{\sin^2\beta d\beta}{(p^2+k^2-2pk\cos\beta)^2} \\
&= -\frac{1}{4p^2k^2}\left(1-\frac{p^2+k^2}{\sqrt{(p^2-k^2)}}\right) \qquad \text{(B.5)}
\end{aligned}
$$

$$
\begin{aligned}
I_1^1(p^2,k^2) &\equiv \frac{1}{\pi}\int_0^\pi \frac{pk\cos\beta\sin^2\beta d\beta}{p^2+k^2-2pk\cos\beta} \\
&= -\frac{1}{4}+\frac{1}{2}(p^2+k^2)I_1^0(p^2,k^2) \qquad \text{(B.6)}
\end{aligned}
$$

$$
\begin{aligned}
I_2^1(p^2,k^2) &\equiv \frac{1}{\pi}\int_0^\pi \frac{pk\cos\beta\sin^2\beta d\beta}{(p^2+k^2-2pk\cos\beta)^2} \\
&= -\frac{1}{2}I_1^0(p^2,k^2)+\frac{1}{2}(p^2+k^2)I_2^0(p^2,k^2) \qquad \text{(B.7)}
\end{aligned}
$$

$$
\begin{aligned}
I_2^2(p^2,k^2) &\equiv \frac{1}{\pi}\int_0^\pi \frac{(pk\cos\beta)^2\sin^2\beta d\beta}{(p^2+k^2-2pk\cos\beta)^2} \\
&= \frac{1}{8}+(p^2+k^2)I_2^1(p^2,k^2)-\frac{1}{4}(p^2+k^2)^2I_2^0(p^2,k^2)\,. \qquad \text{(B.8)}
\end{aligned}
$$

When both $x \equiv p^2$ and $y \equiv k^2$ are real and positive, then the integrals above reduce to the following

$$
\begin{aligned}
I_1^0(p^2,k^2) &= \frac{1}{2\mathrm{max}(x,y)} \qquad \text{(B.9)} \\
I_2^0(p^2,k^2) &= \frac{1}{2\mid x-y\mid \mathrm{max}(x,y)} \qquad \text{(B.10)} \\
I_1^1(p^2,k^2) &= \frac{\mathrm{min}(x,y)}{4\mathrm{max}(x,y)} \qquad \text{(B.11)} \\
I_2^1(p^2,k^2) &= \frac{\mathrm{min}(x,y)}{2\mid x-y\mid \mathrm{max}(x,y)} \qquad \text{(B.12)} \\
I_2^2(p^2,k^2) &= \frac{xy+3\mathrm{min}(x,y)}{8\mid x-y\mid \mathrm{max}(x,y)}\,. \qquad \text{(B.13)}
\end{aligned}
$$

Appendix C

Three Dimensional Integrals

In the process of evaluating the kernels which appear in the finite temperature

$$q^2 = \underline{\mathrm{p}}^2 + \underline{\mathrm{k}}^2 + (\omega_n - \omega_m)^2 - 2\underline{\mathrm{p}}\underline{\mathrm{k}}\cos\theta\,. \tag{C.1}$$

C.1 Integrals for Massless Gluon

The integrals below were evaluated analytically and checked with *Mathematica 2.2.*

$$\begin{aligned} J_1^0(\underline{\mathrm{p}},\underline{\mathrm{k}})_{nm} &= \int_0^\pi d\theta\,\frac{\sin\theta}{q^2} \\ &= \frac{1}{\underline{\mathrm{p}}\underline{\mathrm{k}}}\ln\left(\frac{\underline{\mathrm{p}}^2+\underline{\mathrm{k}}^2+(\omega_n-\omega_m)^2+2\underline{\mathrm{p}}\underline{\mathrm{k}}}{\underline{\mathrm{p}}^2+\underline{\mathrm{k}}^2+(\omega_n-\omega_m)^2-2\underline{\mathrm{p}}\underline{\mathrm{k}}}\right) \end{aligned} \tag{C.2}$$

$$\begin{aligned} J_1^1(\underline{\mathrm{p}},\underline{\mathrm{k}})_{nm} &= \int_0^\pi d\theta\,\frac{\sin\theta\cos\theta}{q^2} \\ &= \frac{\underline{\mathrm{p}}^2+\underline{\mathrm{k}}^2+(\omega_n-\omega_m)^2}{2\underline{\mathrm{p}}\underline{\mathrm{k}}}J_1^0(\underline{\mathrm{p}},\underline{\mathrm{k}})_{nm} - \frac{1}{\underline{\mathrm{p}}\underline{\mathrm{k}}} \end{aligned} \tag{C.3}$$

$$\begin{aligned} J_2^0(\underline{\mathrm{p}},\underline{\mathrm{k}})_{nm} &= \int_0^\pi d\theta\,\frac{\sin\theta}{q^4} \\ &= \frac{2}{(\underline{\mathrm{p}}^2+\underline{\mathrm{k}}^2+(\omega_n-\omega_m)^2)^2-4\underline{\mathrm{p}}^2\underline{\mathrm{k}}^2} \end{aligned} \tag{C.4}$$

$$\begin{aligned} J_2^1(\underline{\mathrm{p}},\underline{\mathrm{k}})_{nm} &= \int_0^\pi d\theta\,\frac{\sin\theta\cos\theta}{q^4} \\ &= \frac{\underline{\mathrm{p}}^2+\underline{\mathrm{k}}^2+(\omega_n-\omega_m)^2}{2\underline{\mathrm{p}}\underline{\mathrm{k}}}J_2^0(\underline{\mathrm{p}},\underline{\mathrm{k}})_{nm} - \frac{1}{2\underline{\mathrm{p}}\underline{\mathrm{k}}}J_1^0(\underline{\mathrm{p}},\underline{\mathrm{k}})_{nm} \end{aligned} \tag{C.5}$$

$$
\begin{aligned}
J_2^2(\underline{p},\underline{k})_{nm} &= \int_0^\pi d\theta \, \frac{\sin\theta \cos^2\theta}{q^4} \\
&= \frac{1}{2\underline{p}^2\underline{k}^2} + \frac{(\underline{p}^2+\underline{k}^2+(\omega_n-\omega_m)^2)^2}{4\underline{p}^2\underline{k}^2} J_2^0(\underline{p},\underline{k})_{nm} \\
&\qquad - \frac{\underline{p}^2+\underline{k}^2+(\omega_n-\omega_m)^2}{2\underline{p}^2\underline{k}^2} J_1^0(\underline{p},\underline{k})_{nm} \,. \qquad \text{(C.6)}
\end{aligned}
$$

C.1.1 Integrals for Massive Gluon

$$
\begin{aligned}
\tilde{J}_1^0(\underline{p},\underline{k})_{nm} &= \int_0^\pi d\theta \, \frac{\sin\theta}{q^2+m_D^2} \\
&= \frac{1}{\underline{p}\underline{k}} \ln\left(\frac{\underline{p}^2+\underline{k}^2+(\omega_n-\omega_m)^2+m_D^2+2\underline{p}\underline{k}}{\underline{p}^2+\underline{k}^2+(\omega_n-\omega_m)^2+m_D^2-2\underline{p}\underline{k}}\right) \qquad \text{(C.7)} \\
\tilde{J}_1^1(\underline{p},\underline{k})_{nm} &= \int_0^\pi d\theta \, \frac{\sin\theta\cos\theta}{q^2+m_D^2} \\
&= \frac{\underline{p}^2+\underline{k}^2+(\omega_n-\omega_m)^2+m_D^2}{2\underline{p}\underline{k}} \tilde{J}_1^0(\underline{p},\underline{k})_{nm} - \frac{1}{\underline{p}\underline{k}} \qquad \text{(C.8)} \\
\tilde{J}_2^0(\underline{p},\underline{k})_{nm} &= \int_0^\pi d\theta \, \frac{\sin\theta}{(q^2+m_D^2)q^2} \\
&= \frac{1}{m_D^2}\left(J_1^0(\underline{p},\underline{k})_{nm} - \tilde{J}_1^0(\underline{p},\underline{k})_{nm}\right) \qquad \text{(C.9)} \\
\tilde{J}_2^1(\underline{p},\underline{k})_{nm} &= \int_0^\pi d\theta \, \frac{\sin\theta\cos\theta}{(q^2+m_D^2)q^2} \\
&= \frac{\underline{p}^2+\underline{k}^2+(\omega_n-\omega_m)^2}{2\underline{p}\underline{k}} \tilde{J}_2^0(\underline{p},\underline{k})_{nm} - \frac{1}{2\underline{p}\underline{k}} \qquad \text{(C.10)} \\
\tilde{J}_2^2(\underline{p},\underline{k})_{nm} &= \int_0^\pi d\theta \, \frac{\sin\theta\cos^2\theta}{(q^2+m_D^2)q^2} \\
&= \frac{1}{2\underline{p}^2\underline{k}^2} + \frac{(\underline{p}^2+\underline{k}^2+(\omega_n-\omega_m)^2)^2}{4\underline{p}^2\underline{k}^2} \tilde{J}_2^0(\underline{p},\underline{k})_{nm}
\end{aligned}
$$

$$-\frac{\underline{\mathrm{p}}^2 + \underline{\mathrm{k}}^2 + (\omega_n - \omega_m)^2}{2\underline{\mathrm{p}}^2\underline{\mathrm{k}}^2}\tilde{J}_1^0(\underline{\mathrm{p}}, \underline{\mathrm{k}})_{nm} - \frac{m_D^2}{2\underline{\mathrm{p}}^2\underline{\mathrm{k}}^2}\tilde{J}_1^0(\underline{\mathrm{p}}, \underline{\mathrm{k}})_{nm} \quad \text{(C.11)}$$

Bibliography

[1] Conceptual design report of the relativistic heavy ion collider. Brookhaven Natl. Lab. Rep. BNL-52195, 1989.

[2] J. Schukraft et al. *Nucl. Phys. A*, 566:311, 1994.

[3] Berndt Müller. Physics and signatures of the quark-gluon plasma. *Rep. Prog. Phys.*, 58:611, 1995.

[4] L. von Smekal, A. Hauck, and R. Alkofer. The infrared behavior of gluon and ghost propagators in landau gauge QCD. hep-ph/9705242, 1997.

[5] A. Bender, D. Blashke, Y. Kalinovksy, and C. D. Roberts. Continuum study of deconfinement at finite temperature. *Phys. Rev. Lett.*, 77:3724, 1996.

[6] D. Atkinson, P. Johnson, W. Schoenmaker, and H. Slim. Infra-red behaviour of the gluon propagator in axial gauges. *Nuovo Cimento*, 77:197, 1983.

[7] R. P. Feynman and A. R. Hibbs. *Quantum Mechanics and Path Integrals.* McGraw-Hill, New York, 1965.

[8] L. H. Ryder. *Quantum Field Theory.* Cambridge University Press, Cambridge, UK, 1985.

[9] H. J. Rothe. *Lattice Gauge Theories: An Introduction.* World Scientific, Singapore, 1992.

[10] F. Karsch. The phase transition to the quark gluon plasma: Recent results from lattice calculations. *Nucl. Phys. A*, 590:367, 1995.

[11] M. R. Frank and C. D. Roberts. Model gluon propagator and pion and rho-meson observables. *Phys. Rev. C*, 53:390, 1996.

[12] F. T. Hawes and A. G. Williams. Chiral symmetry breaking in quenched massive strong-coupling four-dimensional QED. *Phys. Rev. D*, 51:3081, 1995.

[13] D. C. Curtis and M. R. Pennington. Truncating the Schwinger-Dyson equations: How multiplicative renormalizability and the Ward identity restrict the three-point vertex in QED. *Phys. Rev. D*, 42:4165, 1990.

[14] C. Itzykson and J.-B. Zuber. *Quantum Field Theory.* McGraw-Hill, New York, 1980.

[15] P. Maris. *Nonperturbative analysis of the fermion propagator: Complex singularities and dynamical mass generation.* PhD thesis, Institute for Theoretical Physics, Groningen, 1993.

[16] V. A. Miransky. *Nuovo Cimento A*, 90:149, 1985.

[17] V. A. Miransky. *Sov. Phys. JETP*, 61:905, 1985.

[18] P. I. Fomin, V. P. Gusynin, V. A. Miransky, and Yu. A. Sitenko. *Nuovo Cimento*, 6:1, 1983.

[19] D. Atkinson and D.W.E. Blatt. Determination of the singularities of the electron propagator. *Nucl. Phys. B*, 151:342, 1979.

[20] C. J. Burden and C. D. Roberts. Singularity structure of a model quark propagator. *Phys. Lett. B*, 285:347, 1992.

[21] H. J. Munczek and A. M. Nemirovsky. *Phys. Rev. D*, 28:181, 1983.

[22] P. Maris. Confinement and complex singularities in three-dimensional QED. *Phys. Rev. D*, 52:6087, 1995.

[23] D. W. McKay and H. J. Munczek. Study of quark propagator solutions to the Dyson-Schwinger equation in a confining model. *Phys. Rev. D*, 55:2455, 1997.

[24] U. Häbel, R.Könning, H.-G. Reusch, M. Stingl, and S. Wigard. A nonperturbative solution to the Dyson-Schwinger equations for QCD. I. nonperturbative vertices and a mechanism for their self consistency. *Z. Phys. A.*, 336:423, 1990.

[25] U. Häbel, R.Könning, H.-G. Reusch, M. Stingl, and S. Wigard. A nonperturbative solution to the Dyson-Schwinger equations for QCD. II. self-consistency and physical properties. *Z. Phys. A.*, 336:435, 1990.

[26] P. Jain and H. J. Munczek. Calculation of the pion decay constant in the framework of the Bethe-Salpeter equation. *Phys. Rev. D*, 44:1873, 1991.

[27] H. J. Munczek and P. Jain. Relativistic pseudoscalar $q\bar{q}$ bound states: Results on Bethe-Salpeter wave functions and decay constants. *Phys. Rev. D*, 46:438, 1992.

[28] H. J. Munczek and P. Jain. $q\bar{q}$ bound states in the Bethe-Salpeter formalism. *Phys. Rev. D*, 48:5403, 1993.

[29] W. Marciano and H. Pagels. Quantum chromodynamics. *Physics Reports*, 36:137, 1978.

[30] J. Praschifka, R. T. Cahill, and C. D. Roberts. *Int. J. Mod. Phys.*, 4:4929, 1989.

[31] P. Maris. The influence of the full vertex and vacuum polarization on the fermion propagator in QED3. *Phys. Rev. D*, 54:4049, 1996.

[32] F. T. Hawes and A. G. Williams. Proper vertex in studies of dynamical chiral symmetry breaking. *Phys. Lett. B*, 268:271, 1991.

[33] J. Ball and T.-W. Chiu. Analytic properties of the vertex function in gauge theories. I. *Phys. Rev. D*, 22:2542, 1980.

[34] J. Ball and T.-W. Chiu. Analytic properties of the vertex function in gauge theories. II. *Phys. Rev. D*, 22:2550, 1980.

[35] D. C. Curtis and M. R. Pennington. Nonperturbative study of the fermion propagator in quenched QED in covariant gauges using a renormalizable truncation of the Schwinger-Dyson equation. *Phys. Rev. D*, 48:4933, 1993.

[36] K.-I. Kondo. Transverse Ward-Takahashi identity, anomaly and Schwinger-Dyson equation. hep-ph/9608100, 1996.

[37] A. Bashir and M.R. Pennington. Constraint on the QED vertex from the mass anomalous dimesion $\gamma_m = 1$. *Phys. Rev. D*, 53:4694, 1996.

[38] S.D. Odintsov and Y.U.I. Shil'nov. Schwinger-Dyson equations in QED at non-zero temperature. *Mod. Phys. Lett. A*, 707:707, 1991.

[39] A. Cabo, O.K. Kalshnikov, and E.Kh. Veliev. Bootstrap calculation of the dynamical quark mass in QCD4 at finite temperature. *Nucl. Phys. B*, 299:367, 1988.

[40] A. Bender, D. Blashke, Y. Kalinovsky, and C.D. Roberts. Continuum study of deconfinement at finite temperature. *Phys. Rev. Lett.*, 77:3724, 1996.

[41] P. Alkofer, P.A. Amudsen, and K. Langfeld. Chiral symmetry breaking and pion properties at finite temperatures. *Z. Phys. C*, 42:199, 1989.

[42] I.J.R. Aitchison, N. Dorey, M. Klein-Kreisler, and N.E. Mavromatos. Phase structure of QED3 at finite temperature. *Phys. Lett. B*, 294:913, 1992.

[43] J.I. Kapusta. *Finite-temperature field theory.* Cambridge University Press, Cambridge, UK, 1989.

[44] T. Toimela. *Nucl. Phys. B*, 273:719, 1986.

[45] P. Henning. *Phys. Lett. B*, 272:181, 1991.

[46] J.J. Rusnak and R.J. Furnstahl. Two-point fermion correlation functions at finite density. *Z. Phys. A*, 352:345, 1995.

[47] J.F. Donoghue, B.R. Holstein, and R.W. Robinett. Quantum electrodynamics at finite temperature. *Ann. of Phys.*, 164:233, 1985.

[48] W.H. Press, S.A. Teukolsky, W.T. Vetterling, and B.P. Flannery. *Numerical Recipes in C.* Cambridge University Press, Cambridge, UK, 1992.

Biography

Name:	Michael Thomas Strickland
Date of Birth:	November 23, 1969
Place of Birth:	New York, New York
Education:	University of North Carolina at Chapel Hill B.S. in Physics, 1992 Duke University (1992-1997) M.A. in Physics, 1995 Ph.D. in Physics, August, 1997

Publications:

M. Strickland. Thermal photons and dileptons from non-equilibrium quark-gluon plasma. *Phys. Lett. B*, 331:245, 1994.

S.B. Liao and M. Strickland. Renormalization group approach to field theory at finite temperature. *Phys. Rev. D*, 52:3653, 1995.

M. Pichowsky, M. Strickland, and M. Kennedy. Two-body bound states and the Bethe-Salpeter equation. HUGS@CEBAF Proceedings, 1995.

M. Strickland. Deuteron photodisintegration above pion threshold. HUGS-@CEBAF Proceedings, 1995.

S.B. Liao and M. Strickland. Dimensional Crossover and Effective Critical Exponents. *Nucl. Phys. B.*, 497:611, 1997.

Books:

B. Müller, J. Reinhardt, and M. Strickland. *Neural Networks: An Introduction.* Springer-Verlag, Frankfurt, 1995.